Demonstration of Remote Sensing Fenceline Monitoring Methods at Oil Refineries and Ports

FINAL REPORT
(January 2015)

Prepared for the
South Coast Air Quality Management District
21865 Copley Dr, Diamond Bar, CA 91765

by

Principal Investigator: Dr. Jochen Stutz
Dr. Olga Pikelnaya

Department of Atmospheric and Oceanic Sciences
University of California Los Angeles
7127 Math Sciences, Los Angeles, CA 90095-1565
Tel. 310-825-5364
Email: jochen@atmos.ucla.edu

Executive Summary

Remote sensing offers unique opportunities for fenceline monitoring of pollutant emissions from industrial facilities. The ability of modern remote sensing instruments to measure along an extended path, or even in a two-dimensional plane parallel to a facility fenceline, increases the probability of detecting pollutant releases compared to conventional in-situ methods. Remote sensing instruments are also highly selective and sensitive, can be built to be fully automated and, unlike most in-situ techniques, do not require calibration or regular maintenance Remote sensing instruments are thus ideally suited for long-term fenceline monitoring.

Despite these advantages, remote sensing fenceline techniques are not yet widely used. This is, in part, due to a lack of experience with these often relatively new methods, and problems with some currently commercially available instruments, which are based on outdated technology. The motivation for this project was therefore to demonstrate and evaluate capabilities of four different remote sensing techniques to monitor trace gas concentrations and quantify trace gas emissions from petrochemical facilities: Long-path Differential Optical Absorption Spectroscopy (DOAS), dual Multi-Axis DOAS, Imaging DOAS, and open-path Fourier Transform Infrared (FTIR) spectroscopy. The following sections summarize the experience in operating the four different methods at the fenceline of a refinery in Carson and other locations in the South Coast Air Basin for extended periods of time. The performance of each method, as well as its suitability for fenceline monitoring are assessed.

LP-DOAS measurement of aromatic hydrocarbons

Long-path differential optical absorption spectroscopy is based on the analysis of narrowband molecular absorptions along an extended absorption path in the open atmosphere. In the UV wavelength region between 250 nm and 280 nm, absorptions of aromatic hydrocarbons, including benzene and toluene, can be used to selectively detect these species. LP-DOAS instruments consist of a light-source connected to a telescope, which sends a collimated light beam through the atmosphere. In most cases, including in our project, this beam is aimed at an array of reflectors, which sends the light back into the main telescope, where it is spectroscopically analyzed using the DOAS technique. The distance between the main telescope and reflector can vary between 100 m and 1000 m for aromatic hydrocarbon measurements, and was 250m in Carson setup. Because we were unsuccessful in using a commercial OPSIS system for the accurate measurement of benzene and toluene, we developed a new state-of-the-art LP-DOAS instrument at UCLA. The first version of this instrument was operated for more than 2 months at the fenceline of the refinery in Carson, observing varying levels of toluene, which correlated well with wind-direction as well as with CO_2, CO, and total hydrocarbons measured by the co-located OP-FTIR. The final version of the LP-DOAS was deployed for 3 months during Summer, 2014. This system was fully automated and did not require any manual operation or maintenance during this time period. This new system has the capability to measure both benzene and toluene simultaneously, as well as other aromatic hydrocarbons. The detection limits of the LP-DOAS system, calculated from the actual measurements, were ~ 0.6 ppb for benzene and ~ 0.45 ppb for toluene for a 60 second measurement time and a reflector distance of 250 m. These characteristics make this system suitable for the purposes of compliance or enforcement requested in a newly proposed EPA requirement for refineries to monitor fenceline benzene concentrations, which establishes a 2-week averaged benzene concentration action level of 3 ppb (http://www.epa.gov/airtoxics/petref.html). Tools to operate this system as a fast alarm system were also developed. The following general conclusions can be drawn for the use of LP-DOAS for the monitoring of aromatic hydrocarbons:

- LP-DOAS systems based on current state-of-the-art technology can reliably monitor ozone and air toxins such as toluene, benzene, and other aromatic hydrocarbons.

- Detection limits of these new LP-DOAS systems are sufficient for the monitoring not only of large accidental releases, but also of fugitive emissions, as required by the EPA's new rules for such fenceline monitoring instruments (http://www.epa.gov/airtoxics/petref.html).
- The high measurement frequency of one minute, together with the near real-time data analysis, which can provide trace gas concentrations within one minute of a measurement, is sufficient to use these systems as alarm systems for accidental releases.
- The new technology employed in UCLA's new LP-DOAS allows for long-term unattended and stable operation, as well as full remote control access. This ability will considerably reduce operating costs, which largely offsets the initial cost of the instrument. No consumables, besides electricity, are needed to operate instrument.
- Due to its novel design, the UCLA LP-DOAS system is capable of measurements on multiple and longer light paths, thus opening up an unprecedented potential for monitoring emissions from an entire facility.
- Co-location of an UV LP-DOAS and open-path FTIR system open new opportunities for emission measurements, as relating observations of trace gases with better-constrained emissions, for example of CO or CO_2, allows for the determination of emission fluxes using a ratioing technique.

We conclude that our efforts in showing the capabilities of LP-DOAS for fenceline monitoring of aromatic hydrocarbons have been successful, and we see no obstacles in using LP-DOAS for long-term fenceline monitoring and alarm systems at industrial facilities.

Dual Max-DOAS technique

The measurement of area-wide fluxes of air pollutants such as NO_2, HCHO, and SO_2, remains a challenge, as sources are spatially distributed and trace gases are consequently unevenly mixed in the horizontal and vertical. The dual MAX-DOAS approach measures the trace gas amount in a vertical slice perpendicular to the main wind direction, upwind and downwind of the targeted area. The difference between the trace gas content in the two slices, together with wind speed and direction allows the determination of the absolute emission fluxes from the area of interest.

As part of this project we developed two highly stable and fully automated MAX-DOAS instruments, which were deployed around two refineries in Carson. While the upwind MAX-DOAS instrument location was not ideal, the dual MAX-DOAS measurements derived NO_x fluxes of 709 tons/yr with a ~40% uncertainty and an assumed NO_2/NOx ratio of 0.3 during typical wind conditions. This value compares well with the 2012 reported emissions of 983 tons of annual NOx emissions from the refineries enclosed by the dual MAX- DOAS system. In addition, measurements with one MAX-DOAS instrument, using a geometric approach to convert path-integrated concentrations to mixing ratios, were successful compared to observations from a nearby air quality monitoring station. Another unique application of MAX-DOAS is the measurement of the HCHO/NO_2 ratio, which is a proxy to the NOx/VOC sensitivity of ozone formation. The long-term measurement of the HCHO/NO_2 ratio could thus be used to follow the success of the current AQMD 2012 Air Quality Management Plan (AQMP) (http://www.aqmd.gov/aqmp/2012aqmp/RevisedDraft/RevisedDraft2012AQMP-Main-clean.pdf) which calls for NOx emissions reductions as a primary effort combating O_3 and PM pollution. The following conclusions can be drawn from our work with the dual MAX-DOAS system:

- The dual MAX-DOAS method is capable of measuring area averaged fluxes of NO_2 and HCHO, provided high quality meteorological data is available. The instruments are fully automated and no operational effort is required once the systems are set up. On the other hand,

identifying the best location for placement of the instruments is crucial for the success of the dual MAX-DOAS approach.

- Emission rates determined by dual MAX-DOAS in Carson under normal wind conditions compare well to those reported in 2012, considering the estimated 40% uncertainty of our observations.
- Accurate meteorological observations are crucial for the determination of the emissions fluxes. The dual MAX-DOAS measurements could be further improved by measuring boundary layer height.
- A single MAX-DOAS instrument can be used for long-term pollutant monitoring. The observations of the HCHO/NO_2 ratio, which provide information on the NOx/VOC sensitivity of ozone formation, could prove to be particularly useful.

In summary, we successfully demonstrated the capability of the dual MAX-DOAS approach under ideal conditions. However, the accuracy of the method depends crucially on the location of the instruments and good meteorological data.

I-DOAS measurements.

Imaging DOAS allows the visualization of pollution plumes, for example from point sources such as flares and smoke stacks, and, in combination with meteorological data, the determination of absolute emission fluxes. Our original proposal was to apply this method to monitor flares of petrochemical facilities in Carson. However, flaring has become so uncommon, and also mostly occurred at night, that no burning petrochemical flare was observed in Carson. We thus expanded our measurements to other point sources in the South Coast Air Basin. Our most successful application was the observation of a burning flare at an Ontario landfill, where formaldehyde emissions of ~3 lbs/hour were observed. We also visualized trace gas plumes above the UCLA campus, but no direct attribution of these trace gases to a single source was possible. We have drawn the following conclusions from our measurements with the I-DOAS system:

- The I-DOAS approach can measure emission fluxes from point sources. The accuracy of the methods depends on the accurate measurements of wind speed and direction.
- Burning flares have become less frequent at petrochemical facilities in the South Coast Air Basin, and thus were not successfully observed by the I-DOAS. However flares at landfills were found to emit HCHO.
- The I-DOAS can be used to visualize plumes of NO_2 and HCHO, for example above a freeway. This application should be further explored in the future.

In summary, the I-DOAS system performed well during all deployment days. When burning flares were observed, fluxes of HCHO could be determined. The I-DOAS is a powerful technique to characterize source emissions from flares and smoke stacks of power plant and ships, and potentially also emission plumes from road traffic.

OP-FTIR observations

The OP-FTIR method measures hydrocarbons, pollutants, and greenhouse gases with a similar setup as the LP-DOAS, where an open air light-path is set up between a sending/receiving telescope and a reflector. The absorptions of the various trace gases are measured in the infrared wavelength range. The advantages of this method are also similar to those of the UV LP-DOAS system.

In the course of this fenceline technology demonstration project, we successfully used a commercial IMACC OP-FTIR system at a refinery fenceline in Carson for a period of six months. Our detailed conclusions / recommendations are summarized below:

- On short light paths and in close proximity to emission sources OP-FTIR is a good method for monitoring of pollutant and greenhouse gas emissions from industrial sources. Detection limits for various hydrocarbons are in the range of 5 - 10ppb. The detection limit for CO_2 is ~11ppm.
- Simultaneous measurements of pollutants from the OP-FTIR, or a co-located LP-DOAS, together with OP-FTIR observations of CO_2 and CO allow estimates of emission fluxes using a ratioing technique.
- Long-term operation of an OP-FTIR system is feasible only if the instrument is equipped with an active detector cooling system. For the automated alignment and possibility of multi-light-path measurements, a motorized azimuth/elevation mount for the FTIR telescope is highly desirable. In areas with many pollution sources, especially those that emit soot particles (e.g. proximity to busy railroad tracks), FTIR retroreflectors must be periodically cleaned in order to maintain good light levels.

OP-FTIR is a powerful method for fenceline monitoring of certain greenhouse gases, pollutants, and hydrocarbons. The main challenge found in the operation of the OP-FTIR in Carson was the maintenance of the detector cooling and regular manual alignment of the telescope. These are obstacles that can be easily overcome with existing technology, and it is thus feasible to operate fully automated OP-FTIR systems over extended time periods.

We conclude that all four methods are capable of monitoring emissions from industrial facilities. The inherent advantages of these methods, such as the ability to measure emissions averaged along a fenceline or integrated in the vertical and horizontal, make them better suited for fenceline monitoring than classical in-situ techniques. Due to the open-path measurement geometry, which precludes sampling artifacts, and the use of an absolute absorption spectroscopy approach, which makes calibrations unnecessary, these systems are ideal for long-term automated measurements with little or no maintenance.

Table of Contents

1 Introduction

Modern atmospheric remote sensing techniques offer unique opportunities for monitoring trace gas emissions from industrial facilities. The remote sensing approach has many advantages over classical in-situ techniques. Because remote sensing methods are often based on absorption spectroscopic techniques, they uniquely identify trace gases and are based on physically constant and well-defined absorption cross sections. Consequently, they do not require instrument calibration. Remote sensing methods are often averaged over extended absorption paths, thus increasing the chance of observing an insulated trace gas plume. This is particularly useful for monitoring along a fenceline, where spatially limited plumes could be missed by in-situ monitors. Spectroscopic remote sensing measurements thus allow an absolute determination of the path-averaged trace gas concentration. Another advantage is that remote sensing methods allow for continuous monitoring of trace gas emissions from outside a facility, thus avoiding possible complications due to safety and security concerns. Finally, remote sensing spectroscopic instruments can be automated such that little operational effort is required. They are also easily remote controlled.

Despite these advantages, remote sensing fence-line techniques are not yet widely used for pollutant monitoring. This is, in part, often due to the difficulty in establishing these relatively new methods as tools for air quality agencies. In addition, the underlying technologies and techniques are not part of typical university curricula and are thus often unfamiliar to all but the researchers developing and applying them. There is thus a need to demonstrate the capabilities of these methods for industrial fence-line monitoring.

In this project we demonstrated four different remote sensing techniques to monitor trace gases or quantify trace gas emissions using the UV-visible Differential Optical Absorption Spectroscopy (DOAS), as well as FTIR long-path spectroscopy:

- Long-path DOAS (LP-DOAS) monitoring of aromatic hydrocarbons and use of this system as an alarm tool for accidental emissions
- Imaging DOAS (I-DOAS) measurements of the emissions of HCHO, NO_2, and SO_2 from point sources
- Dual Multi-Axis DOAS (MAX-DOAS) measurements of facility wide emission fluxes of HCHO, NO_2, and SO_2.
- FTIR long-path spectroscopic measurements of various hydrocarbons downwind of an oil refinery.

The following report outlines our activities over the past year at the Tesoro refinery in Carson, as well as the different instrument development activities. The general location and meteorological conditions of this location, together with a brief description of the reported emissions from the Carson refinery will be given in Chapter 2. It should be noted, however, that the Carson refinery is in a heavily industrialized area, and that other sources could contribute to trace gas levels we report throughout this report.

The LP-DOAS measurements of aromatic hydrocarbons required the development of a new instrument, as the commercial OPSIS instrument originally purchased by the AQMD for this purpose did not perform satisfactorily. We thus put more effort into instrument development than originally proposed. The results of the development efforts and the operation of the new LP-DOAS instrument will be described in Chapter 3 of this report.

Imaging DOAS observations were performed at the Carson refinery and flares of landfills in the LA basin. The results of these measurements are outlined in Chapter 4. We developed and built two MAX-DOAS instruments within this project for the Dual-MAX-DOAS measurements of facility wide emission fluxes. These new instruments will be described in Chapter 5 of this report. One of these systems was

operated for a year at the Carson refinery. However, delay in obtaining the permit to place the second instrument restricted the observation of the facility fluxes to two months. Despite this shorter deployment, this period was sufficient to show the feasibility of this approach, as we will explain in the second part of Chapter 5.

Chapter 6 will describe our experience with a IMACC open-path Fourier Transform System, which we borrowed from the US EPA. This system was successfully operated at the Carson refinery fenceline. The OP-FTIR system was also operated in parallel with a test-version of our new LP-DOAS instrument. The results of this combined monitoring approach will be described in Chapter 3, together with the LP-DOAS data.

The conclusions from our work will be summarized in Chapter 7. We will also make specific recommendations for the operation of remote sensing fenceline monitoring measurements to help guide future efforts.

2 Site Description

Most of the activities described in this report, with the exception of some Imaging-DOAS measurements, were performed at AQMD's Fenceline Monitoring Laboratory (FML) near the Tesoro refinery in Carson (Figure 2.1). The FML is located on the grounds of Ventura Transfer Co., which shares a fenceline with the Tesoro Carson refinery. The Tesoro refinery extends to the south and south-west of the FML (and Figure 2.1). Two major freeways, I405 and I710, run to the north and east of the FML. There are also a number of other industrial facilities near the FML.

During the project we deployed two path-averaging active remote sensing instruments, a long-path-DOAS and open-path FTIR, at the FML. In all cases the main instrument was located at the FML, with reflector arrays mounted on light posts on the grounds of the Tesoro refinery. The light paths thus extended from the FML, across the Dominguez Channel to the respective retroreflector arrays. The insert in Figure 2.1 shows a map of the area with marked locations of the FML and LP-DOAS light path. The

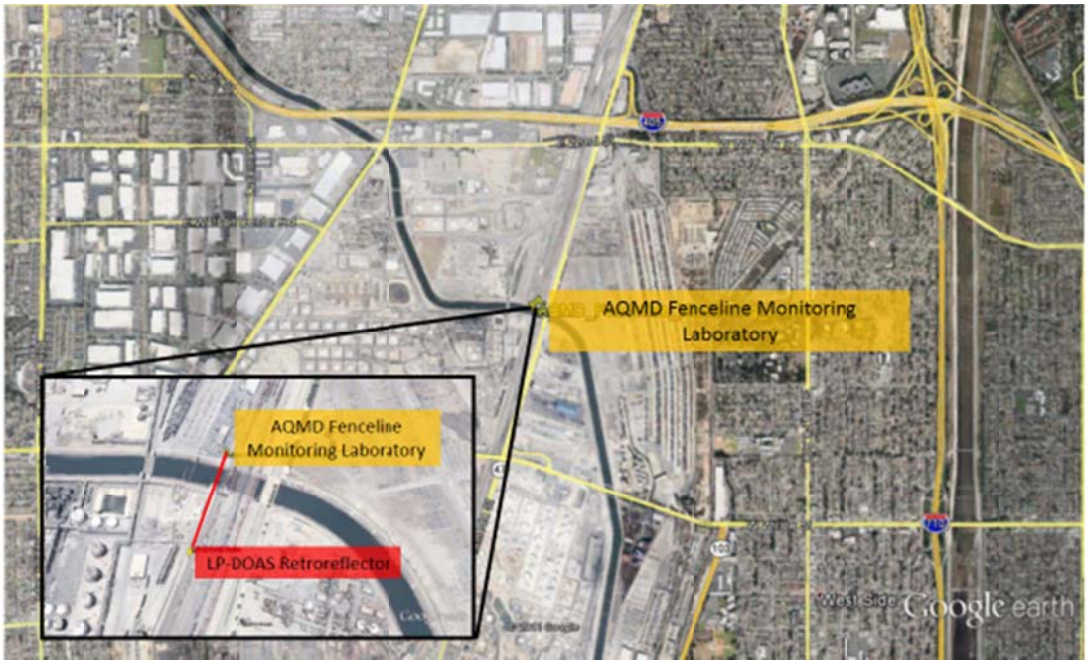

Figure 2.1: Map of the area around the Carson Tesoro refinery with locations of the AQMD Fenceline Monitoring Laboratory and LP-DOAS light path marked.

light paths were running in parallel to the refinery fenceline. The instruments line of sight was almost due south (at an azimuth of 193°). This line of sight is perpendicular to the main wind direction (Figure 2.2).

One of the Dual-Max DOAS instruments was also located at the FML, looking perpendicular to the main wind direction (Figure 2.2) at an azimuth angle of 193°. The second instrument was located at a school looking at an azimuth of 18°. The viewing paths were thus parallel, running upwind and downwind of the refinery. Further details of this setup will be given in Chapter 5.

Figure 2.2: Google Earth Map of the area around Carson BP refinery Red lines indicate light paths for dual MAX-DOAS experiment. Nominal diurnal wind pattern is indicated by the large yellow arrow. Red lines show MAX-DOAS lines of sight.

2.1 General meteorological conditions

The AQMD Fenceline Monitoring Laboratory in Carson is located at the western side of the Los Angeles Air Basin, approximately 1.6 miles SW of the intersection of I405 and I710 freeways, and approximately 4 miles north of the Terminal Island in the Port of Long Beach. This location is close to the coast and therefore highly influenced by the sea-coast wind pattern. Prior to conducting observations, we analyzed four years of meteorological data provided by the Tesoro Refinery Carson. Wind patterns from 2007 through 2011 were analyzed to determine prevailing wind direction for the area. This analysis was particularly important for Dual MAX-DOAS experiment site selection because it required for wind direction to be approximately normal to the MAX-DOAS lines of sight during daylight hours. Figure 2.3 shows the distribution of daytime (7am through 6pm local time) wind directions (winds from) for four years. The area experiences fairly consistent wind patterns, with a narrow distribution of winds mostly blowing from the north-west to south-east. During winter-time (see top panel of Figure 2.3) the wind direction spread is wider, with a number of data points with winds from the north-east. However, for other seasons the wind direction distribution is fairly narrow, as illustrated in Figure 2.3.

As mentioned earlier, selections of instrument locations and their lines of sight were based on this analysis of meteorological data. For example, line of sight for the LP-DOAs and OP FTIR were selected so that, for majority of times, it is normal to the wind direction. Similarly, locations for the Dual MAX-DOAS experiment were selected based on the nominal wind patterns for the area. Throughout this report we define the wind direction as the direction from which the wind is blowing.

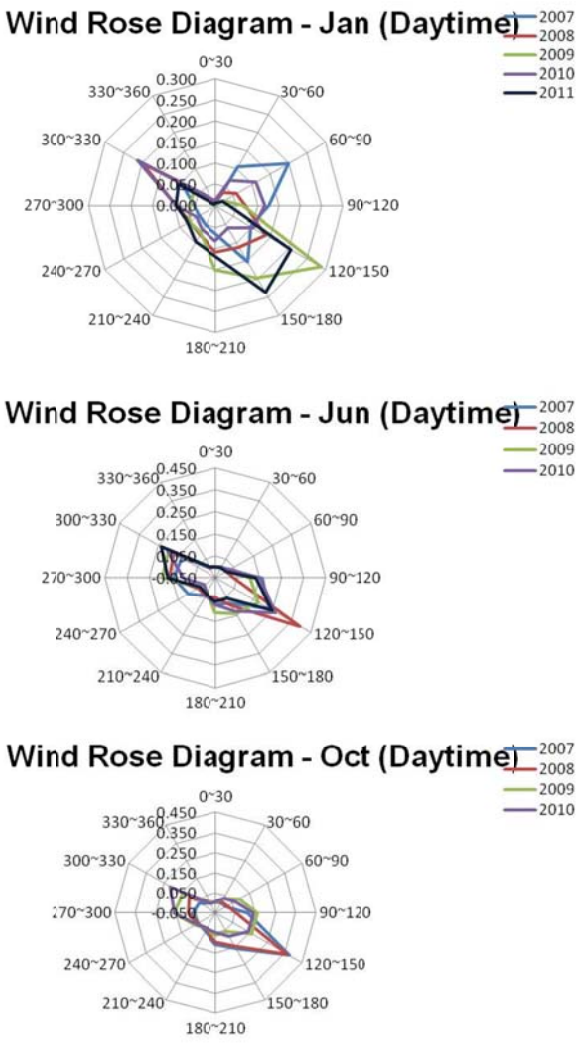

Figure 2.3: Monthly wind direction data for January, June and October at Carson BP refinery, CA for five years 2007 – 2011. All other months (not shown) experience very narrow wind direction spread, similar to the June and October examples presented here.

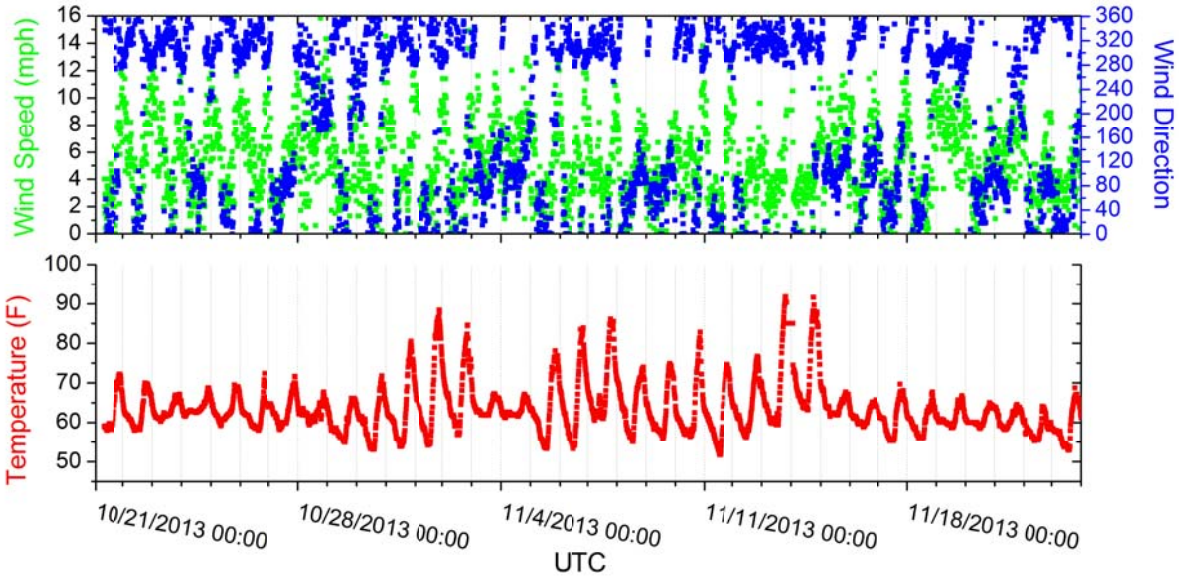

Figure 2.4: Overview of meteorological conditions at the Carson Fenceline Monitoring Site in Fall 2013

Because this report will focus on two main observational periods in the years 2013 and 2014 we will briefly present the meteorological conditions during these time periods in the following sections.

2.1.1 Fall 2013

During the months of October and November of 2013, when the OP-FTIR and test version of the new LP-DOAS were operated, the Carson fenceline monitoring site mostly experienced sea-land breeze conditions normal for Southern California. During the day, the winds were coming from west/north-west, shifting east/south-east during late afternoons and into the night. Wind speed also exhibited clear diurnal variations with the highest wind speeds of up to 16 mph observed during late afternoon, and calm nights. Daytime maximum temperatures ranged from the mid-seventies to low nineties during the day. Minimum nighttime temperatures were in the mid-fifties. Figure 2.4 shows temperature, wind speed and wind direction near the Carson FML for a four week period in Fall 2013. This data was provided by the Tesoro refinery and represents observations from the meteorological station on the grounds of the refinery.

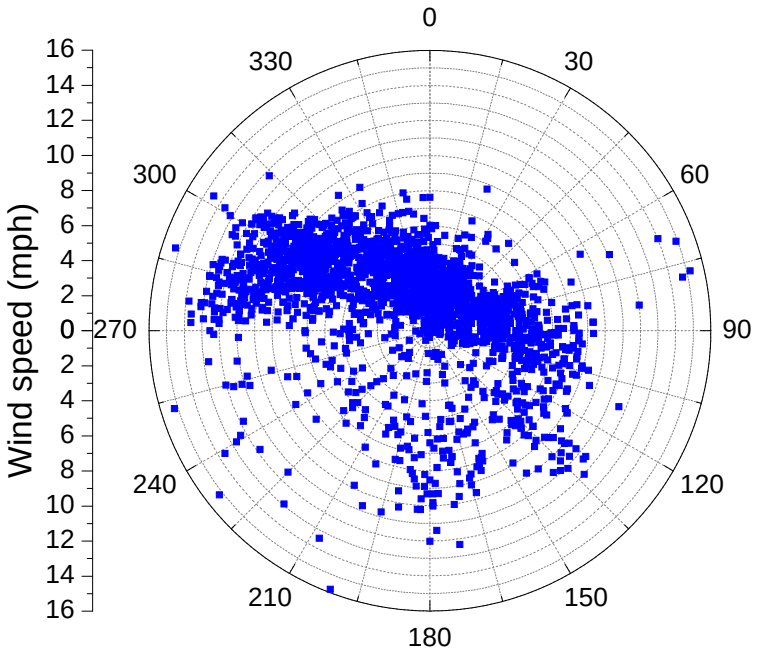

Figure 2.5: Wind speed and wind direction at the Carson Tesoro Refinery in Fall 2013.

The wind rose in Figure 2.5 shows that for most of the time, wind at the Carson site was coming either from the west/north-west (between azimuths 250 – 370 degrees) or from the east/south-east (between azimuths 80 – 130 degrees). These wind directions are almost perpendicular to light path of the various instruments.

2.1.2 Summer 2014

Meteorological conditions during the second Phase of our LP-DOAS and dual MAX-DOAS measurements (presented in Figure 2.6) were generally similar to Phase 1, with temperatures between 60F and 90FThe wind direction and speed during Phase 2 also follow the characteristic patterns observed during Phase 1 (see Figure 2.5 and Figure 2.7).

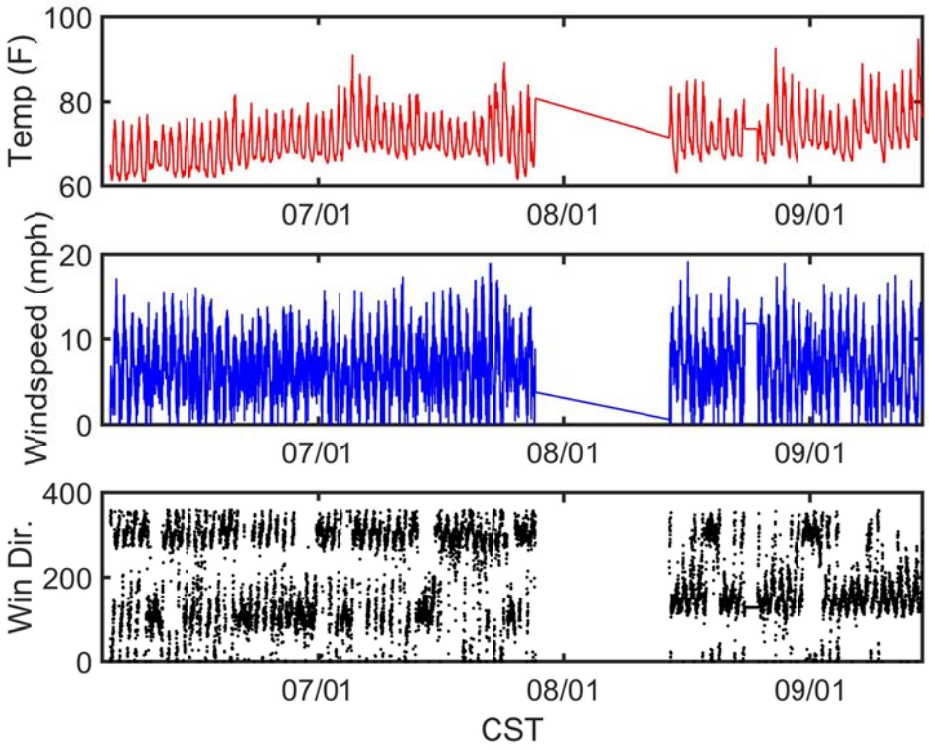

Figure 2.6: Overview of the meteorological observations during the LP-DOAS and dual MAX-DOAS Phase 2 observations. The gap in the data is due to a malfunction of the meteorological data, which was provided to us by the Tesoro Refinery.

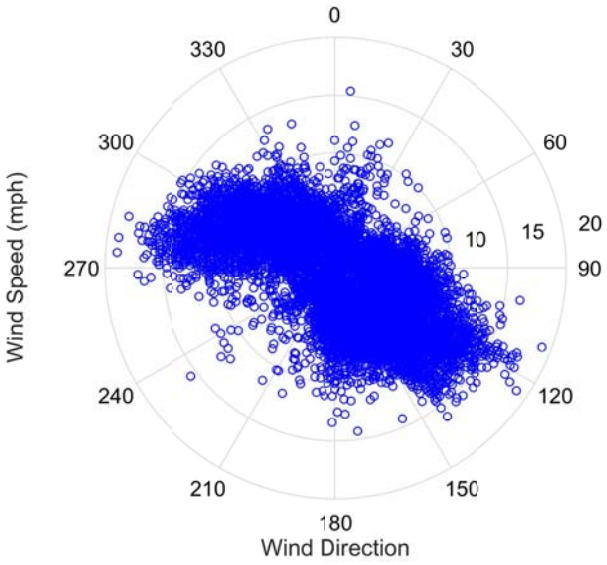

Figure 2.7: Wind rose of the Phase 2 observational period at Tesoro Carson Refinery.

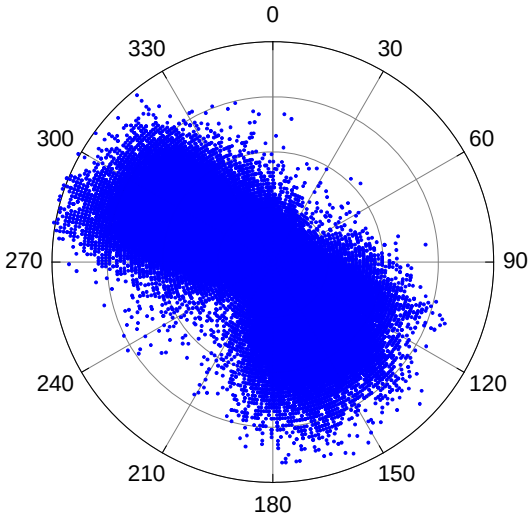

Figure 2.8: Wind rose of the Phase 2 observational period at SPPS.

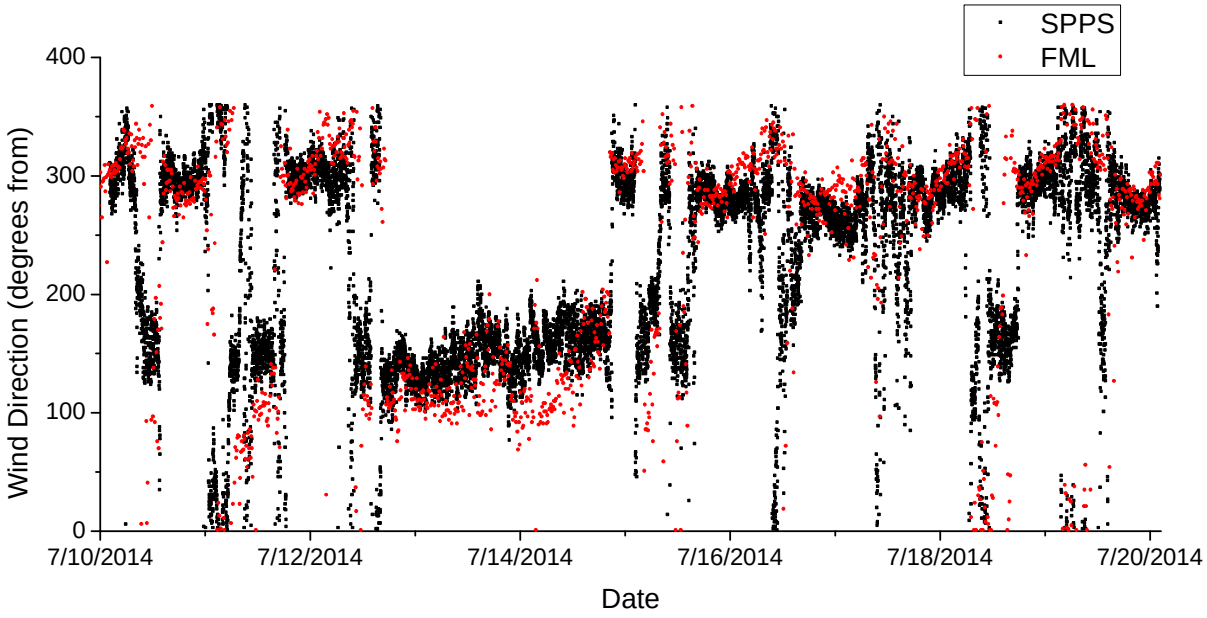

Figure 2.9: Comparison of wind direction measured at Carson Tesoro refinery and Saint Peter and Paul School.

2.2 Reported Emissions near FML

As the main goal of our project was to demonstrate emission techniques from industrial facilities near the FML, we compiled a list of the emissions from these facilities reported to the AQMD.

Refineries operating in the Los Angeles Air Basin are required to submit annual emissions reports to the SCAQMD. This information is publicly available through the SCAQMD web-site. Since emissions of Toluene are not reported to the SCAQMD we also extracted data from the Toxic Release Inventory web-site of the US Environmental Protection Agency. Annual emissions for Tesoro Wilmington and INEOS polypropylene plant, both of which are near the FML, were not available

Table 2.1: Annual emissions (tons) of selected compounds reported by the refineries in Carson, CA

Facility	Pollutant ID/CAS	Pollutant	Annual Emissions 2012	Annual Emissions 2013
Tesoro Carson (formerly BP)				
	NOx	Nitrogen Oxides	650.402	698.164
	SOx	Sulfur Oxides	418.397	508.73
	CO	Carbon Monoxide	670.889	608.88
	50000	Formaldehyde	1.493	2.896
	71432	Benzene AQMD/EPA TRI	0.921 / 0.2125	0.814 / 1.906
	108883	Toluene AQMD/EPA TRI	NA / 0.043	NA / 2.84
Source:	http://www3.aqmd.gov/webappl/fim/prog/emission.aspx?fac_id=131003 http://oaspub.epa.gov/enviro/tris_control.tris_print?tris_id=90749RCPRD1801E			
Phillips 66 Carson				
	NOx	Nitrogen Oxides	332.584	335.592
	SOx	Sulfur Oxides	231.752	240.683
	CO	Carbon Monoxide	266.864	285.581
	50000	Formaldehyde	0.188	0.188
	71432	Benzene AQMD/EPA TRI	0.278 / 0.335	0.330 / 0.35
	108883	Toluene AQMD/EPA TRI	NA / 0.945	NA / 0.99
Source:	http://www3.aqmd.gov/webappl/fim/prog/emission.aspx?fac_id=171109 http://oaspub.epa.gov/enviro/tris_control.tris_print?tris_id=90745NCLCR1520E			
Valero Wilmington (formerly Ultramar)				
	NOx	Nitrogen Oxides	257.311	268.949
	SOx	Sulfur Oxides	144.477	146.518
	CO	Carbon Monoxide	102.152	116.699
	50000	Formaldehyde	1.010	1.154
	71432	Benzene AQMD/EPA TRI	0.382 / 0.046	0.532 / 0.0465
	108883	Toluene AQMD/EPA TRI	NA / 0.0785	NA / 0.108
Source:	http://www3.aqmd.gov/webappl/fim/prog/emission.aspx?fac_id=800026 http://oaspub.epa.gov/enviro/tris_control.tris_print?tris_id=90744HNTWY1651A			

3 Long Path Differential Optical Absorption Spectroscopy

Long Path Differential Optical Absorption Spectroscopy (LP-DOAS) is a powerful method for identifying and quantifying pollutants in the UV/visible spectral region using their unique narrow-band absorption features. Before describing the details of our work, we will review the principles of DOAS, as it applies to the instruments in this chapter as well as instruments in the following two chapters.

Originally we pursued a strategy based on AQMD's commercial OPSIS LP-DOAS system, which was already installed near the BP Refinery in Carson, CA. Our plan was to assess the quality of data produced by the OPSIS system, to develop the software tools to automate the system, remote control it, and to implement automated data analysis. The system then was to use a threshold value to send alarm emails to UCLA and AQMD in case elevated aromatic hydrocarbon levels were encountered. During our assessment of the OPSIS LP-DOAS system, we deemed it unusable for the measurement of aromatic hydrocarbons, and shifted our effort to developing our own LP-DOAS system for measurement of aromatic hydrocarbons.

The following sections describe the details of the new LP-DOAS instrument, its performance characteristics, and the first data acquired with this instrument. Please note that we will present our work with UV LP-DOAS to measure aromatic hydrocarbons in different section, as different observations were performed with different versions of our LP-DOAS system. Section 3.2 will describe the preliminary version of the instrument, while section 3.3 will show some of the results from the final version of the new instrument

3.1 Differential Optical Absorption Spectroscopy

DOAS is a well-established method to measure path-integrated trace gas absorptions and concentrations in the open atmosphere [*Platt and Stutz*, 2008]. The basis of DOAS is the identification and quantification of narrow-band absorptions in the UV-vis wavelength range along an open absorption path in the atmosphere (Figure 3.1). DOAS is based on Beer-Lambert's law:

$$I(\lambda) = I_0(\lambda) \times \exp\left(-\sum_j \sigma_j(\lambda) \times C_j \times L\right) \tag{3.1}$$

where $I(\lambda)$ is the intensity at wavelength λ, as observed by a spectrometer, $I_0(\lambda)$ is the intensity of the light sources, for example a lamp or the sun, σ_j is the molecular absorption cross section of trace gas j, and C_j is the concentration of trace gas j.

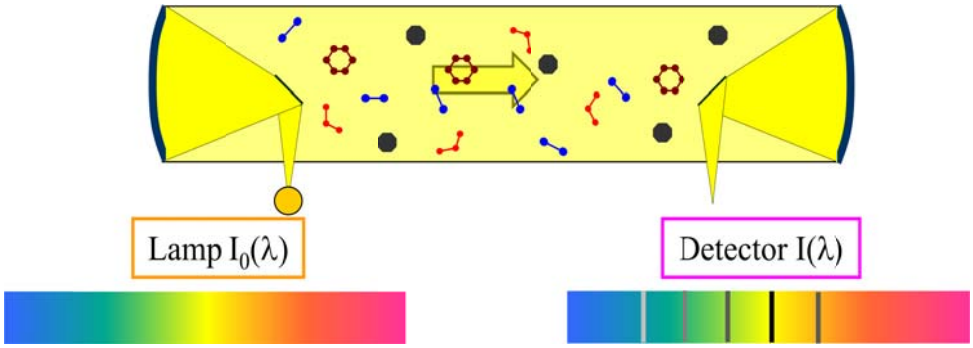

Figure 3.1: Principle of DOAS. Light from a sources, lamp or sun, undergoes intensity changes as it travels through the atmosphere before it is collected by a detector. Processes that can change the intensity are the absorption by trace gases, extinction by air molecules and aerosol, as well as turbulence.

Because many processes in the atmosphere, such as aerosols, turbulence, etc., can influence the intensity I(λ) the basic idea of DOAS is the separation of the narrow and broad band structures both for the absorption cross section and the intensity:

$$\sigma_j(\lambda) = \sigma_{j0}(\lambda) + \sigma'_j(\lambda) \qquad (3.2)$$

σ_{j0} in equation 3.2 varies 'slowly' with the wavelength λ, for instance describing a general 'slope', for example caused by Rayleigh and Mie scattering, while $\sigma'_j(\lambda)$ shows rapid variations with λ due to an absorption band. Beer-Lambert's law thus can be transformed with respect to a differential absorption cross section, $\sigma'_j(\lambda)$, and an intensity term that also includes all broadband features changing intensity, I'(λ):

$$I(\lambda) = I'_0(\lambda) \times \exp\left(-\sum_j \sigma'(\lambda)_j \times C_j \times L\right) \qquad (3.3)$$

Figure 3.2 shows examples of trace gases and their narrow band, i.e. differential, absorption structures in the UV-Visible wavelength range. These absorption cross sections are well known physical constants and uniquely identify and quantify each trace gas. Because the light path is in the open atmosphere, DOAS is commonly considered an absolute analytical technique, as it does not require calibration and is insensitive to interferences from other trace gases, aerosol/dust, or any sampling artifacts. Simply speaking, DOAS takes a "spectroscopic photograph" of the composition of the atmosphere.

The analysis of DOAS spectra is usually performed on the logarithm of the ratio of I(λ) and I'(λ), which is also known as optical density:

$$D'(\lambda) = \ln\frac{I'_0(\lambda)}{I(\lambda)} = L\sum_j \sigma_j'(\lambda) \times c_j \qquad (3.4)$$

Using a linear least squares fit approach that simulates D'(λ) using a linear combination, F(λ), of the various differential absorption cross sections, degraded to the instrument resolution, and a polynomial $P_n(\lambda)$, the trace gas concentration can be determined.

$$F(\lambda) = P_n(\lambda) \times \sum_j \sigma_j'(\lambda) \times a_j \qquad (3.5)$$

The fitting procedure returns the scaling factor which is proportional to the trace gas concentration and the path-length, $a_j = c_j \times L$. This column density can then be used directly, or converted to a concentration: $c_j = a_j / L$. It should be added that the fitting procedure also returns the error of a measurement, thus directly characterizing the uncertainty of the retrieved concentration. The details of the DOAS method and examples of its application have been recently published by the PI in a book [*Platt and Stutz*, 2008].

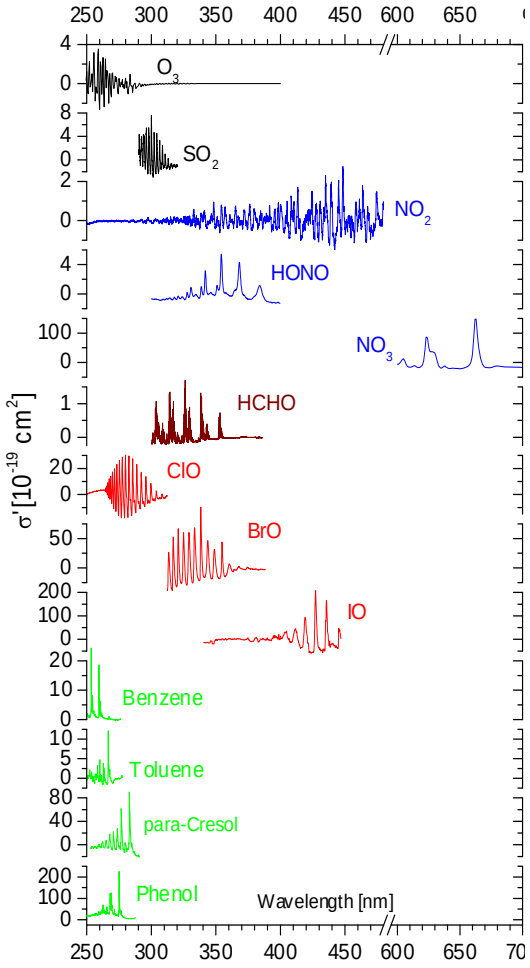

Figure 3.2: Examples of differential absorption cross-sections of various atmospheric trace gases observable by DOAS.

DOAS can be used in a variety of configurations using active light sources, i.e. lamps, and passive light sources, i.e. scattered sun light. In Active Long-Path DOAS, light from an artificial light source is collimated and sent through the open atmosphere and collected by a spectrometer-detector combination. This atmospheric absorption spectrum is then analyzed using the DOAS methods. In Passive DOAS, sunlight scattered by air molecules is used as the light source. Passive DOAS instruments measure a slant column density, SCD, i.e. the trace gas concentration integrated along the light path through the entire atmosphere. To eliminate the solar spectral structure, a spectrum is typically analyzed relative to a spectrum with lower trace gas SCD, often called solar reference, in the DOAS analysis. The results of this analysis are then reported as differential slant column densities: $DSCD = SCD - SCD_{reference}$. The passive DOAS approach is used in the I-DOAS and the dual MAX-DOAS measurements described in Chapters 4 and 5.

3.2 LP-DOAS Development Phase 1

After determining that the AQMD owned OPSIS system was unable to accurately measure aromatic hydrocarbons, we decided to use our own spectrometer and detector, and explore if we could use telescope and light source of the OPSIS system. Unfortunately we were unable to drive these components with our computer due to the proprietary and undocumented OPSIS hardware. Due to the limited resources in our original proposal we thus developed a test version of a new telescope-light source setup. Later in the project we were able to leverage our efforts through a grant from the Houston Advanced Research Center that allowed us to build a completely new sending-receiving telescope system. This final instrument will be described in Section 3.3.

3.2.1 Test-Instrument Description

For the test version of the new LP-DOAS system we retrofitted a commercial astronomical telescope, Celestron Astromaster, as a sending/receiving telescope and developed a small fully automated telescope mount. In order to make this new instrument more compact and increase long-term stability, we elected to use an UV LED as our light source. The LED also solves one of the major problems with LP-DOAS measurements of aromatics, stray light in the spectrometer-detector system. In short, the use of a classical XE-arc lamp introduces a large amount of light at wavelengths not used for the aromatics measurement into the spectrometer, i.e. light above 300nm. Some of this light bounces around in the spectrometer and negatively influences the spectroscopic measurements. We theorize that this problem may be the cause for the poor performance of the OPSIS system. The LED setup solves this problem, as LEDs only emit in the spectra region that is used for aromatic hydrocarbon measurements.

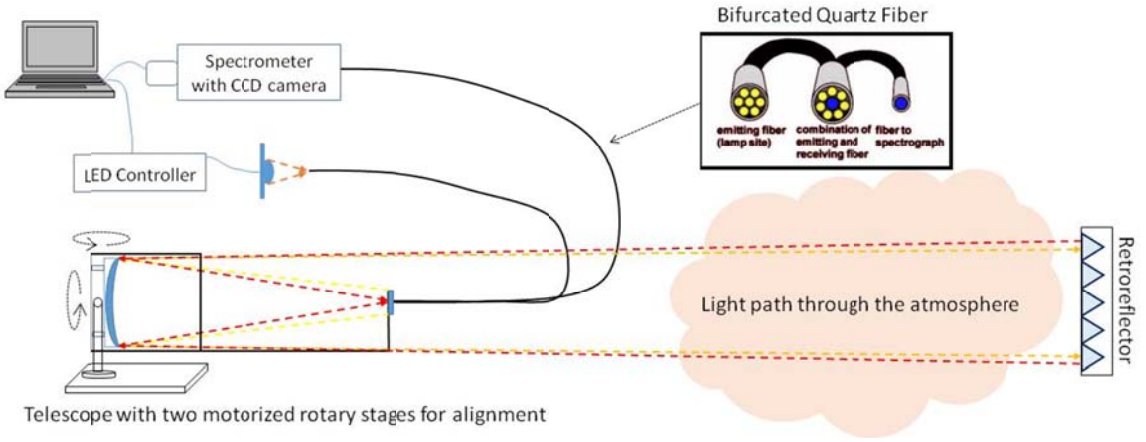

Figure 3.3: Sketch of the new UCLA Mini LP DOAS instrumental setup. The insert shows the ends of the bifurcated fiber – common end to the telescope, the fiber bundle to the light source, and receiving fiber to the spectrometer.

The new telescope setup (Figure 3.3) is based on the design by *Merten et al*. [2011], and uses a single fiber bundle that combines transmitting and receiving fibers at the focal plane of the telescope mirror. The telescope end of this bifurcated fiber consists of a single 300 µm fiber surrounded by seven 200 µm fibers. These fibers were distributed into two ends: the first ends in seven 200 µm fibers tightly packed into a 660 µm circle; the second end consists of the single 300 µm fiber (see insert in Figure 3.3). The seven 200 µm fibers bundle is used to transmit light from the LED light source and the single fiber is used to receive the light returning from the retroreflector into the grating spectrometer.

The test version LP-DOAS system (see Figure 3.4) consisted of components listed in the Table 3.1.

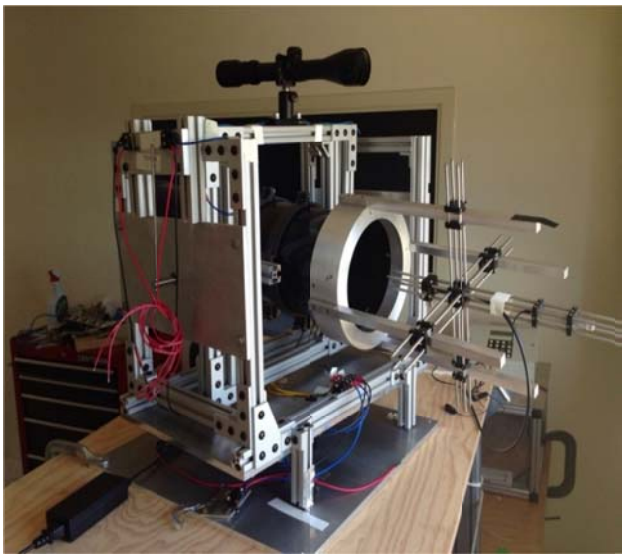

Figure 3.4: Photograph of the new UCLA Mini LP-DOAS system during testing at the Bunche Hall rooftop lab on UCLA campus.

Table 3.1: Components of the test version of the LP-DOAS system

Part	Component
Sending/receiving telescope	modified Celestron Astromaster 130 telescope (Figure 3.4) with custom build stepper motor based alignment system
Spectrometer	Acton 500 grating spectrometer, with measurements performed using 1800 g/mm holographic grating covering 50 nm range, with spectral resolution of ~0.3 nm
Detector	Princeton Instrument, PIXIS 256 CCD detector
Light source	265nm UV LED (see Figure 3.5 for LED spectrum) powered by Mightex high resolution LED driver
Reflector	Solid quartz corner cube reflector array mounted on light pole in 250m distance
Alignment Aids	- Camera to aid in alignment of telescope and to remotely check visibility - Green alignment laser – for initial on-retroreflector alignment - Green LED that can replace UV LED for alignment purposes
Computer / Software	Laptop Dell Latitude computer running DOASIS

The instrument is controlled by a laptop computer and is designed to run unattended for extended periods of time. This LP-DOAS system took measurements at the Carson FML site in from October to December, 2013.

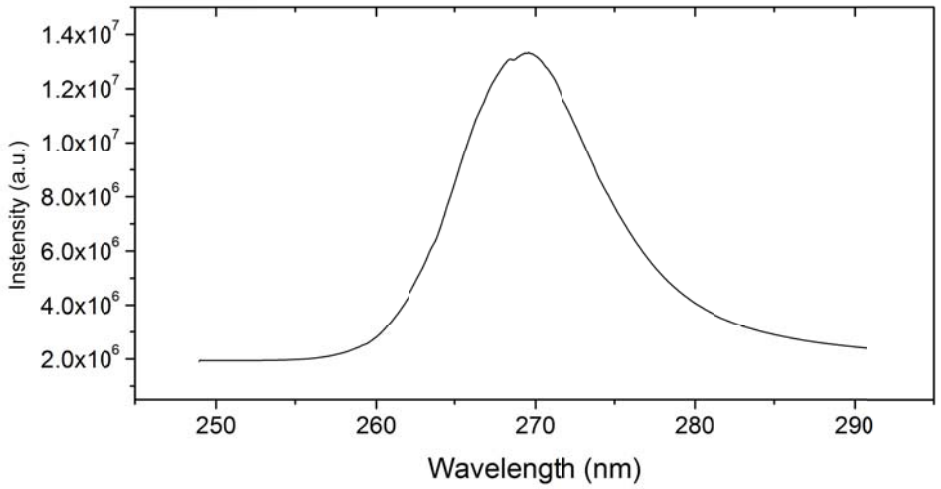

Figure 3.5: Spectrum of the 265 nm LED used as a light source for LP-DOAS instrument in Phase 1.

3.2.2 Operation of instrument

During these first measurements at the Carson fenceline monitoring site, the test version of the LP-DOAS system performed very well. The only difficulty we experienced with the instrument was the initial telescope alignment to the retroreflector. In order to assist with the alignment to the retroreflector, prior to transporting instrument to the FML, the LED light beam (invisible by the human eye) was aligned with the green alignment laser. The position of the green laser image on the retroreflector was recorded on the camera. However, after installation at the FML site the position of the green laser did not coincide with the LED beam. This was caused by the shift of the green alignment laser during transport of the instrument to the site. Therefore, in order to align to the retroreflector, we temporarily replaced the UV LED with a visible green LED. The light from this green LED was not strong enough to see during daylight, but could be seen during the night. Therefore, using this configuration, we were able to align the instrument to the retroreflector at night and begin LP-DOAS measurements. We have since found a better way to align the instrument, which will be described in Section 3.3.

In order to minimize signal-to-noise, we performed scans averaged over 10 minutes. However, we recently discovered that we have been using incorrect settings for the Mightex controller that is powering the LED. By adjusting the Mightex controller settings, we increased the LED output 10 times. Shorter integration times were thus used in Phase 2.

During the LP-DOAS Phase 1 deployment from October through December 2013, the instrument maintained a good alignment to the retroreflector. We only had to perform manual re-alignment to the retroreflector on average once every 2-3 days. It should be noted, however, that the retroreflector we used for this deployment was larger than the LP-DOAS light beam, and therefore slight changes in the beam position did not result in a misalignment. In the Phase 2 instrument, the alignment was fully automated and no manual alignment was required (Section 3.3).

3.2.3 LP-DOAS spectral retrievals

The LP-DOAS instrument measures absorption spectra in the open atmosphere along the fenceline light path. To derive the path-averaged concentrations a spectral retrieval that separates the various overlying absorption structures and quantifies each trace gas is needed. We therefore developed an analysis algorithm that is suitable for the measurement of aromatic hydrocarbons within this project. This spectral retrieval was performed using a combination of linear and non-linear least squares fits, as described in *Platt and Stutz*, [2008]. The wavelength interval between 263 and 269.5 nm was used for the spectral retrieval of toluene. In addition to the trace gas references outlined in Table 3.2, spectra of the LED light signature were included in the spectral retrieval. To allow for uncertainties in the grating position, spectral shift of trace gases during evaluation was allowed in the limits of +/- 2 pixels. During the evaluation, all trace gases were shifted and squeezed in wavelength with one single set of parameters, and spectral shift typically did not exceed 2 pixels. The statistical error of the fit was multiplied by a factor of three according to *Stutz and Platt* [1997] to yield the correct measurement error. It should be added that no calibration is necessary in this analysis. However, the uncertainties in the absorption cross sections, which are also listed in Table 3.2, introduce an additional, non-statistical, error that should be considered.

Figure 3.6 shows the result of a toluene spectral retrieval from the LP-DOAS spectrum recorded on 11/13/2013 at 11:34 UTC. The toluene mixing ratio was found to be 7.9 +/_ 0.4 ppb.

Table 3.2: Trace gas references used for LP-DOAS spectral analysis.

Trace gas	Reference	Uncertainties
O_2	*Fally et al.*, 2000	5 – 15%
O_2N_2	*Fally et al.*, 2000	5 – 15%
O_2O_2	*Fally et al.*, 2000	5 – 15%
O_3	*Voigt et al.*, 2001	5%
Toluene	*Fally et al.*, 2009	<8%
Benzene	*Fally et al.*, 2009	<8%
O-Xylene	*Fally et al.*, 2009	<8%
P-Xylene	*Fally et al.*, 2009	<8%
M-Xylene	*Fally et al.*, 2009	<8%

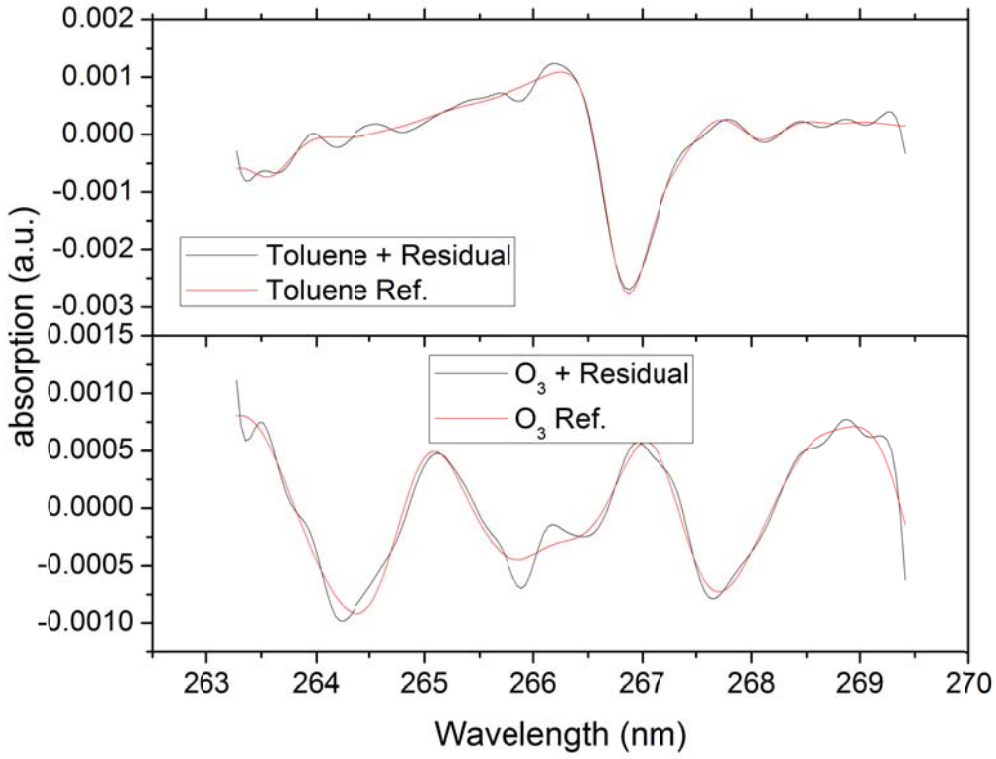

Figure 3.6: Example of a retrieval of O_3 and Toluene from the new UCLA LED LP-DOAS measurements taken in Carson, CA on 11/13/13 @11:34UTC.

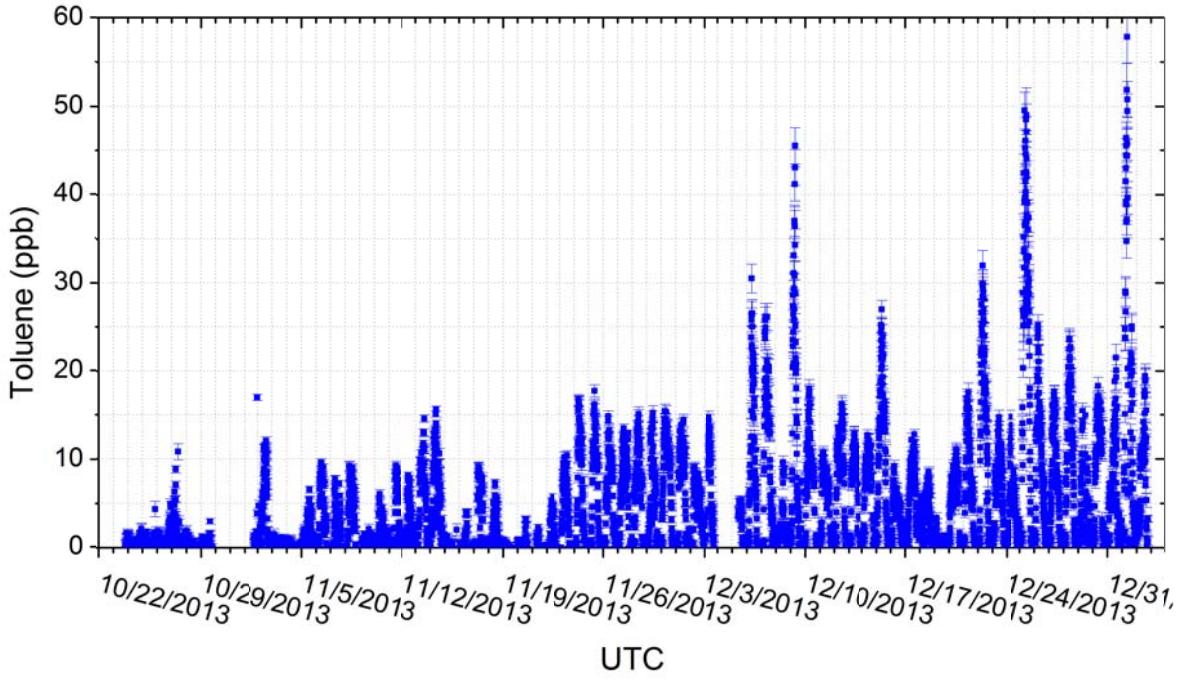

Figure 3.7: Toluene mixing ratios measured at the FML in Carson, CA by the phase 1 LP-DOAS instrument.

3.2.4 Results

The LP-DOAS observations at the Carson fenceline monitoring site began on October 22, 2013 and ended on January3, 2014. Due to the single LED setup only detection of toluene was possible, since the main absorptions of benzene are at shorter wavelength. Toluene was detected on many occasions above the instrument's average toluene detection limit of 0.8 ppb. Maximum toluene levels of 58 ppb were observed on November 01, 2013 at 08:35 UTC (00:35 local time). The majority of elevated levels of toluene were observed during the night-time hours, between midnight and 4 am. Only during a few days were elevated levels of toluene detected during the day – on December 17, 2013, around 8am, with a maximum of 15 ppb; December 25, around 9am local time with a maximum of 40 ppb; December 31, around 6am with the maximum of 22 ppb, and on January 01, 2014 around 10am local time, with a maximum of 25 ppb. No elevated toluene levels were detected on November 03, 09, 10, 15, 19; December 19, 24, 25 and 28. Figure 3.7 presents an overview of toluene measurements at the Carson fenceline monitoring site.

Figure 3.8 examines the relationship between toluene levels observed at the site and wind direction. Meteorological data was collected on the grounds of the Tesoro Carson refinery and provided by refinery personnel. During this time period, a very clear dependence between observed toluene concentrations and wind direction can be observed. Majority of the elevated toluene mixing ratios (above 4 ppb) were observed when winds were coming from the directions between azimuths of 270 and 75 degrees (west to north-east). The highest frequency of high toluene (up to 16 ppb) was observed when winds were coming from north-west, from the direction of northern part of the Carson Tesoro refinery. Frequently, elevated levels of toluene were also observed with the winds coming from the north and north-east. The Tesoro refinery expands to the north of the monitoring site; however the I405 freeway is in that direction as well. The INEOUS propylene plant is located north-east of the site, and behind it lays the I710 freeway. Some freeway tunnel (e.g. *Hwa et al.,* 2002; *Chiang et al*., 2007) and roadside emission (e.g. *Kawashima et al*., 2006) studies in Asia found toluene as one of the VOCs emitted from the on-road vehicles. However,

during the CalNex 2010 field study on the grounds of Caltech in Pasadena, CA, large toluene emissions associated with on-road vehicles were not observed.

In addition, observed toluene levels were rising and falling rapidly, which is more consistent with the source related to industrial operations than a constant source such as a freeway. In order to illustrate this point even further, we took a closer look to the timing of wind direction changes and observed toluene excursions. Figure 3.9 shows wind direction and toluene measured on November 13 through 15 2013 at the FML site. Starting from about 8:00 pm local time on 11/13/2013 toluene levels begun to increase, reaching a maximum of ~16 ppb at 3:00 am on 11/14/13. For the next few hours toluene mixing ratios declined to ~3 ppb at 5:30 am, followed by increase to ~9 ppb for the next few hours. During this time period winds were relatively consistently coming from north-western direction. At approximately 10 am on 11/14/23 winds began to shift and originated from the east. This wind shift coincided with the reduction in observed toluene levels. Between 2 pm and 8 pm on 11/14/13 winds shift again to the north-west, but no elevated toluene levels observed. Starting from 8 pm on 11/14/13 through 6 pm on 11/15/13, winds are from the east/south-east with no elevated toluene. If the I405 and I710 freeways were the source of observed toluene, one would expect to observe consistently elevated levels of toluene. However, our observations show changes in toluene mixing ratios while wind direction remained relatively stable. In addition, if observed toluene were a product of traffic emissions, one would expect to observe higher levels during the day, when there are more vehicles on the road, however, this was not the case (see example of the afternoon on November 14, 2013 in Figure 3.9). Differences in toluene levels observed during Phase 1 and Phase 2 (see section below) of the LP-DOAS experiment also point at source(s) other than the freeways as it is unlikely for traffic emissions to change drastically in 6 month. We therefore strongly suspect that freeways are not the main source of observed toluene, and conclude that moderately elevated levels of toluene observed when winds were coming from the north and north-east were more likely results of releases from units on the grounds of the refinery and/or the chemical plant located in that direction. On some occasions, elevated toluene levels were also observed when winds were coming from the south-west, where the southern part of the Tesoro Refinery as well as Phillips 66 Refinery are located, and therefore either could be suspected as a source of observed toluene. It should, however, be noted that no clear statement of the exact source for observed toluene can be made at this point in time.

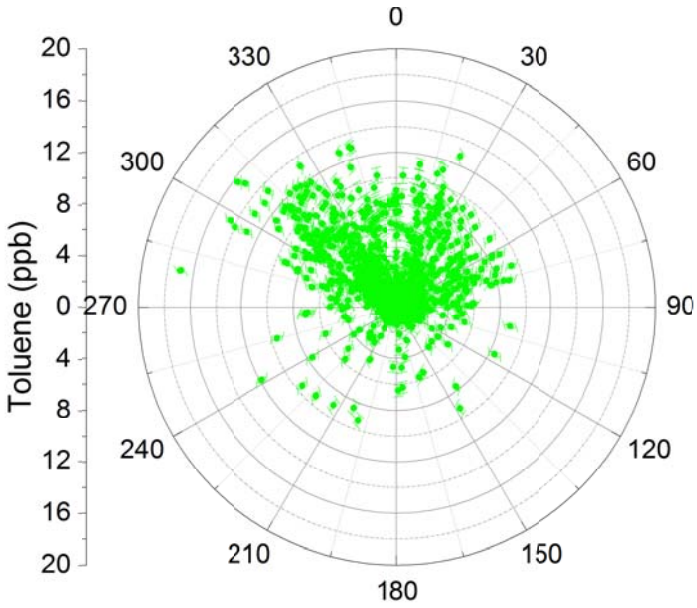

Figure 3.8: Wind rose of Toluene measured at the Carson fenceline monitoring site from October 24 to November 24, 2013.

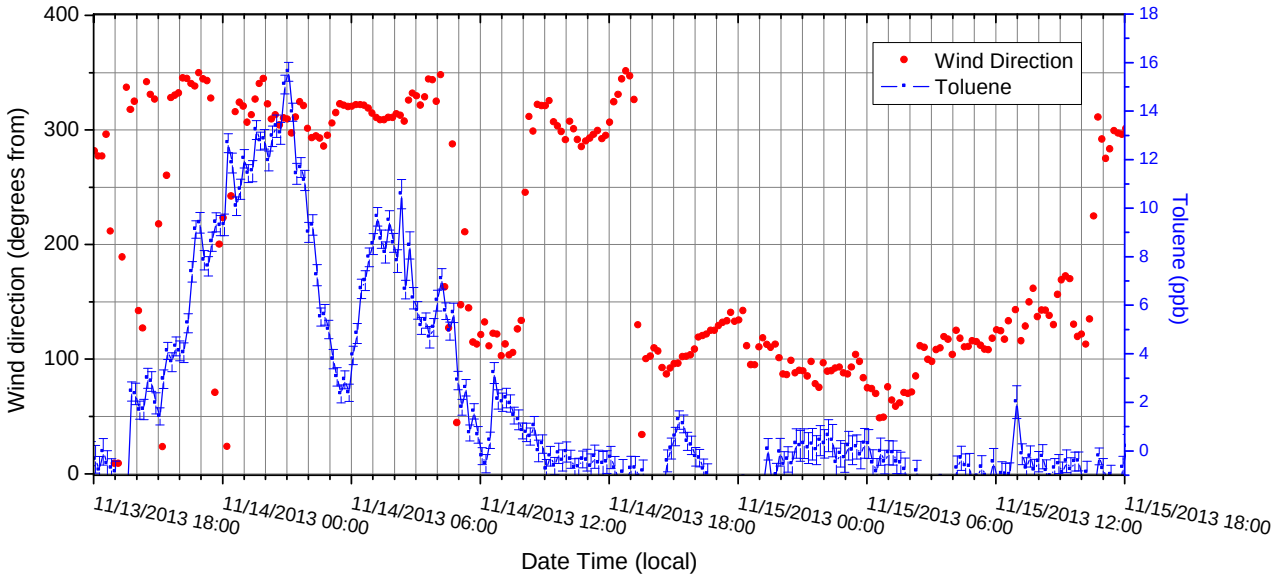

Figure 3.9: Wind direction and toluene mixing ratios measured at the FML site for two days in November 2013.

To further analyze our toluene observations with respect to the emission strength, we compared the LP-DOAS toluene observations with the CO_2 observations from the open-path FTIR co-located at the site (see Chapter 6 for details on the CO_2 measurements).

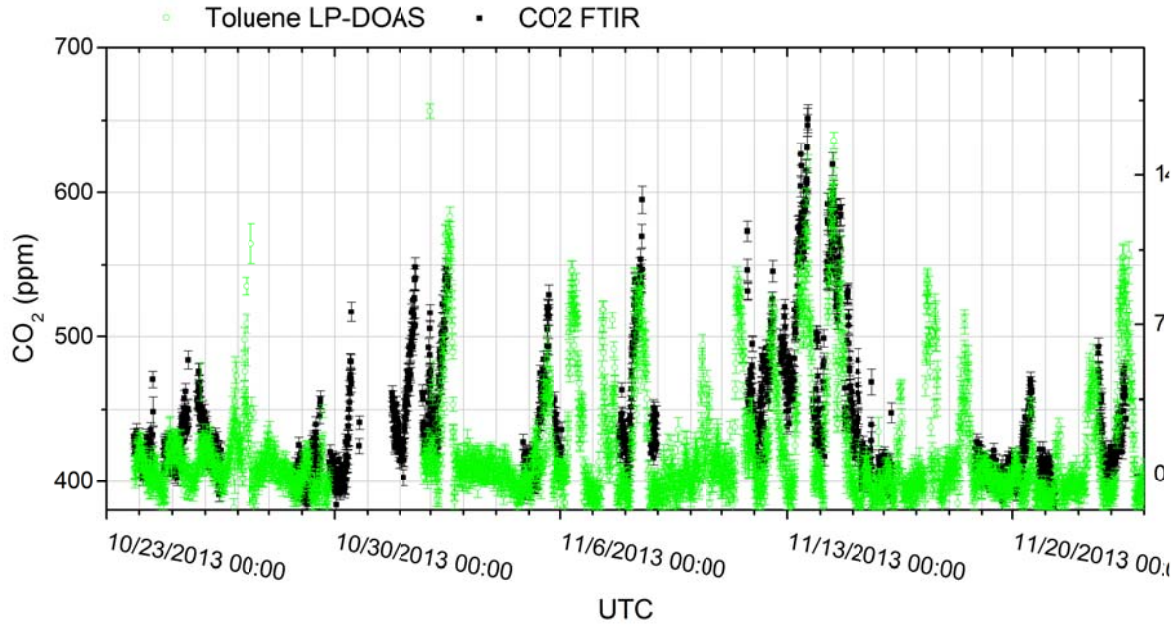

Figure 3.10: Toluene and CO_2 mixing ratios measured at the FML in Carson, CA by the UCLA Mini LP-DOAS and IMAC FTIR instrument respectively.

Figure 3.10 shows toluene and CO_2 concentrations measured at the FML. On many occasions, elevated levels of toluene coincided with elevated levels of CO_2. On November 15, 2013 three periods with elevated CO_2 were observed, only two of them were accompanied by elevated toluene levels. Because of the gaps in the FTIR data, it is unclear if there were instances of elevated toluene that were not accompanied by elevated CO_2. Figure 3.11 shows a very good correlation between CO_2 and toluene described by the linear relationship presented in Equation 1 with an R=0.80.

$$[Toluene] = -33.5\ ppb + 0.0783\ ppb/ppm \times [CO_2] \quad \text{with R=0.80} \qquad (3.6)$$

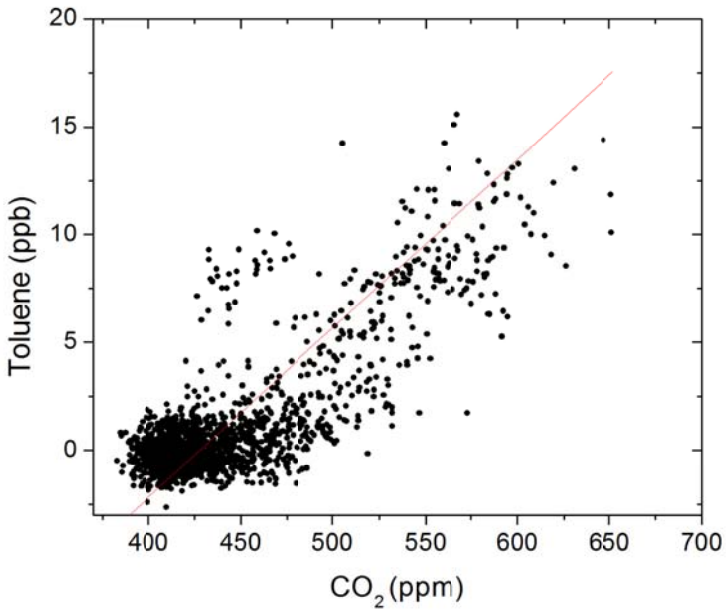

Figure 3.11: . Correlation between Toluene and CO_2 mixing ratios measured at the FML in Carson, CA.

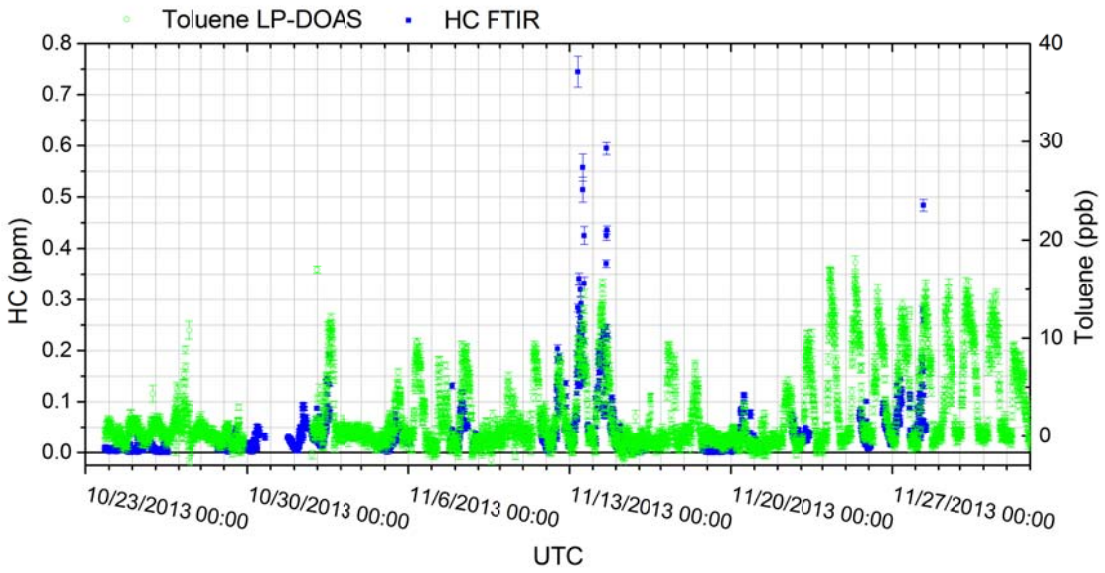

Figure 3.12: Toluene and hydrocarbon continuum (HC) mixing ratios measured at the fenceline monitoring laboratory in Carson, CA by the UCLA LP-DOAS and IMAC FTIR instrument, respectively.

A tight correlation between toluene and CO was also observed (see Figure 3.14, and Equation 3.7).

$$[Toluene] = -2.75\ ppb + 8.33\ ppb/ppm \times [CO] \qquad \text{with R=0.85} \qquad (3.7)$$

Since the refinery is likely the main source of CO_2 and CO near the monitoring site, It leads us to suspect that the observed toluene originates from the refinery.

A correlation between toluene and hydrocarbons measured by the IMACC FTIR was also observed. Figure 3.12 presents toluene and hydrocarbon continuum (HC) measured at the fenceline monitoring site. Figure 3.13 shows the correlation between these two species, which can be described by the linear relationship in Equation 3.7. This correlation, like the one with CO_2, is also very strong, except for a few instances when high levels of HC (up to 0.8 ppm) were observed at relatively moderate levels of toluene (between 7 and 12 ppb).

$$[Toluene] = -1.29\ ppb + 71.42\ ppb/ppm \times [HC] \qquad \text{with R=0.73} \qquad (3.7)$$

Overall, the various correlations give us confidence that the LP-DOAS is indeed measuring toluene emissions originating from refineries and/or other industrial facilities in the vicinity of FML. They also point to the potential of using co-located LP-DOAS and open-path FTIR to determine emission ratios, or even emission rates from an industrial facility.

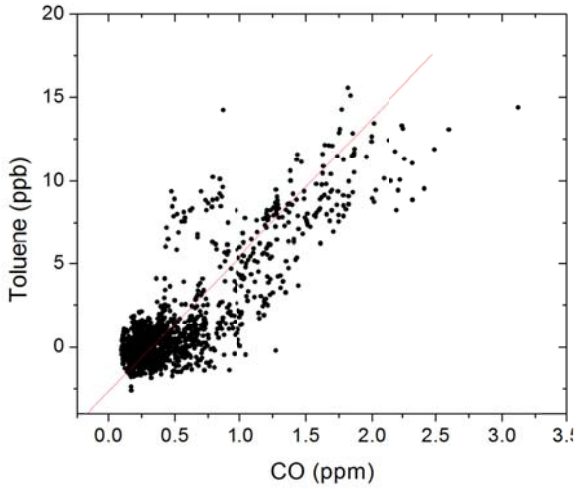

Figure 3.14: Correlation between Toluene and CO mixing ratios measured at the FML in Carson, CA

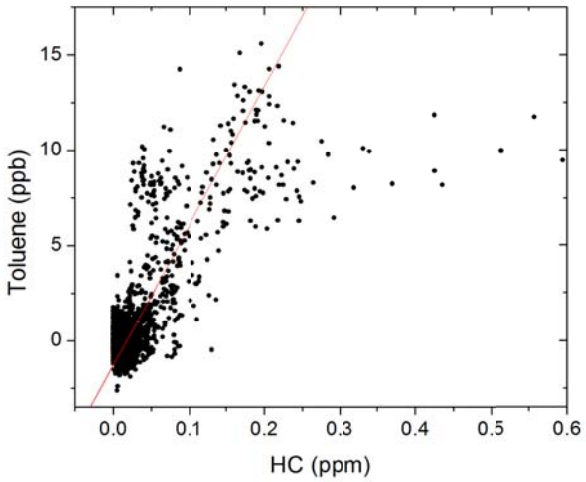

Figure 3.13: Correlation between Toluene and HC mixing ratios measured at the FML in Carson, CA

3.3 LP-DOAS Phase 2

After our initial measurements in Phase 1, we built the final version of the new LP-DOAS instrument. The equipment for this instrument was predominately financed through a grant from the Houston Advanced Research Center.

The final instrument follows the same general principle as the one described above (Figure 3.3), but has a larger and optically more sophisticated telescope (Figure 3.15). The telescope is mounted in a frame that can be rotated in the horizontal (+/- 170°) and vertical (+/- 10°) using high-precision rotation stages with stepper motors, thus allowing the computer controlled sequential use of multiple senders/reflectors and light paths. This setup, together with the updated software, is now also able to perform auto-alignments and, through the use of a camera as aiming scope, finding the retroreflector can now be achieved remotely. In addition, the LED emission spectrum can now also be measured automatically using a stepper motor controlled diffuser that rotates in front of the fiber. The new system combines two UV LED's into one light source. This allows the simultaneous measurement of benzene and toluene. In principle, it is possible to also measure xylene's and ethyl-benzene, but levels were low at Carson, so we will focus on benzene and toluene in this report. Table 3.3 gives an overview of the main characteristics of the new LP-DOAS instrument.

Table 3.3: Components of the final version of the LP-DOAS system

Part	Component
Sending/receiving telescope	Homebuilt telescope based on 120cm focal length, 12 inch diameter spherical main mirror. Rotation capability in azimuth and elevation using two high accuracy rotational stages. Automated short-cut system to measure LED emission spectrum.
Spectrometer	Acton 500 grating spectrometer, with measurements performed using 1800 g/mm holographic grating covering 50 nm range, with spectral resolution of ~0.3 nm
Detector	Princeton Instrument, PIXIS 256 CCD detector
Light source	Combination of 255nm and 265nm UV LED (see Figure 3.16 for LED spectrum) powered by Mightex high resolution LED driver
Reflector	Solid quartz corner cube reflector array in 250m distance
Alignment Aids	- Fully automated alignment capability, using UV LED and detector. Alignment frequency selectable, but typically every 1 - 4hours. - Camera to aid in alignment of telescope and to remotely check visibility
Computer / Software	Industrial PC running DOASIS. Connected to Dropbox folder via wireless modem for online backup. Data analysis can be performed on secondary computer at remote location.
Measurement Frequency	~60 seconds.
Detection Limits on 500m total light path	Benzene: ~ 0.6 ppb Toluene: ~ 0.45 ppb

Figure 3.15**:** Photos of the new UCLA long-path DOAS telescope at the FML in August 2013.

3.3.1 LP-DOAS spectral retrievals

Spectral retrievals were performed with the same methodology and absorption cross sections as described in Section 3.2.3. A wavelength interval from 252.5 – 260nm was used for the benzene retrievals. Figure 3.18 shows the clear identification of the benzene absorption structure at a mixing ratio of 4.3 ± 0.3 ppb in a measurement taken in Carson on 6/20/14 at 14:31 UTC. Similarly, Figure 3.17 shows the clear retrieval of 4.0 ± 0.3 ppb of toluene in the same spectrum. Detection limits determined from the error analysis of the retrievals, i.e. calculated based on all data are ~ 0.6 ppb for benzene and ~ 0.45 ppb for toluene. These detection limits are for a 60 second measurement frequency for a reflector array at 250m distance. Averaging of the data and longer light paths would improve these detection limits. A proposed EPA requirement for refineries to monitor fenceline benzene concentrations establishes a 2-week averaged benzene concentration action level of 3ppb (http://www.epa.gov/airtoxics/petref.html). The detection limits of the new LP-DOAS system are therefore sufficient for monitoring of fenceline benzene concentrations outlined in the rule. The system can be used by refineries as alternative method to verify compliance.

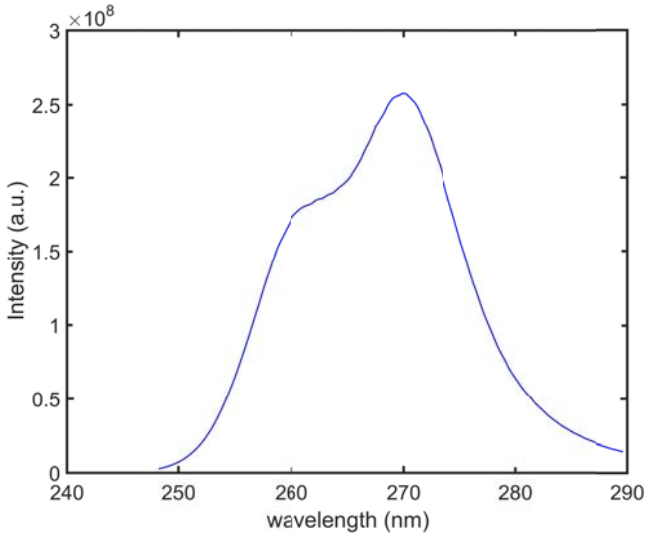

Figure 3.16: Light source spectrum of a combination of a 255nm and 265nm UV-LED. A comparison with the single LED spectrum in Figure 3.5 shows the expanded wavelength range towards shorter wavelength that allows the measurement of benzene.

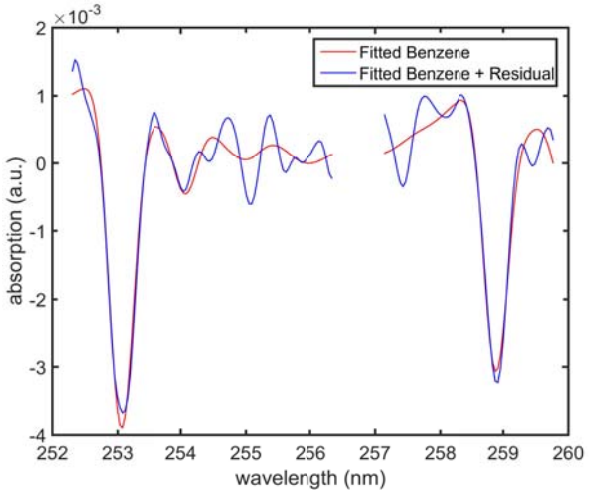

Figure 3.18: Example of a benzene spectral retrieval on 6/20/14 14:31 UT. The red curve shows the benzene reference spectrum, which is compared to the identified spectral structure in blue (retrieved benzene spectrum + unexplained structures of retrieval). The retrieval clearly identified 4.3 ± 0.3 ppb of benzene in the atmospheric spectrum.

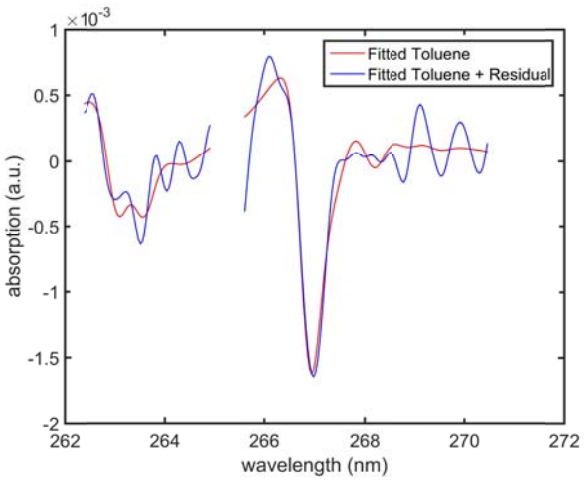

Figure 3.17: Example of a toluene spectral retrieval on 6/20/14 14:31 UT. The red curve shows the toluene reference spectrum, which is compared to the identified spectral structure in blue (retrieved toluene spectrum + unexplained structures of retrieval). The retrieval clearly identified 4.0 ± 0.3 ppb of toluene in the atmospheric spectrum.

3.3.2 Operation of instrument

We operated the instrument during a three month period from June to August 2014 at the FML. Figure 3.20 gives an overview of the data, showing that, except for three periods, the instrument operated continuously. The first two gaps in the data were caused by a power failure at the FML, while the third gap was caused by a broken uninterruptable power supply. The extent of the measurement gaps was determined by our access to the FML which is restricted to weekdays. During the three months no other instrument failures were encountered. Aside from the three gaps, no direct work on the instrument was needed. We conclude from this experience that is it realistic to operate the instrument with minimal human interaction, providing considerable cost-savings. In addition, in contrast to other methods of detection for aromatics, no consumables, except electricity, are needed to continuously operate the instrument.

The stability of the instrument, and in particular of the LED light sources, allowed us to use one single retrieval procedure for the entire 3 month period. This is quite important, as adjustments to the spectral retrieval procedure are time-consuming. Our experience indicates that, once the retrieval routine for an instrument has been established and tested after setup, it can be used for extended periods of time. In addition, the instrument does not require maintenance and the lifetime of the LEDs is quite long, so we do not expect that they need to be changed frequently.

While the data analysis shown here was performed off-line, we have also developed and tested the tools to perform near real-time analysis. Our approach was based on storing the measured absorption spectra on a directory on the measurement computer, which was synchronized with an online backup service. A second computer at UCLA performed the spectral retrieval as soon as the spectrum arrived, typically within 30-60 seconds after the measurement. This setup provides the additional advantage, that one can follow the operation of the instrument in real-time. It is also possible to locate the second computer with the instrument, or to run the analysis software on the instrument computer.

Finally, it should be noted that the detection limits of the new system are sufficient to distinguish background levels of benzene and toluene from even slightly elevated levels of these compounds from petrochemical facilities, as we will discuss in the next section.

3.3.3 Results

During Phase 2 of the LP-DOAS deployment we acquired a 3 month long dataset of concentrations of benzene, toluene and ozone mixing ratios at the fenceline of the Tesoro Carson refinery (Figure 3.20). As we did not have the OP-FTIR available during Phase 2, we relied on an UV-absorption ozone monitor (2B Technology) to provide a verification of the general behavior of our instrument via a comparison of O_3 mixing ratios measured by the two instruments. Figure 3.19 shows the close agreement of the two instruments during a six day period in June 2014. Ozone varied between 50 ppb and values close to zero. It shows the typical diurnal variation with low values at night, due to its reaction with NO, and higher values during the day, when the $NO\text{-}NO_2\text{-}O_3$ stationary state and photochemical ozone formation are active.

LP-DOAS benzene observations show a baseline of ~0.75 ppb, with frequent peaks of 3-4 ppb during the entire 3 month period (Figure 3.20). The toluene data shows a similar behavior, with a baseline of about 1 ppb and peaks of up to 4 ppb. Maximum toluene levels observed in June through September 2014 were generally lower those measured in October through December of 2013.

The reason for the observed benzene behavior becomes clear when the mixing ratios are compared to the wind direction (Figure 3.22). High benzene levels are associated with certain wind-directions between 300° and 120°, the general direction of the refinery, the chemical plant, tank farm, and/or other industrial operations located in these directions (Figure 3.21). In general, the benzene wind-rose agrees with the toluene wind-rose observed in Phase 1 (Figure 3.8), and the same arguments as described above apply.

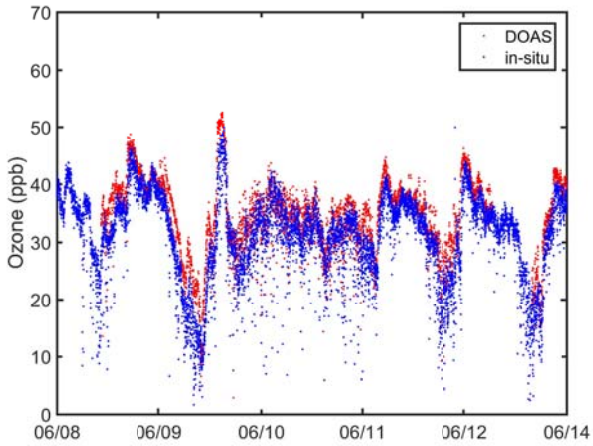

Figure 3.19: Comparison ozone measured by the LP-DOAS and an in-situ UV-absorption instrument.

It is quite surprising that the benzene mixing ratios do not exceed 4 ppb and that the maximum values appear to be highly reproducible throughout the 3 month period. While it is not

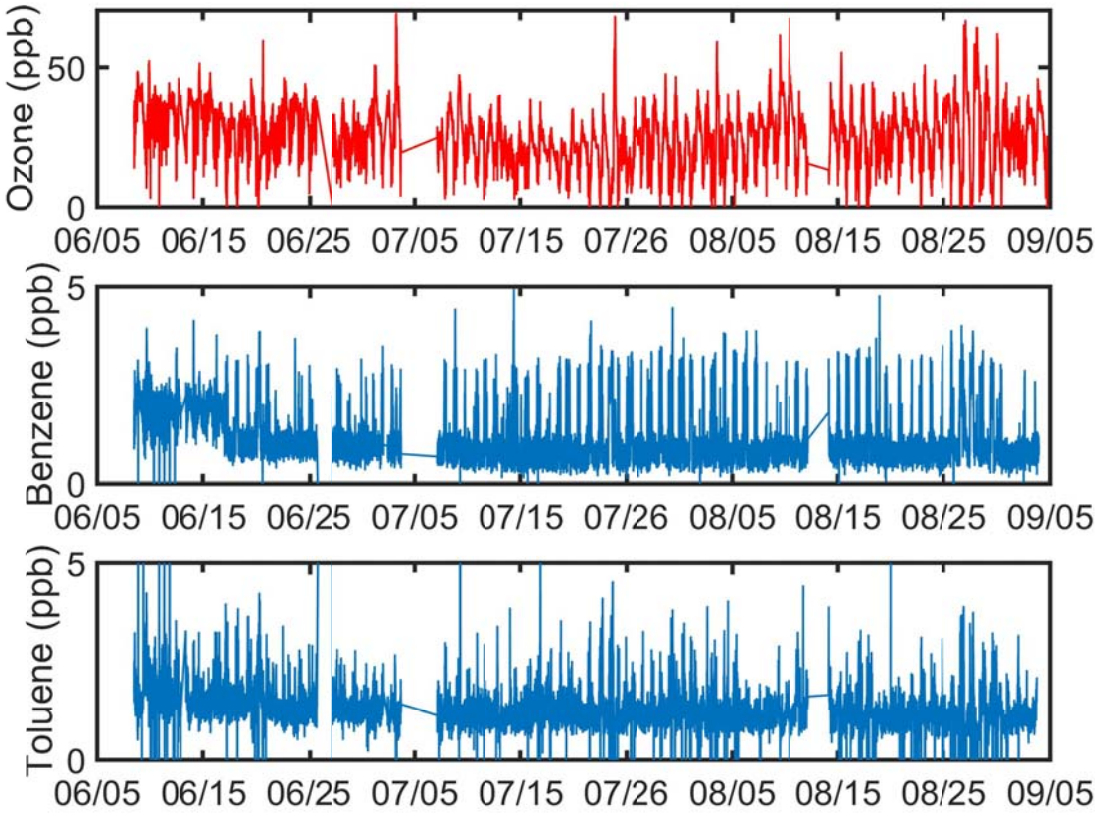

Figure 3.20: Overview of ozone, benzene, and toluene during the Phase 2 deployment at the FML in Carson. The gaps in data are due to power problems at the FML.

possible to unequivocally identify the refinery as the source of the benzene, the data suggests a relatively constant source, for example from fugitive emissions. To show that these emissions are from the refinery, a second upwind system would be required.

Our experience and observations during the second phase of the LP-DOAS deployment clearly show that it is possible to run such an instrument fully automated for an extended period of time. We do not anticipate that the behavior would change over longer deployment periods than were tested here.

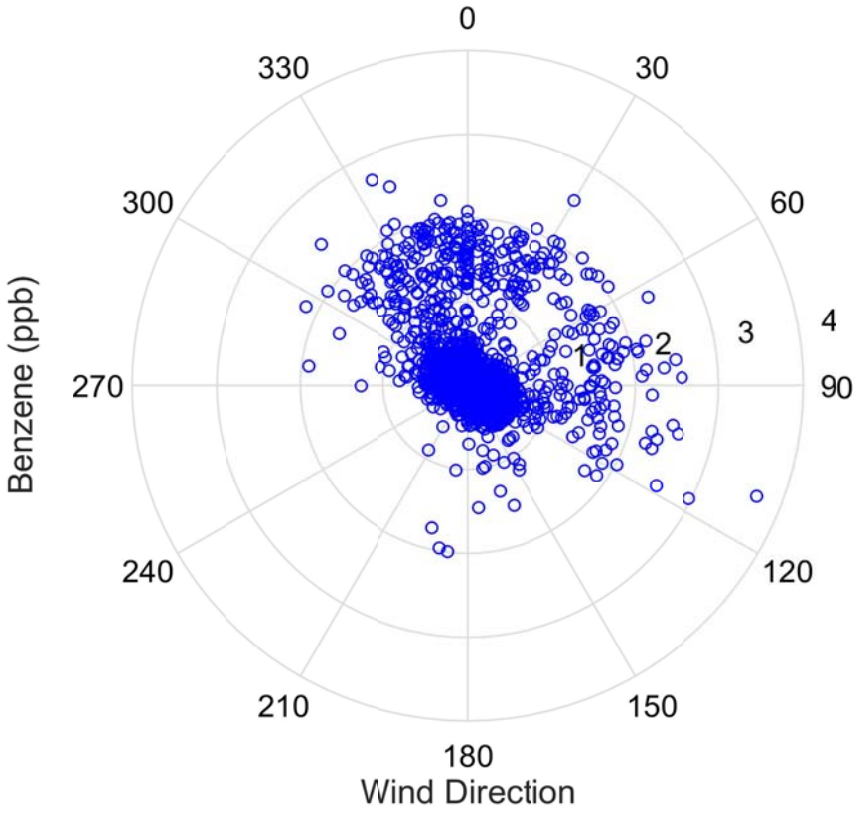

Figure 3.21: Windrose of benzene mixing ratios.

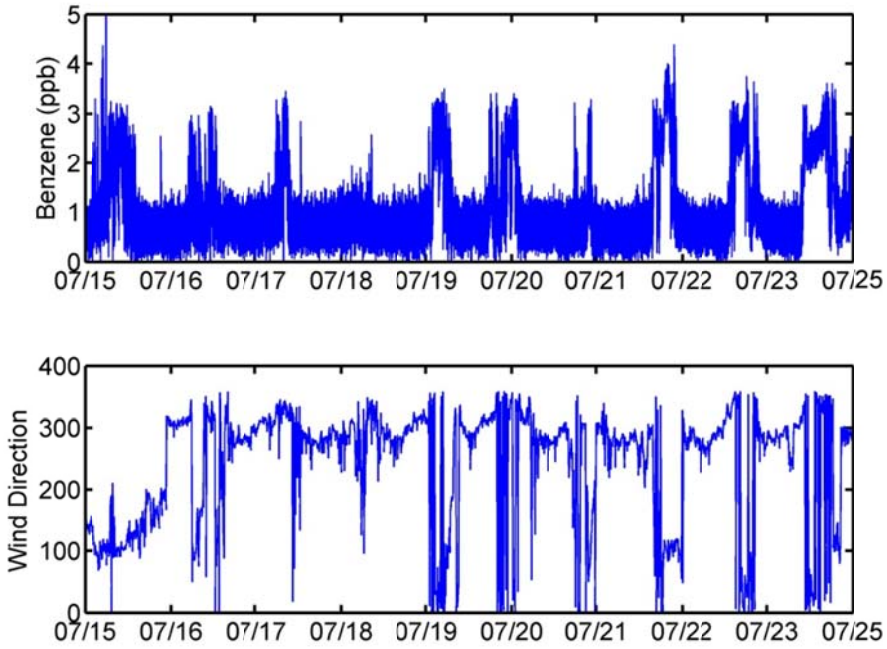

Figure 3.22: Example of 10 days of benzene and wind direction observations at the fenceline of the Carson Refinery. Elevated benzene levels are clearly correlated with wind direction, indicating an upwind source.

The performance of the instrument demonstrates that changes in benzene and toluene mixing ratios of around 0.5 ppb can be observed at a 1 minute time resolution. This is sufficient for fenceline monitoring of aromatic hydrocarbons. This system is not only capable of detecting large accidental releases, but can also be used for routine identification of small fugitive emissions. Small fugitive refinery emissions of aromatic hydrocarbons contribute to air pollution and chronic exposure of neighboring communities. Fugitives also represent a loss of product stream and therefore economic losses for refineries.

LP-DOAS system(s) can be operated to warn the refinery and the surrounding neighborhood about an accidental release within less than a minute after a measurement has been completed. Continuous LP-DOAS data can also be used by refineries to identify and correct sources of small fugitive emissions. While the detection limit of the LP-DOAS is sufficient to measure emissions from industrial sources at the fenceline, for measurements of emissions fluxes requires the use of at least two systems or other creative measurement setups, in order to characterize air masses upwind and downwind of a refinery.

4 Multi-Axis Differential Optical Absorption Spectroscopy

As a part of the remote sensing technology demonstration for SCAQMD, we proposed to develop and deploy two identical Multi-Axis DOAS (MAX-DOAS) instruments to be used for measurements of area-averaged fluxes of pollutants such as HCHO, NO_2 and SO_2. The setup for these measurements requires that one instrument is deployed upwind and the other downwind of the facility, as illustrated in Figure 4.1. Each instrument measures scattered sunlight at various viewing elevation angles, thus determining the number of trace gas molecules in a slice through the atmosphere using the DOAS method.

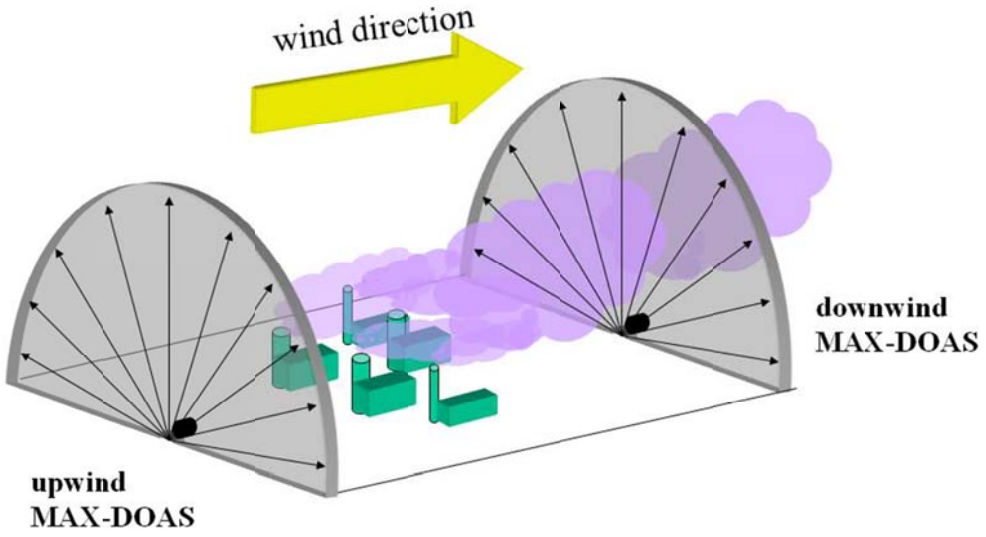

Figure 4.1: Experimental setup for area-wide emission measurements using the dual MAX-DOAS method.

To perform these flux measurements, two identical MAX-DOAS systems are required. We therefore constructed two instruments during this project. The MAX-DOAS instrument design and details of the spectral analysis are described in Section 4.1. Because of delays in obtaining the permits to deploy the upwind instrument, we divided the measurement aspect of the dual MAX-DOAS task into two phases. During Phase 1, one instrument was deployed at the FML and compared with in-situ measurements from a nearby monitoring station. The results from Phase 1 will be described in Section 4.2. During Phase 2, described in Section 4.3, the upwind instrument was also deployed and we were able to determine facility averaged fluxes.

4.1 MAX-DOAS Instrument Design and Development

The UCLA MAX-DOAS instruments consist of three main components:

1 - Telescope: containing light-collecting assembly in weatherproofed enclosure;

2 – Temperature-controlled enclosure containing the spectrometer/detector combination;

3 – Enclosure for electronics: containing all electronic components for temperature control and an industrial computer for data acquisition and storage.

The MAX-DOAS telescope must be placed outdoors with a clear line of sight towards the viewing direction(s). The spectrometer enclosure can be indoors or outdoors, while the electronics enclosure needs to be indoors. All cables, and the optical fiber connecting the three elements together, are 5m long, and can be arranged up to 5m away from each other. In order to fasten the MAX-DOAS telescope to a mast or platform in the field, an adapter must be designed once a location for the instrument is selected. For our deployment we used a holder that allowed deployment on a flat roof, using flat aluminum plated and aluminum tubing. Figure 4.2 shows the schematic layout of these components, and Figure 4.3 presents a photo of the telescope and spectrometer enclosure. Table 4. lists dimensions, weight and specifications of the UCLA MAX-DOAS instrument.

Table 4.1: MAX-DOAS component description and specifications.

Component	Dimensions (WxLxH), in	Weight, lb	Requirements	Notes
Telescope	4 x 20 x 6	10	Outdoors	Fiber to the Spectrometer Enclosure – 5m Cabling to the Electronics Enclosure – 5m
Spectrometer Enclosure	17.5 x 20 x 10	40	Outdoors or indoors	Cabling to the Electronics Enclosure – 5m
Electronics Enclosure	17.5 x 20 x 7	20	Indoors Requires one 115V AC outlet Maximum power consumption – 300 W Internet connection for remote access	

The controlling computer has both wired and wireless internet capabilities, thus allowing for remote control of the instrument, as well as data transfer. The instrument is also equipped with a web-cam, allowing for remote monitoring and documentation of cloudiness at the measurement site.

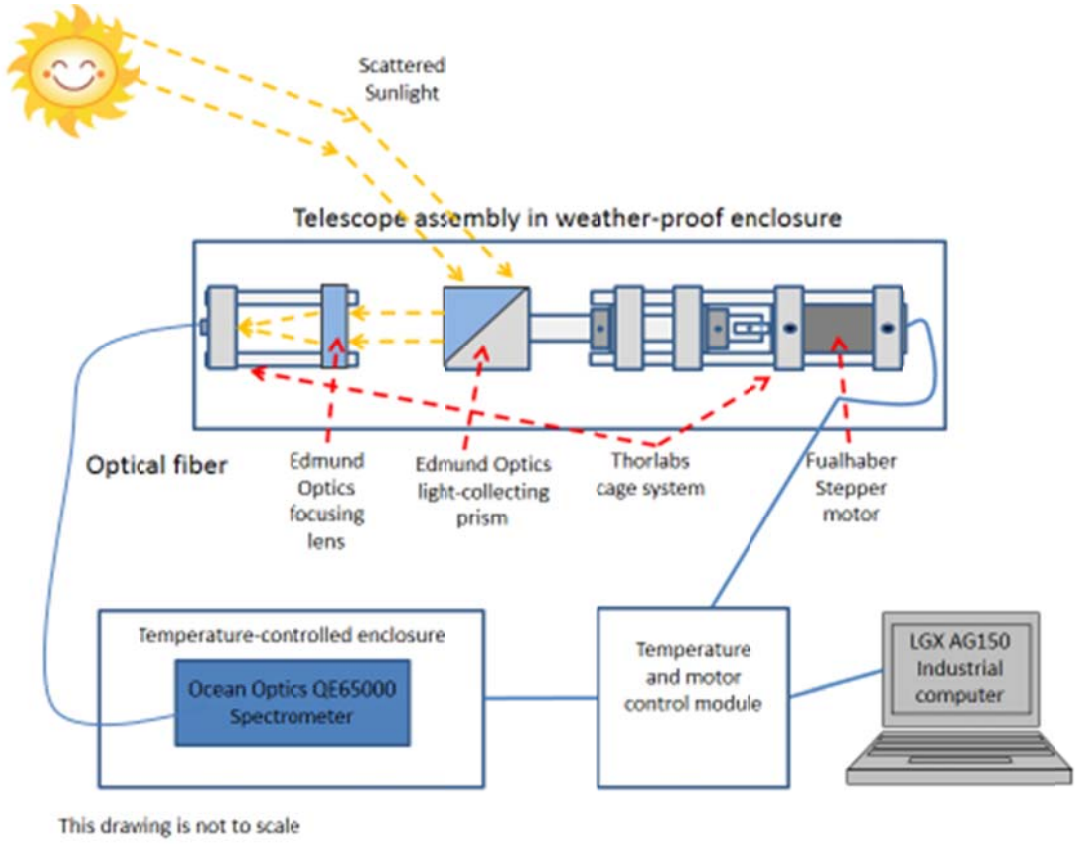

Figure 4.2: Schematic of UCLA MAX-DOAS instrument. Main components of the system are1 - MAX-DOAS telescope assembly; 2 – Temperature-controlled spectrometer enclosure; 3 – Temperature and motion control units enclosure. Drawing is not to scale.

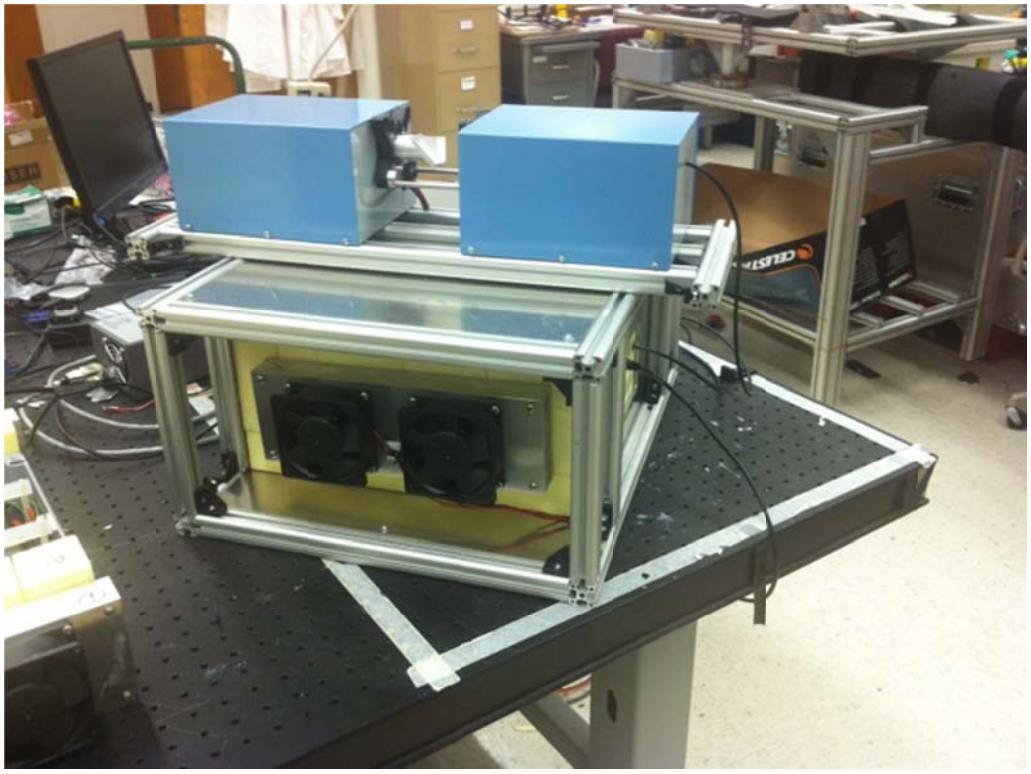

Figure 4.3:. Photograph of UCLA MAX-DOAS telescope (top, Component 1 in Figure 4.2) and spectrometer Temperature Control Enclosure (bottom, Component 2 in Figure 4.2).

4.1.1 Spectrometer and detector

In the original proposal to SCAQMD for the MAX-DOAS instrument development, we planned and budgeted for an Acton 150i spectrometer coupled with Apogee Alta U1107 camera equipped with the Hamamatsu back-illuminated CCD array, necessary for high sensitivity in the applications in UV spectral region. After detailed evaluation of a test version of this system, it was determined that the detector did not meet the requirements for the MAX-DOAS measurements.

We thus had to investigate other products available on the market that would satisfy our performance requirements and budgetary constraints. We settled for an Ocean Optics QE65000 spectrometer. This system was more costly than the Acton spectrometer/Apogee CCD detector combination, but still within the project budget. One advantage of using the Ocean Optics system was its small dimensions, thus making the MAX-DOAS system design more compact that initially planned. One large disadvantage of it, however, is that is it equipped with only one fixed grating, which can be set to only one wavelength range. The fact that we had to redesign the instruments and that the Ocean Optics spectrometers had to be sent back twice to the manufacturer for re-alignment and repair, lead to a delay in deploying the MAX-DOAS instruments, compared to the original proposal time line.

The Ocean Optics QE65000 spectrometers purchased for the MAX-DOAS instrument are equipped with H10 1800 g/mm holographic gratings and Hamamatsu S7031-1006 back thinned FFT CCD detector arrays. The gratings cover a spectral range of 115 nm, between 305 and 420 nm, with a spectral resolution of 0.6 nm. This spectral range allows for simultaneous detection of important pollutants such as SO_2, NO_2, and HCHO, as well as O_4, which is a proxy for radiative transfer conditions during the measurements.

4.1.2 Spectrometer temperature control enclosure

Spectrometer temperature stabilization is essential for long-term stability of MAX-DOAS measurements. For the dual MAX-DOAS setup, temperature stability is of even greater importance because the two systems must be as identical as possible. After a number of design iterations, we found a design that provided the desired 0.01 degrees temperature stabilization for the spectrometer.

The spectrometer temperature control system is schematically presented in **Error! Reference source not found.** and **Error! Reference source not found.** lists components used in this design. The spectrometer is maintained at slightly elevated temperature (24^{o}C) using a highly precise temperature control system. The heated spectrometer is insulated and then placed into a larger insulated temperature controlled box that is cooled to a temperature slightly below ambient temperature (18^{o}C). In such an arrangement, the cooled outer temperature control box "absorbs" any fluctuations in ambient temperature, therefore insuring complete temperature stability of the spectrometer.

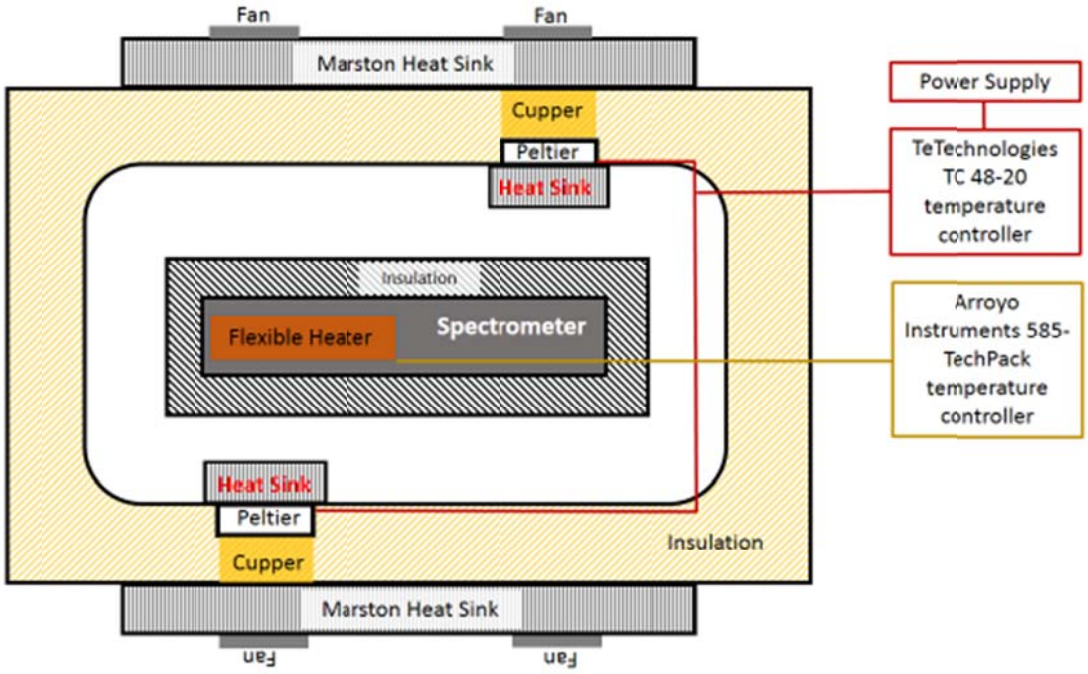

Figure 4.4: Schematics of the spectrometer temperature stabilization assembly.

The Ocean Optics QE65000 spectrometer is heated to 24^{o}C using a flexible heater attached to the bottom of the spectrometer. The flexible heater is controlled by an Arroyo Instruments high precision temperature controller. The spectrometer is encased in flexible 1/2"-thick insulation and placed inside the larger enclosure (Allied Electronics Aluminum die cast weather-proofed box), which is encased in 1.5"-thick Styrofoam insulation. The environment inside the cast aluminum box is cooled to 18^{o}C by means of two Peltier coolers (TETechnologies) placed at two opposite sides of the box. The Peltier coolers are attached to the outer walls of the aluminum box using thermal paste. The cold sides of Peltier coolers are facing the box. Small heat sinks manufactured by Cool Innovations are attached to the inner walls of the cooling box in order to facilitate heat transfer inside the box. The hot sides of the two Peltier coolers are

connected to a large Marston heat sinks through copper blocks. The Peltier coolers are connected in parallel to a 36V power supply and controlled by a TETechnologies controller. Heat transfer through the connecting surfaces (e.g. surfaces between Peltier elements and the box or between the hot side of the Peltier element and copper block, etc.) is enhanced by using thermal paste.

Table 4.2:. List of components for spectrometer temperature control

Component	Description	Part number
Spectrometer temperature control enclosure	Allied Electronics aluminum die cast weather-proofed box 11.02inX9.06inX4.37in	Type AL 2823-11 Cat. No. 150-015
2 cooling elements to cool the inside of the spectrometer enclosure	TETechnologies thermoelectric (Peltier) module	HP-199-1.4-1.5
Heat sinks for hot sides of peltier elements	HS Marston Ultra-Fin high density heat sinks	890SP-03000-A-100
Heat sinks for cold sides of peltier elements	Cool Innovations Splayed Aluminum Pin Fin Heat Sinks	3-202008P3M8815
Fans for Marston heat sinks	Papst DC axial fan 3300 series, 92mmX92mmX32mm	3312
Spectrometer Heating	Polyimide Film low voltage heater, 5W/in^2, with adhesive backing	Omega.com product #KHLV-103/5-P
Spectrometer heating control	Arroyo Instruments high precision temperature controller (allowing for 0.01^{o}C precision control)	TECPak 585
Cooling control	TETechnologies thermoelectric cooler temperature controller	TC-48-20
Cooling power supply	UGRACNC 36V, 11A, 400W power supply	400-36-11
T control box insulation	1-1/2” thick, Lightweight Polystyrene Foam Insulation High Density	McMaster Carr product # 9255K2
Spectrometer insulation	½” thick ultra-Flexible Foam Rubber Insulation	McMaster Carr product # 9349K2

4.1.3 MAX-DOAS telescope

The purpose of the MAX-DOAS telescope is to collect scattered sunlight and focus it onto an optical fiber, which then transfers the collected light to the spectrometer (Figure 4.2). For the purpose of the Dual MAX-DOAS experiment, scattered sunlight needs to be collected from a number of elevation viewing angles. We use a prism to collect scattered sunlight, and a quartz lens to focus the light onto an optical fiber. In order to point the prism to different elevation viewing directions, it is mounted to a computer-controlled miniature motor (see Figure 4.2). Table 4.1 lists all components of the MAX-DOAS telescope.

Table 4.1: List of components for MAX-DOAS telescope

Component	Description	Part number
Motor for prism rotation	Faulhaber 24 mm DC-Servomotor	2444V0055
Motor controller	Faulhaber Motion Controller	MCBL3006S
Focusing lens	25 mm Edmund Optics quartz lens	
Light collecting prism	Edmund Optics, quartz	
Edmund Optics 30mm cage system	Edmund Optics 30mm cage system	
Optical Fiber	Fiberoptic Systems custom made fiber bundle, 5m length	

4.1.4 MAX-DOAS Spectral Retrieval

The MAX-DOAS systems record spectra of scattered sunlight that need to be further processed to retrieve trace gas slant column densities. Spectral retrieval from the MAX-DOAS measurements in Carson was performed using a combination of a linear and non-linear least squares fits, as described in *Platt and Stutz*, [2008]. Wavelength intervals between 352 - 391 nm; 399 – 418 nm; 320 - 347 nm, and 310-331 nm were used for spectral retrieval of O_4, NO_2, HCHO, and SO_2 respectively. For HCHO, small intervals between 331 - 332, 334 – 336 and 340 - 341 nm were excluded from the fit. Table 4.2 presents the trace gas references used for spectral fitting and Table 4.3 lists the reference absorption cross sections used. In addition to the trace gas references outlined in Table 4.3, a temporally close zenith spectrum was included in the fit as solar Fraunhofer reference. Simulated Ring spectra of the solar reference scan, along with the linear and quadratic expansion of the Ring spectra [*Vountas et al*., 1998; Langford et al., 2007], were also fitted, as well as a polynomial to account for smooth changes in the spectrum. To allow for uncertainties in the grating position, a spectral shift and squeeze of trace gases during evaluation was allowed within the limit of +/- 2 pixels. During the evaluation, all trace gases were linked in shift and squeeze to each other, and spectral shift typically did not exceed 2 pixels.

Figure 4.5, Figure 4.6 and Figure 4.7 show examples of MAX-DOAS spectral retrieval for O_4, NO_2 and HCHO.

Table 4.2: MAX-DOAS Spectral Evaluation Information.

Species	Fitting window (nm)	Trace gas reference fitted	Degree of polynomial
HCHO	320 – 347 with intervals between 331 - 332, 334 - 336, 340 - 341 excluded	HCHO, NO_2, HONO, O_3	5
NO_2	399 - 418	NO_2, O_4,	3
SO_2	320 - 331	SO_2, NO_2, HCHO, O_3	4
O_4	352 - 391	O_4, NO2, HCHO, HONO	3

Table 4.3: Trace Gas References used for MAX-DOAS analysis.

Trace Gas	References	Uncertainties
HCHO	*Meller and Moorgat*, 2000	5%
NO_2	*Voigt et.al.*, 2002	4%
HONO	*Stutz et al.*, 2000	5%
O_4	*Hermans et al.*, 2011	10%
O_3	*Voigt et al.*, 2001	5%
SO_2	*Vandaele et al.*, 1994	5%

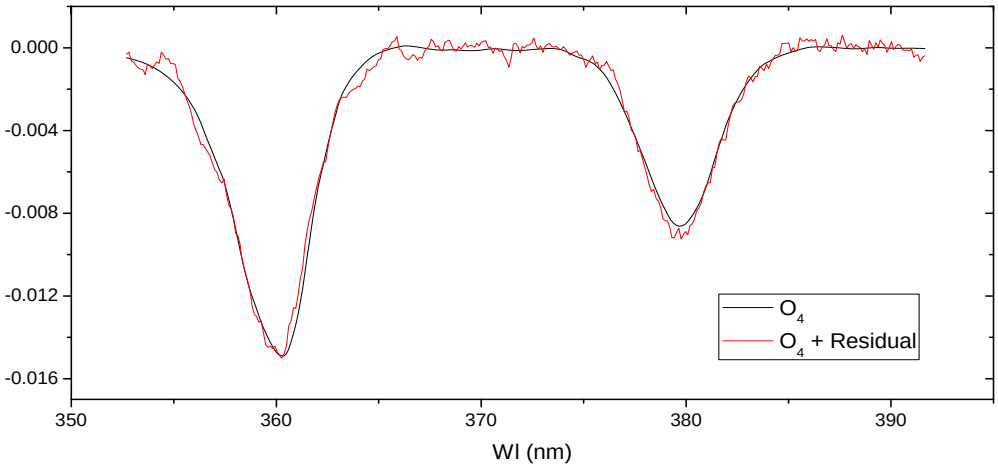

Figure 4.5: Example of O_4 spectral evaluation for 8° elevation viewing angle spectrum recorded on April 21, 2013 at 21:51 UT. The comparison of the pure O_4 absorption spectrum (black line) with the O_4 absorption spectrum retrieved from the atmospheric measurements (red line) shows the quality of the measurement. O_4 DSCD in this spectrum is 3.17 +/_ 0.10 x10^{43} molec^2/cm^5.

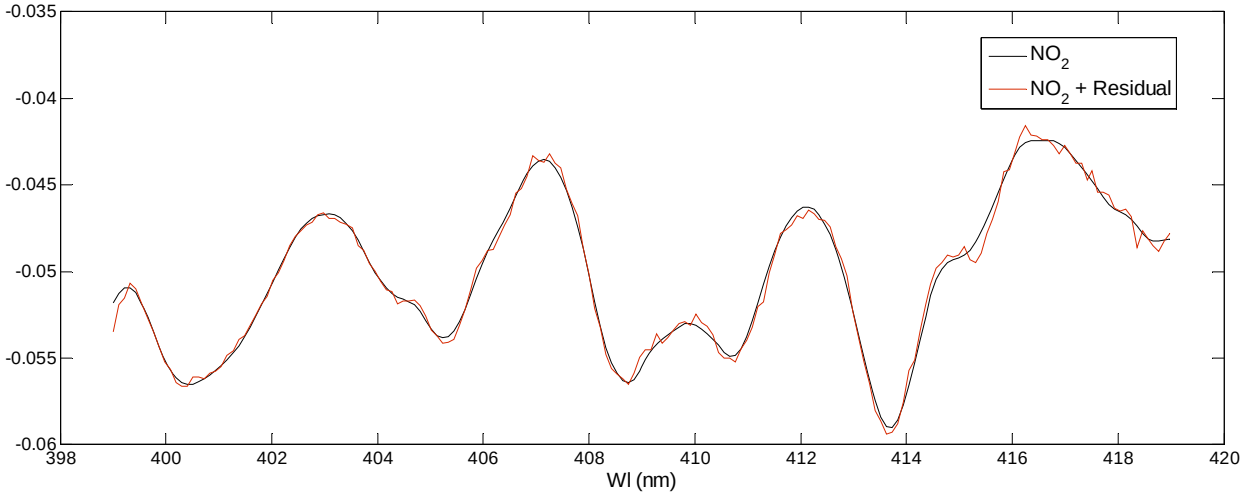

Figure 4.6: Example of NO_2 spectral evaluation on May 13, 2013 at 17:39UT. The comparison of the pure NO_2 absorption spectrum (black line) with the NO_2 absorption spectrum retrieved from the atmospheric measurements (red line) shows the quality of the measurement. NO_2 DSCD in this spectrum is 0.83 +/_ 0.02 x 10^{17} molec./cm^2.

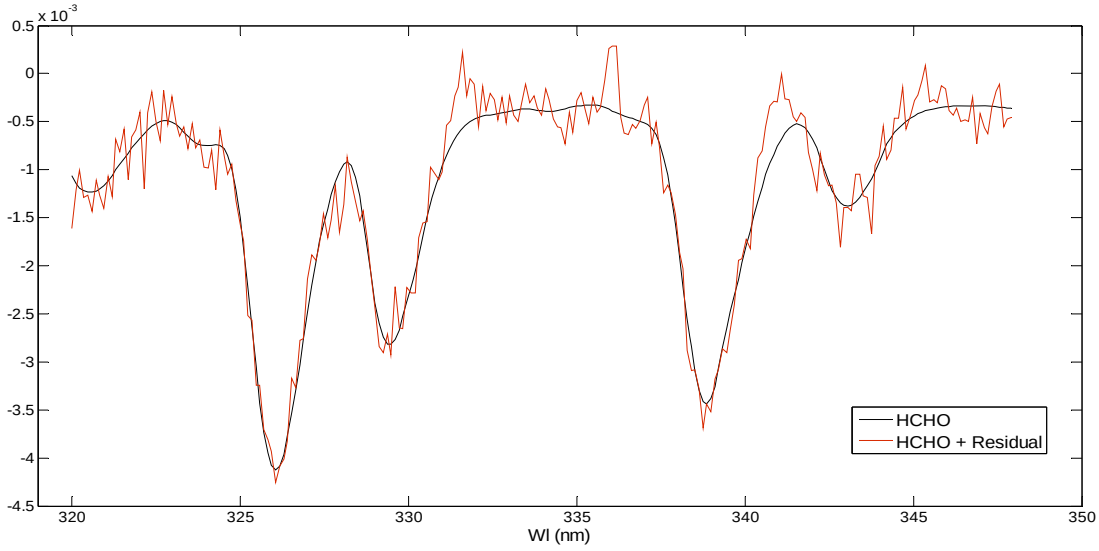

Figure 4.7: Example of HCHO spectral evaluation on May 13, 2013 at 15:13 UT. The comparison of the pure HCHO absorption spectrum (black line) with the HCHO absorption spectrum retrieved from the atmospheric measurements (red line) shows the quality of the measurement. HCHO DSCD in this spectrum is 0.23 +/_ 0.058 x 10^{17} molec/cm^2.

4.1.5 Timeline of MAX-DOAS measurements in Carson

On July 15, 2013, one of the MAX-DOAS instruments (designated AQMD2) was moved to the Fenceline Monitoring Laboratory (FML) in Carson, CA, which served as a downwind location for the dual MAX-DOAS experiment. Originally, Banning High School was selected for placement of the upwind MAX_DOAS instrument (designated AQMD2). In Spring of 2014, it became clear that permission from LAUSD will not be granted. After an extensive search of the area, we settled on the Port of Los Angeles Wilmington Community Monitoring Site on the grounds of the Saint Peter and Paul School (SPPS) in Wilmington, CA. Advantages of this location were availability of roof space for the MAX-DOAS telescope as well, as climate-controlled lab space for the instrument's spectrometer and controls enclosures. The site also provided stable power and security. However, this location is farther from the refinery fenceline than we desired, therefore increasing the likelihood of contributions from other non-refinery sources in the area. In June 2014, we received all necessary permits and executed agreements with the Port and SPPS for placement of MAX-DOAS instrument on the school's grounds. The instrument performed measurements at the site until October 03, 2014.

MAX-DOAS measurements for this project therefore had two distinct time periods:

Phase One: July 2013 – June 2014 – Single MAX-DOAS measurements with theAQMD2 unit at the FML

Phase Two: July 2014 – October 2014 – Dual MAX-DOAS measurements with both AQMD1 and AQMD2 units operating in concert at SPPS and the FML respectively.

In order to estimate area-averaged pollutant fluxes, the dual MAX-DOAS setup is required. However, nearly one-year of measurements of the single MAX-DOAS unit at the FLM provided a wealth of information that would be beneficial to explore. We therefore describe data and conclusions derived from both single and dual MAX-DOAS phases of operation below.

4.2 Phase One of MAX-DOAS measurements

4.2.1 Overview of single MAX-DOAS measurements at the FML

During Phase 1 of the MAX-DOAS experiment, all measurements were performed at the FML site. The MAX-DOAS instrument, designated AQMD2, was placed at the FML in July 2013, and has been continuously collecting data since that time. The telescope of the AQMD2 MAX-DOAS unit was placed on the roof of the FML, where it continuously collects scattered sunlight from 20 elevation viewing angles (1, 2, 3, 4, 5, 6, 7, 8, 9, 10, 12, 16, 20, 30, 40, 80, 85, and 90 degrees relative to the horizon) at the azimuth of 198 degrees (to the South). This viewing direction is parallel to the LP-DOAS and FTIR light paths, looking across the Dominguez Channel and "skimming" the eastern boundary of the Tesoro refinery (Figure 2.2). From the collected MAX-DOAS spectra, differential slant column densities (DSCD) - the number of molecules in a cm^2 column along an average photon path between the instrument and the sun - of NO_2, HCHO and O_4 are retrieved using the spectral fitting procedure described in section 4.1.4.

Figure 4.8, Figure 4.9 and Figure 4.100 show an overview of the measured DSCDs for O_4, NO_2, and HCHO, respectively. DSCD for NO_2 and HCHO are expressed in units of molecules/cm^2, because oxygen dimer is a product of two oxygen molecules, O_4 DSCDs are commonly reported in units of molec^2/cm^5. Periods of missing data are due to power outages at the site. Warmer colors represent lower elevation viewing angles of the measurements. During our measurements, SO_2 was often below the detection limit of 2.7×10^{16} molec/cm^2 of the MAX-DOAS instrument, and is thus not reported here.

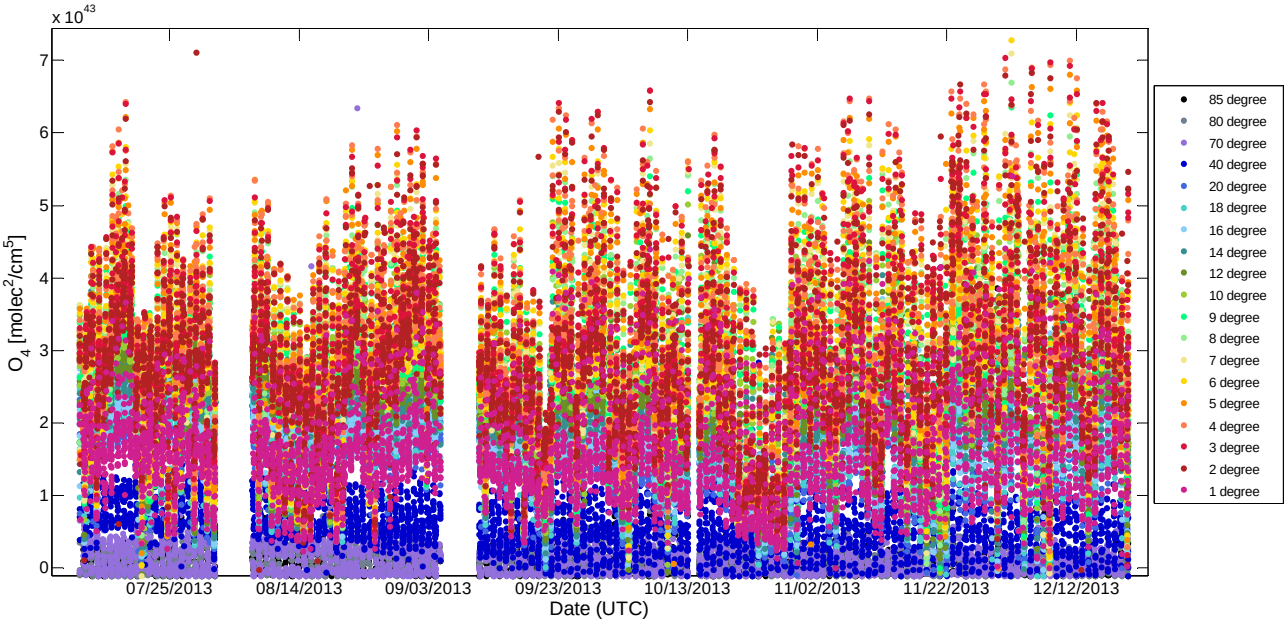

Figure 4.8: Overview of the O_4 DSCDs measured at the FML in Carson, CA. Warmer colors represent lower elevation viewing angles. Clear separation between elevation viewing angles can be observed during most days.

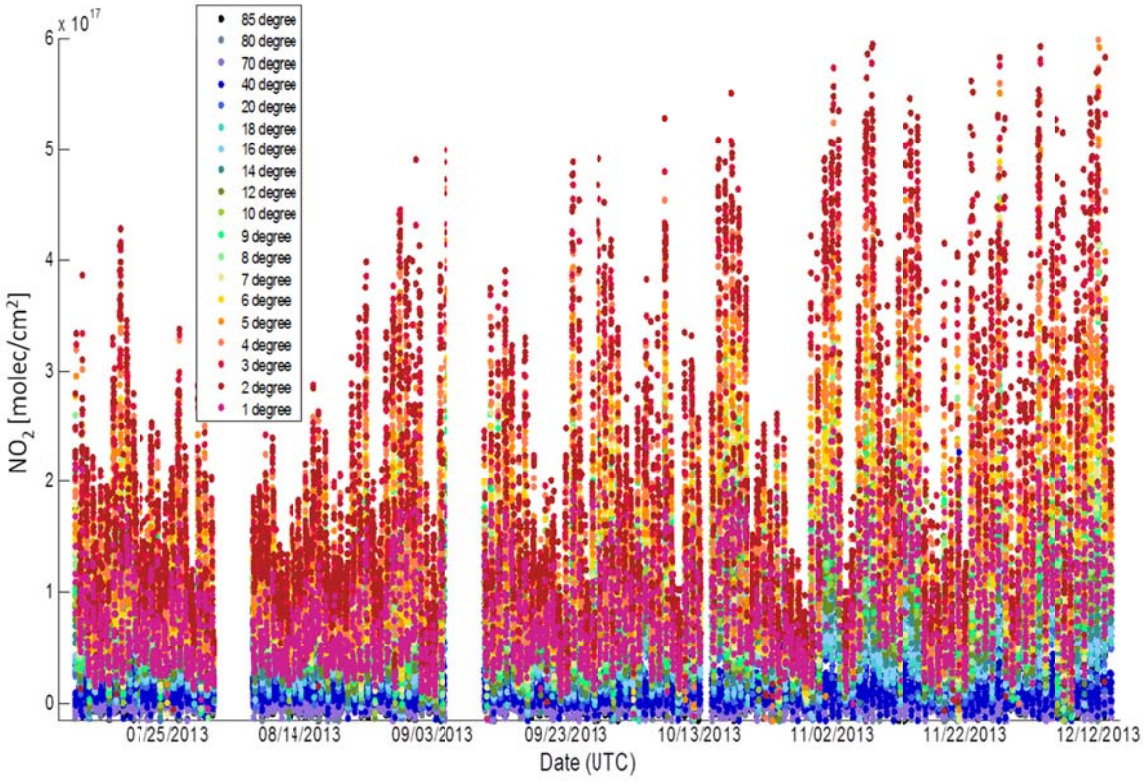

Figure 4.9: Overview of the NO_2 DSCDs measured at the FML in Carson, CA. Warmer colors represent lower elevation viewing angles.

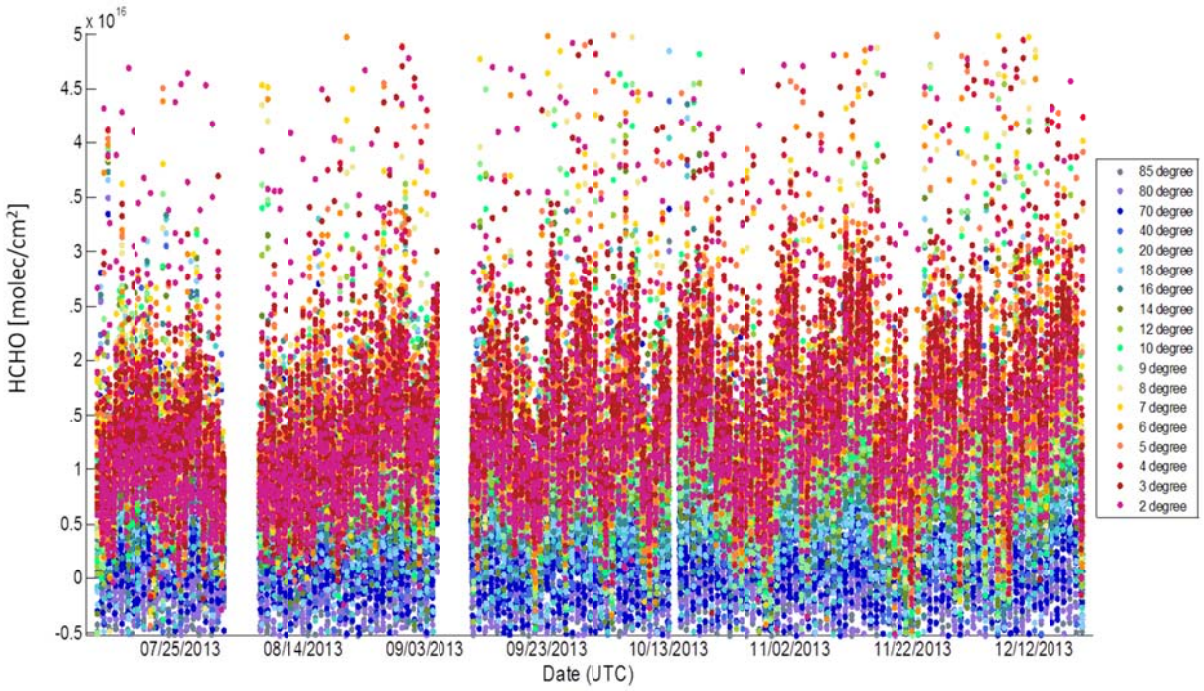

Figure 4.10: Overview of the HCHO DSCDs measured at the FML in Carson, CA. Warmer colors represent lower elevation viewing angles.

In all three figures (Figure 4.8, Figure 4.9 and Figure 4.10) lower elevation angles show higher DSCDs. The only exception is the lowest elevation viewing angle of 1^o, where measured DSCDs are significantly lower. This is most likely due to an obstacle on the line of sight of the instrument, which results in a reduction of the light path. Therefore, 1^o elevation viewing angles will be excluded from the future data analysis. For all other elevation viewing angles (2^o – 85^o), a clear separation between DSCDs is observed in the O_4 and NO_2 data, with slightly weaker separation for HCHO (see Section 4.2.2 for an explanation for the separation).

O_4 is a collisional complex of oxygen molecules in the atmosphere, and therefore is a function of atmospheric pressure and temperature only. For our experiment we can assume the O_4 atmospheric vertical profile remains constant in time and space. As a result, MAX-DOAS O_4 DSCDs can be used as a measure of radiative transfer (RT) conditions at the time of the observations. This then allows the retrieval of aerosol extinction profiles. But even simple visual examination and comparison of measured DSCDs of other trace gases with the O_4 DSCDs, can provide useful qualitative information about the trace gas vertical distribution.

For example, on August 21 – 23, 2013, O_4 DSCDs show a clear separation between elevation viewing angles, suggesting a clear day. During these days, NO_2 DSCDs also show good separation between elevation viewing angles, suggesting a fairly even vertical distribution of NO_2 in the boundary layer. At the same time, HCHO DSCDs exhibit slightly weaker dependence on the elevation viewing angles, which leads to the conclusion that HCHO along the MAX-DOAS lines of sight has a more complex spatial distribution. This statement is true for the entire dataset of MAX-DOAS observations collected in Carson thus far. This is partially due to the fact that RT conditions are different at the wavelength range of the HCHO retrieval, but spatial inhomogeneity of HCHO distribution may also play a role.

4.2.2 Boundary layer averaged concentration from MAX-DOAS measurements

While we could not estimate area-averaged fluxes using only one MAX-DOAS system, measurements from a single instrument still provided a wealth of valuable information. For example, we used collected MAX-DOAS data to determine boundary layer NO_2 and HCHO concentrations using the geometric air mass factors (AMF). In short, the AMF is a measure of the light path enhancement through the atmosphere compared to a vertical column, i.e. trace gas concentration integrated with altitude. The AMF is a function of observation geometry (elevation viewing angle) and radiative transfer conditions at the time of measurements. Normally, radiative transfer calculations are required to estimate AMF. However, for clear days with low aerosol load, AMFs can be estimated as $\frac{1}{\sin \alpha}$, where α is MAX-DOAS viewing elevation angle. Trace gas concentration of species C within the boundary layer can then be calculated using DSCDs measured at a certain elevation angle α ($DSCD^{\alpha}$), boundary layer height (BLH) and $\sin \alpha$ using Equation 4.1. Essentially, this approach assumes a geometric path-length through the boundary layer as described in Figure 4.11.

$$[C] = {}^{SCD_{\alpha}}/_{BLH \cdot \sin \alpha} \qquad (4.1)$$

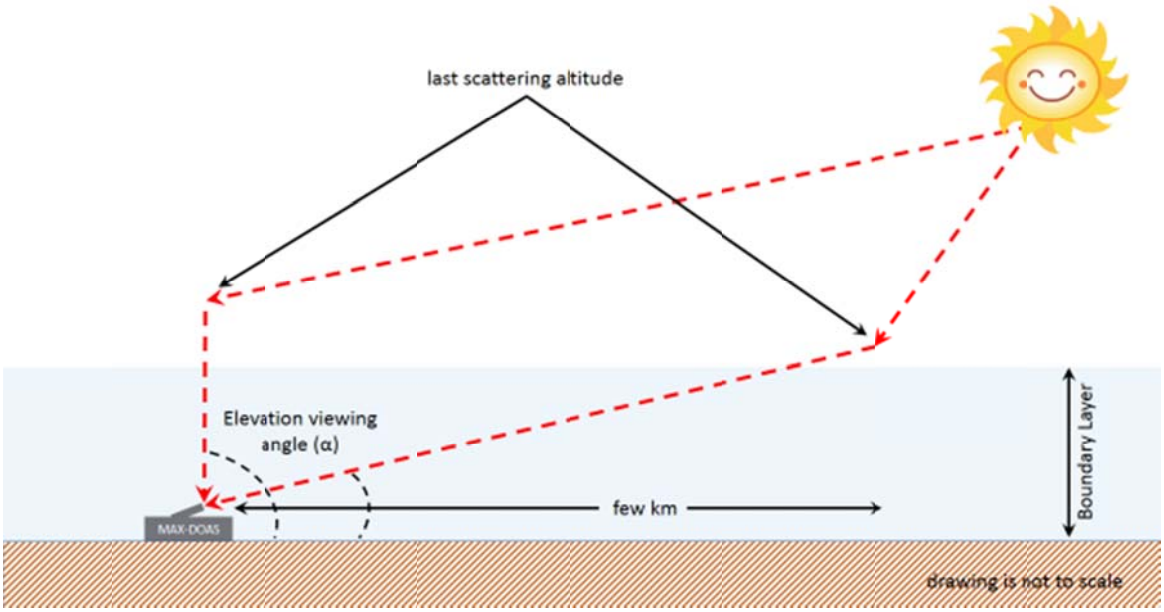

Figure 4.11:. Sketch of MAX-DOAS viewing geometry. For low elevation viewing angles, the last scattering altitude occurs at altitudes similar to the boundary layer height allowing application of a geometrical approximation for the air mass factor. Drawing is not to scale.

Our examination of the data for boundary layer heights in the vicinity of Carson (data from profiles at nearby airports (http://profilerops.sonomatechdata.com/map.jsp) revealed that boundary layer heights remained relatively unchanged throughout many days, with an average height of around 350 m. The boundary layer height of 350 m was thus used in our calculations.

Figure 4.12 shows NO_2 mixing ratios derived from the MAX-DOAS SCD measured at the 5° viewing elevation angle using a 350 m boundary layer height. The choice of the 5° elevation viewing angle was based on radiative transfer calculations. For this angle light can be assumed to have a straight path from the last scattering altitude to the instrument throughout the boundary layer (see Figure 4.11). For comparison, NO_2 data from the CARB North Long Beach station is also plotted. Observed NO_2 levels are similar, but do not always agree temporally. This may be a result of the placement of the two instruments, since they were not co-located. In addition, the two locations are also separated by two major freeways – I405 and I710. Therefore the discrepancies in NO_2 mixing ratios measured at the two sites can be attributed to additional emissions from freeways which, depending on the wind direction, can affect one site but not the other. Nevertheless, NO_2 mixing ratios measured at the North Long Beach monitoring station maintained by the SCAQMD, and those derived from the MAX-DOAS measurements, are in fairly good agreement. Figure 4.13 shows relationship between the NO_2 mixing ratios measured at FML and at the North Long Beach Site. The two datasets show a correlation with R values of 0.76. We believe that this is very good, considering differences in instrument locations and measurement techniques (MAX-DOAS is path-averaged method, while North Long Beach data is from in-situ measurement). This comparison therefore provides confidence that, for most of the time, geometric air mass factors can be used successfully to derive boundary layer averaged mixing ratios from MAX-DOAS observations

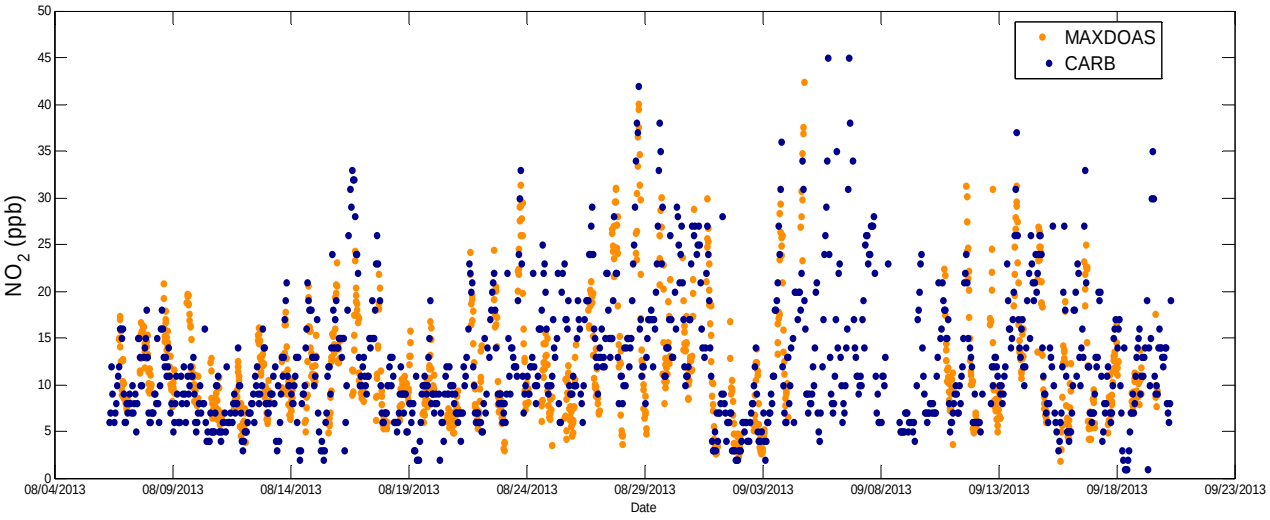

Figure 4.12: NO_2 mixing ratios retrieved using measured NO_2 DSCDs at an elevation viewing angle of 5° and geometric AMF approach; as well as NO_2 mixing ratios reported from the North Long Beach Station.

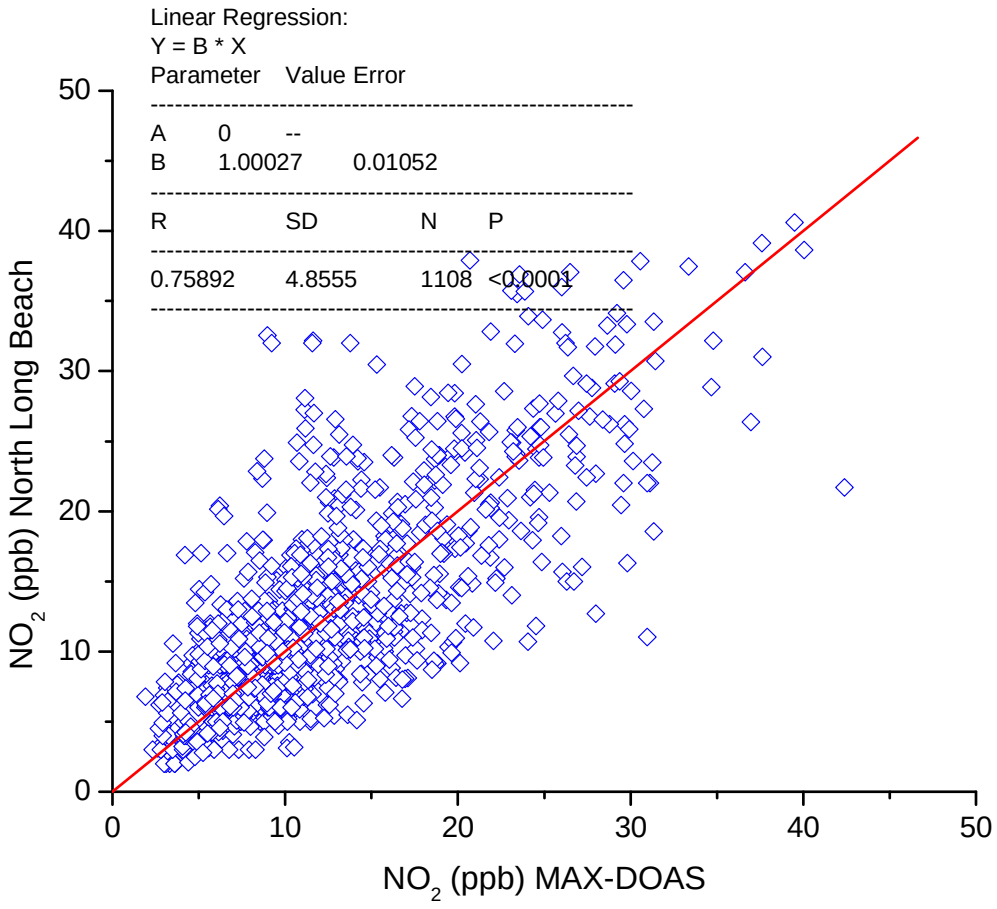

Figure 4.13. Correlation between NO_2 mixing ratios measured at the FLM using a MAX-DOAS instrument and those recorded at the North Long Beach monitoring station.

The same approach was applied to derive boundary layer averaged HCHO mixing ratios. Figure 4.14 presents the HCHO mixing ratios derived from HCHO DSCDs measured at the 5^o viewing elevation angle using the geometric AMF approximation. On average, daytime HCHO mixing ratios at the FML site ranged between 1 – 2 ppb, with occasional excursions of up to 7.5 ppb.

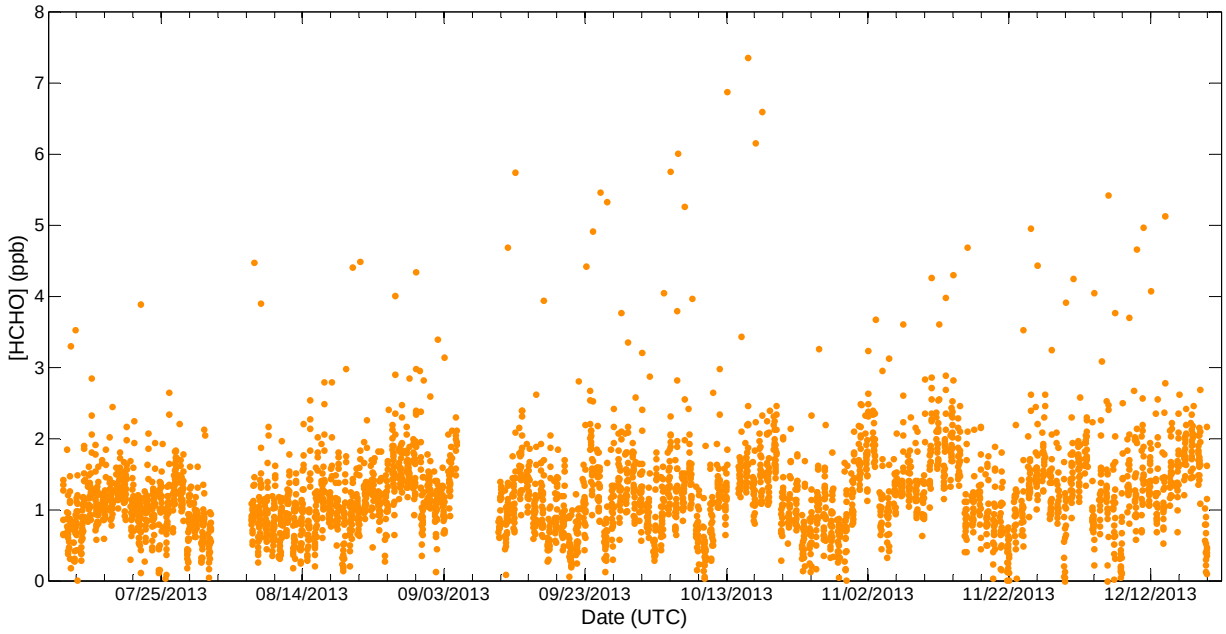

Figure 4.14: HCHO mixing ratios retrieved using measured HCHO DSCDs at a viewing elevation angle of 5^{o} using a geometric AMF approximation.

4.2.3 HCHO to NO_2 ratios

Since both HCHO and NO_2 spectral retrieval is possible from the same wavelength interval, MAX-DOAS data can be used to directly derive ratios between these two species. Derivation of such ratios for the area is important, as it can provide information on which emission reduction measures will result in a greater decrease in ozone. Ozone formation is controlled by complex interactions between nitrogen oxides (NOx) and volatile organic compounds (VOCs). Reduction in VOCs or NOx can result in various degrees of reduction of ozone production, depending on which species are in excess. These conditions are often referred to as NOx- or VOC-limited photochemical regimes. According to *Sillman* [1995] HCHO can be used as a proxy for VOC reactivity, and ratios of $HCHO/NO_2$ have been used to determine the photochemical regime. A study by *Duncan et al.* [2010], using tropospheric NO_2 and HCHO columns from OMI measurements, showed that at $HCHO/NO_2 < 1$, instantaneous ozone production rate (PO_3) decreases with reduction of VOCs, and at $HCHO/NO_2 > 2$, NO_2 reduction will lead to reduction in PO_3. The regime between 1 and 2 is a transitional regime.

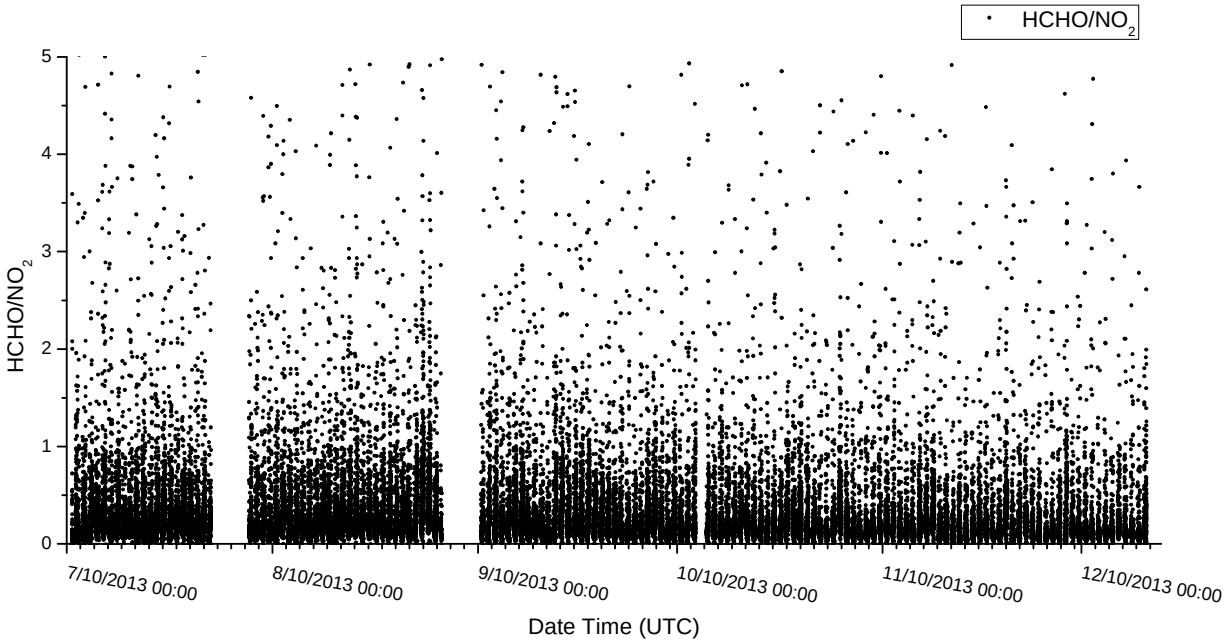

Figure 4.15:HCHO/NO_2 ratios for all MAX-DOAS data collected at the Carson fenceline monitoring laboratory.

Figure 4.15 presents HCHO/NO_2 ratios calculated for the entire MAX-DOAS dataset collected at the Carson fenceline monitoring site, including all elevation viewing angles. This overview graph shows that, for a large portion of the data collected, the ratio is below 1, and therefore in the VOC-limited regime. There are still a significant number of data points in the intermediate (ratio between 1 and 2), and a small fraction is in the NOx-limited regime (ratio above 2).

It is important to keep in mind that different elevation viewing angles "probe" different parts of the troposphere, therefore allowing for differentiation between the boundary layer and the rest of the troposphere. In order to isolate these differences we examined the HCHO/NO_2 ratio for individual viewing elevation angles. Figure 4.16 and Figure 4.17 present the ratio for viewing elevation angles of 5° and 40° respectively. The 5° elevation angle direction is more representative of the boundary layer, while the 40° angle probes a larger altitude interval in the troposphere, i.e. up to around 5-7km altitude (this assessment is based on radiative transfer calculations for an atmosphere with urban aerosol, which were conducted by our group prior to measurements in Carson). For the 5° elevation angle the majority of values are below 0.6, with an average ratio value of 0.12, and only a hand-full of data points that are between 1 and 2. This low HCHO/NO_2 ratio observed in Carson may be an indication that this area is in the VOC-limited regime for ozone formation rates. For the 40° elevation angle most of the data is still below 1, but there is a greater portion that is between 1 and 2, and some number of points above 2 (see frequency plot in Figure 4.17).

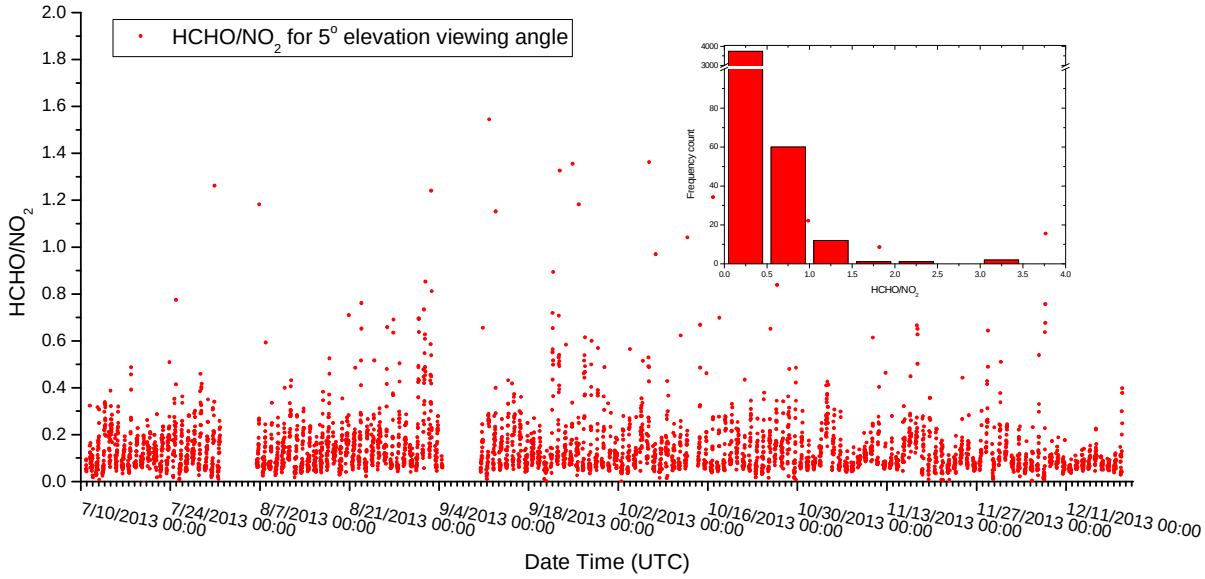

Figure 4.16: $HCHO/NO_2$ ratios for all MAX-DOAS data at the 5° viewing elevation angle collected at the Carson fenceline monitoring laboratory. Insert graph shows frequency count for the observed ratio values.

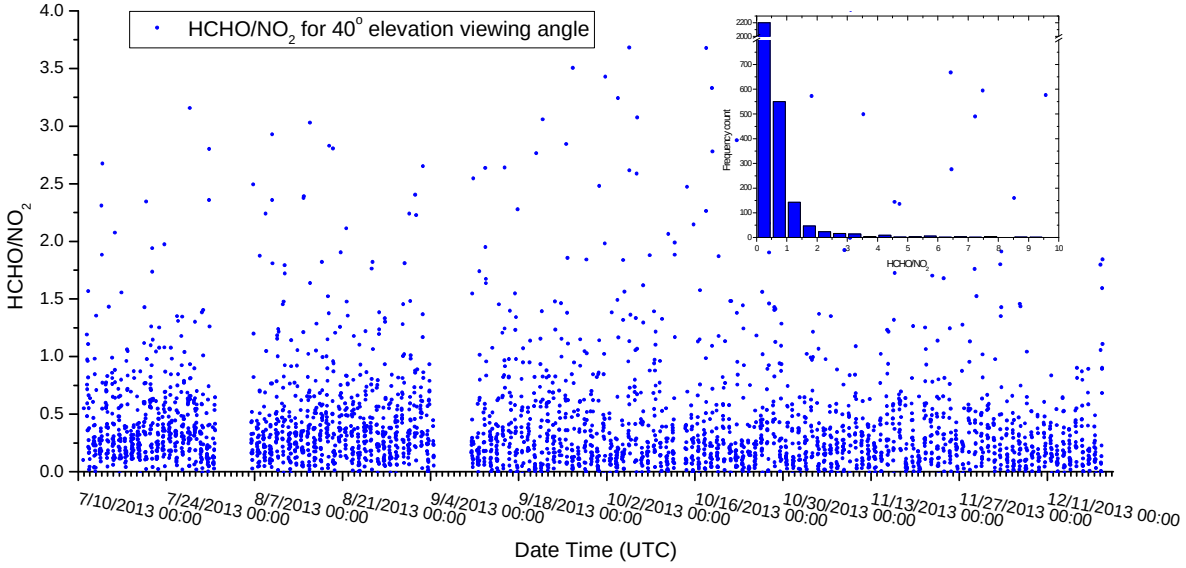

Figure 4.17: $HCHO/NO_2$ ratios for all MAX-DOAS data at the 40° viewing elevation angle collected at the Carson fenceline monitoring laboratory. Insert plot shows frequency count for the observed ratio values.

The ratio of HCHO to NO_2 derived from the MAX-DOAS measurements near the Carson Tesoro refinery therefore suggest that, for Carson, the chemical regime for instantaneous ozone production is mostly VOC-limited.

It is important to note that the proximity to the refinery, which is a direct source of both HCHO and NO_2 emissions, complicates the interpretation of HCHO/NO_2 ratios. The influence of direct refinery emissions will be greater for low viewing elevation angles and therefore more care must be taken in the interpretation of the ratio from low elevation viewing angles. However, higher elevation viewing angles are much less influenced by the direct refinery emissions. Therefore the ratio calculated from higher angles (e.g. 40^o in Figure 4.17) can be directly interpreted.

The HCHO/NO_2 ratio derived from the MAX-DOAS measurements can therefore be used as an important piece of information for determination of factors influencing ozone production in the region. The current AQMD 2012 Air Quality Management Plan (AQMP) (http://www.aqmd.gov/aqmp/2012aqmp/RevisedDraft/RevisedDraft2012AQMP-Main-clean.pdf) calls for NOx emission reductions as a primary effort to combat O_3 and PM pollution. Our observations in Carson, however, suggest that for this area of the basin, VOC emission controls are also important for further ozone reduction.

These results also illustrate that ground-based MAX-DOAS instruments, which are easy to operate, could play an important role in future efforts by the AQMD to design and monitor the effectiveness of air pollution mitigation strategies, as the HCHO/NO2 ratio provides a direct observation of the ozone formation regime, and its long-term changes as a result of mitigation policies.

4.3 Phase Two of MAX-DOAS measurements

4.3.1 Overview of Dual MAX-DOAS measurements

For Phase Two of the MAX-DOAS demonstration in Carson, the MAX-DOAS instruments were placed upwind and downwind of the refinery complex to perform measurements of area-wide emissions. The locations and viewing directions for the upwind and downwind stations were selected based on historical meteorological data (see Section 2.1). The wind data analysis revealed that, during the day, winds in the area often come from the west. Located at the NE boundary of the Tesoro Carson refinery, the FML was chosen as the downwind site because it primarily experiences winds coming from the direction of the refinery. The Saint Peter and Paul School location (where the second MAX-DOAS instrument was placed) was designated as the upwind site because of its location west of the Tesoro Carson fenceline. Along the instruments' lines of sight, the distance between the two sites is approximately 4.5 km and the two sites are offset from each other in the East-West direction by approximately 2 km. MAX-DOAS instruments at both locations performed measurements at 20 elevation viewing angles (1, 2, 3, 4, 5, 6, 7, 8, 9, 10, 12, 16, 20, 30, 40, 80, 85, 90 degrees relative to the horizon). Azimuth viewing angles of the two instruments were almost parallel to each other, with the AQMD1 upwind instrument azimuth viewing direction of 18°, and the AQMD2 downwind azimuth viewing angle of 198°. Figure 4.18 shows the locations, as well as the lines of sight, for both MAX-DOAS instruments. Two large refining facilities, Tesoro Carson and Philips 66 Carson, are located inside the rectangle defined by the lines of sight of the two MAX-DOAS instruments and lines of the East-West wind directions. Dual MAX-DOAS observations will thus result in area-averaged emission fluxes in the rectangle denoted in Figure 4.18**,** and thus the measured fluxes will include contributions from both facilities.

Figure 4.18: Map of the area surrounding the FML and SPPS sites, with locations of Tesoro Carson, Phillips 66 Carson and Port of Long Beach marked by the green markers. The area sampled by the two MAX-DOAS instruments is indicated by the orange rectangle. Red lines represent the approximate extent of MAX-DOAS instruments lines of sight.

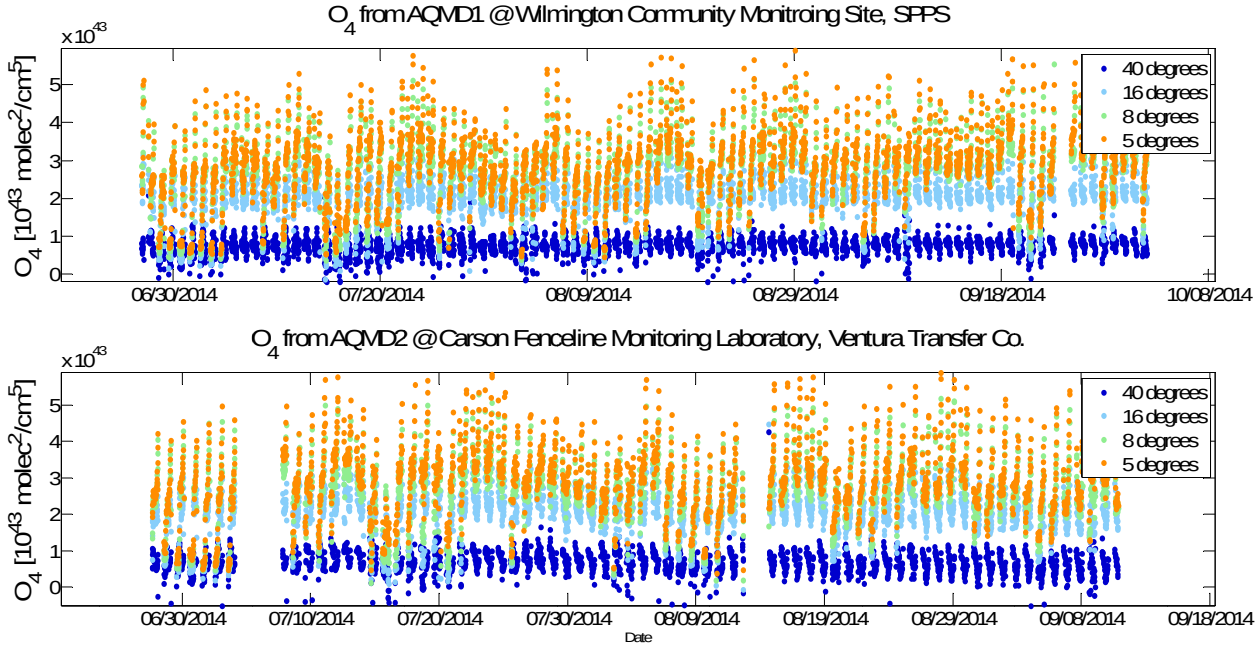

Figure 4.19: O_4 DSCDs measured at the FML and SPPS during the dual MAX-DOAS Phase. For clarity, only selected elevation viewing angles are displayed.

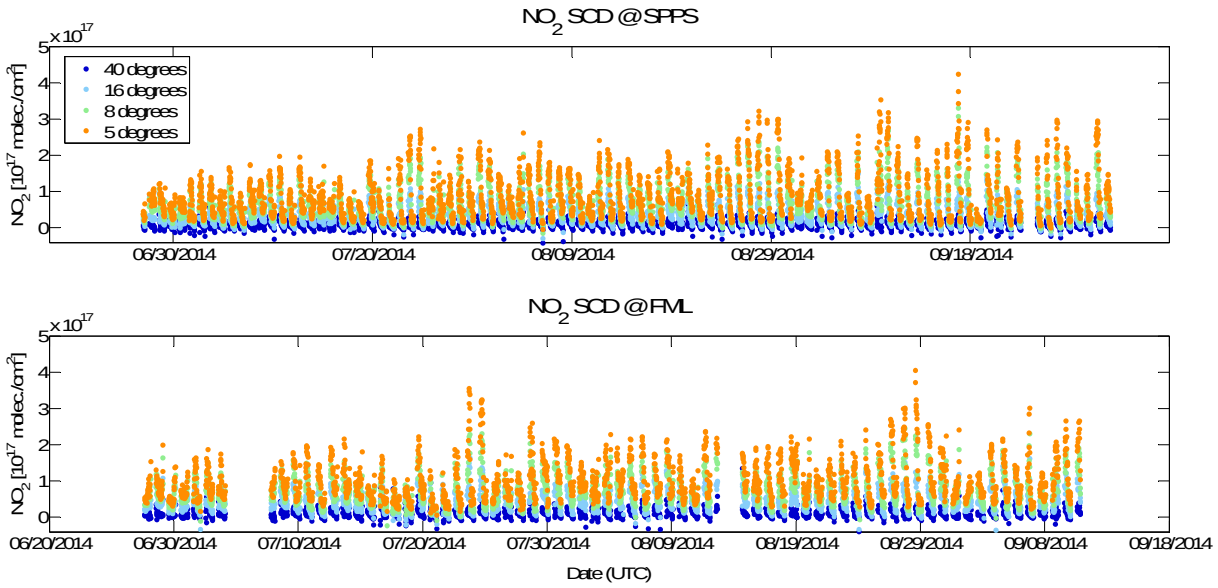

Figure 4.20: NO_2 DSCDs measured at the FML and SPPS during the dual MAX-DOAS Phase. For clarity, only selected elevation viewing angles are displayed.

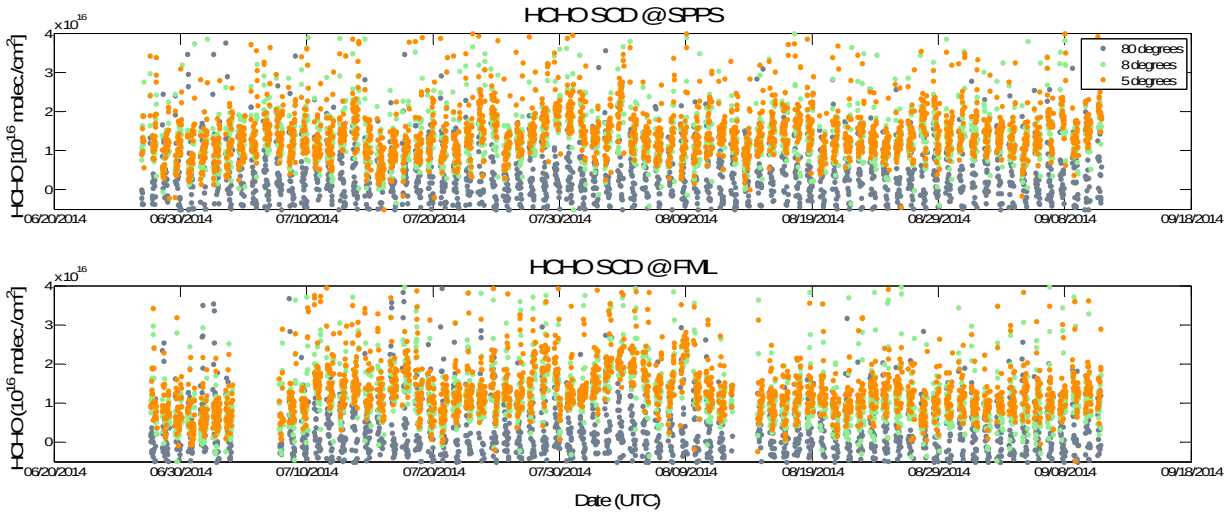

Figure 4.21: HCHO DSCDs measured at the FML and SPPS during the dual MAX-DOAS Phase. For clarity, only selected elevation viewing angles are displayed.

Figure 4.19, Figure 4., and Figure 4.21 show time series of O_4, NO_2, and HCHO SCDs measured at both sites. Gaps in the data correspond to periods of power outages at the sites. For most of the time the O_4 data is similar at both sites, suggesting similar radiative transfer conditions. The fact that the radiative conditions are similar allows a direct comparison of the trace gas SCD's between the two sites.

In the case of NO_2 and HCHO there are clear differences in the SCDs measured at the upwind and downwind site. These differences are due to contributions of local emissions from the area between the

two instruments. To further investigate these difference and the radiative transfer similarities, Figure 4.22, Figure 4.23, and Figure 4.24 show time periods between July 10 and 24, 2014. This time period contained days with various conditions observed throughout the dual MAX-DOAS experiment. For example, July 16, 2014 was a foggy and cloudy. These conditions are evident in the O_4 data, which show lower O_4 SCD values and decreased separation between elevation viewing angles than the other days. The afternoon of July 15 and all of July 20, 2014 were cloudy, which is reflected in more scattered O_4 SCDs. The period from July 23 – 25 was clear, thus the diurnal variation of the O_4 SCD is smoother and the elevation angles are more separated. In general, O_4 SCDs show suppressed values in the morning due to frequent coastal fog in Carson. Because of the potential impact of fog on the atmospheric radiative transfer, the following flux calculations were performed only for data in the afternoons.

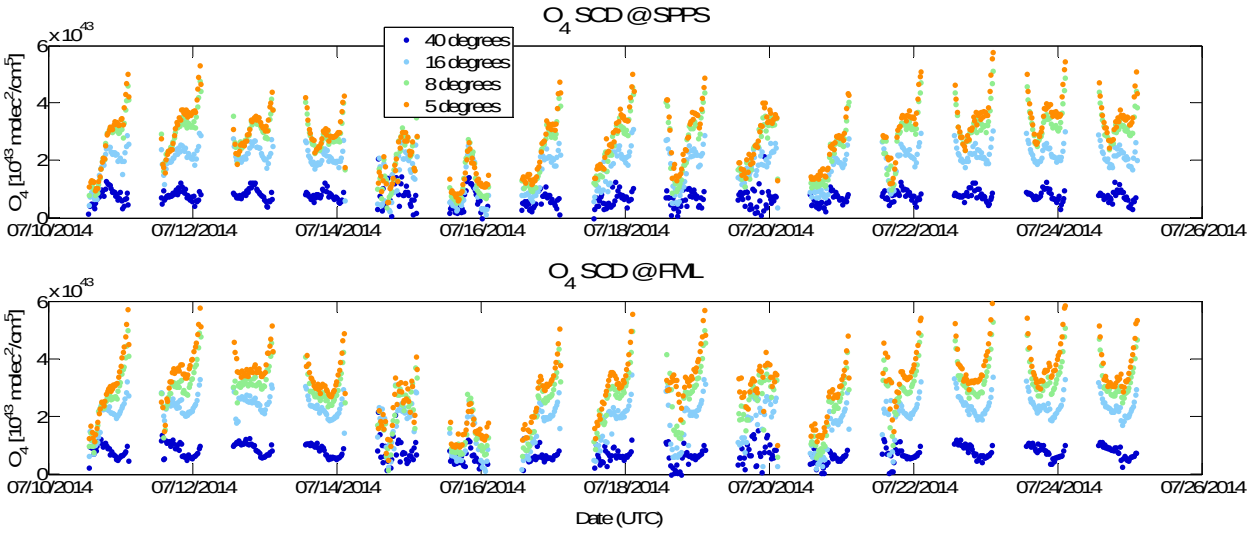

Figure 4.22: Excerpt of the O_4 DSCDs measured at the FML and SPPS July 10 through July 24 2014. For clarity, only selected elevation viewing angles are displayed.

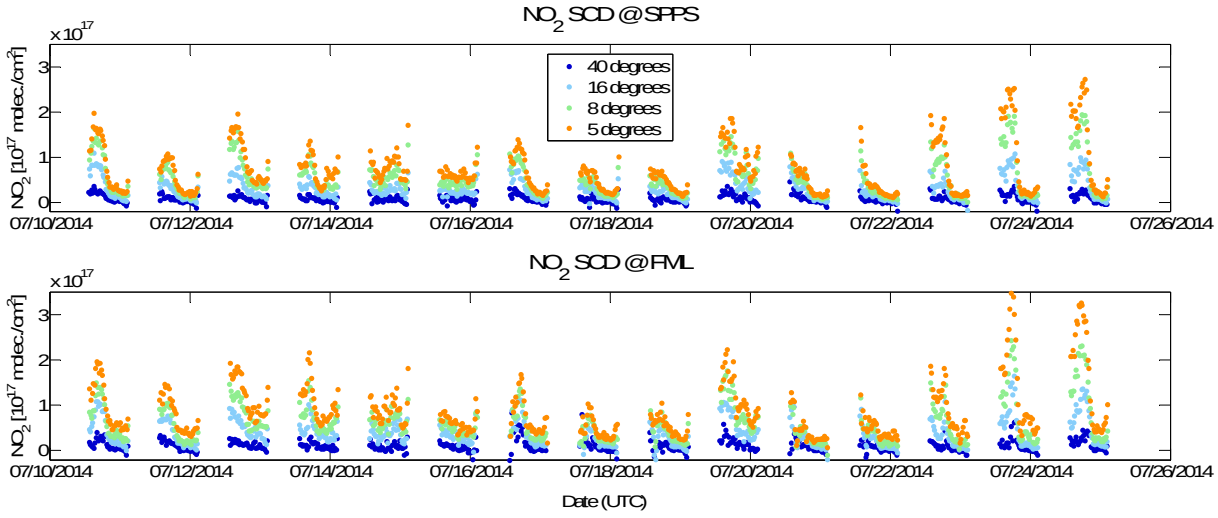

Figure 4.23: Excerpt of the NO_2 DSCDs measured at the FML and SPPS July 10 through July 24, 2014. For clarity, only selected elevation viewing angles are displayed.

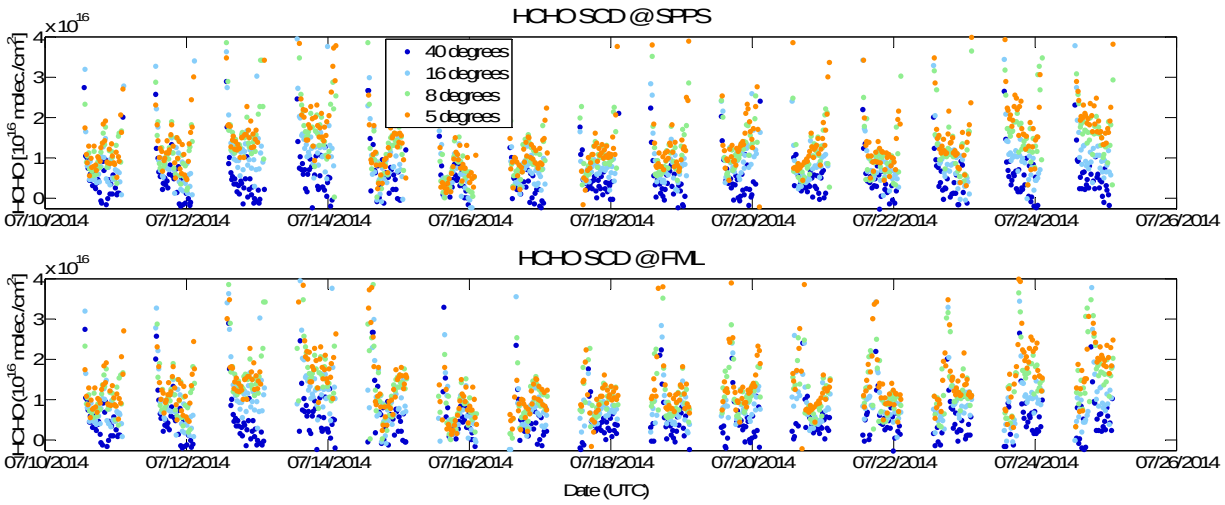

Figure 4.24: Excerpt of the HCHO DSCDs measured at the FML and SPPS. For clarity, only selected elevation viewing angles are displayed.

For the first part of the dual MAX-DOAS measurements period, the wind conditions in the area were "normal" – i.e. for most of the daylight hours wind was coming from the west. However, during the second part of the measurement period, wind reversals frequently occurred during the day. This flow reversal is evident in the wind data shown in Figure 4.25. During these flow reversal times, SPPS became a downwind site and the FML an upwind site. For the flux calculations, we thus had to take into account these wind direction changes.

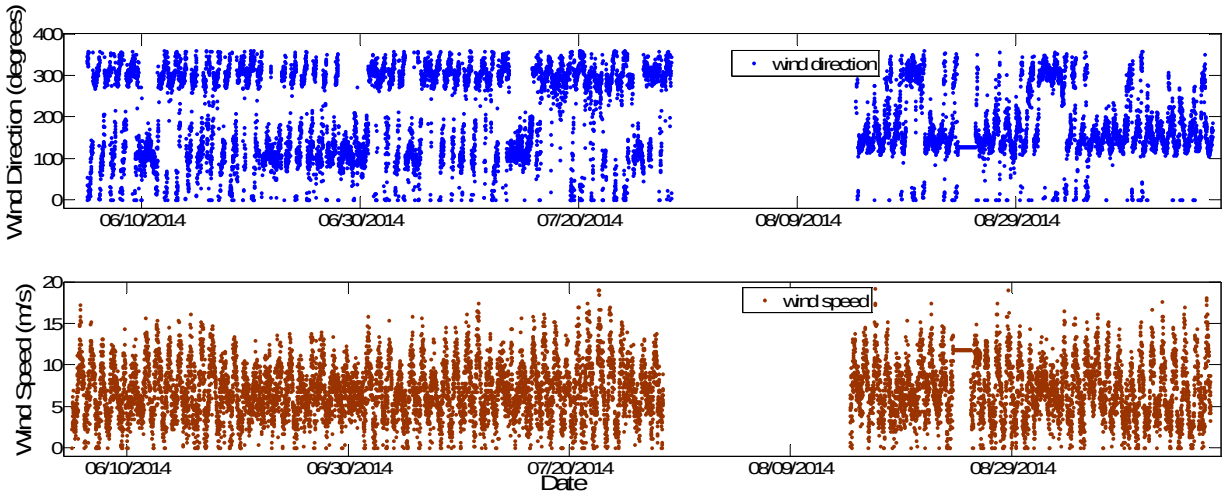

Figure 4.25: Wind direction (upper panel) and wind speed (lower panel) measured at the Tesoro Carson refinery. Facility's meteorological station was malfunctioning July through August 2014, resulting in missing data.

4.3.2 Area-Averaged Emissions Calculation Procedure

Area-wide emissions can be calculated using the combination of the data produced by two MAX-DOAS instruments and meteorological data. Using the geometric approximation described earlier in Section 4.2.2 (Equation 4.1), the average trace gas VCD for each MAX-DOAS "sweep" (set of consecutive measurements at elevation viewing angles 90° through 2°) can be derived using Equitation 4.2. In this equation, VCD_a is a vertical column density at elevation viewing angle a, and n is a number of elevation viewing angles.

$$\overline{VCD} = \frac{1}{n}\sum_1^n VCD_a \tag{4.2}$$

The difference between average VCD derived at upwind and downwind sites can then be calculated using Equation 4.3:

$$\Delta\overline{VCD} = \overline{VCD}_{downwind} - \overline{VCD}_{upwind} \tag{4.3}$$

For the well-mixed boundary layer, the average VCD, combined with the meteorological information, can be converted to an area-averaged flux by Equation 4.4. In this equation, BLH corresponds to the boundary layer height, u is wind speed, and ϕ is angle between the instrument's line of sight and the wind direction at the time of the measurement.

$$Flux = \Delta\overline{VCD} \times BLH \times u \times sin\emptyset \tag{4.4}$$

4.3.3 Area-Averaged Trace Gas Emissions

The methodology outlined in Section 4.3.2 was applied to calculate area-averaged emissions in Carson. All calculations presented here were performed for MAX-DOAS data during afternoon hours, when the wind direction was within ± 30 degrees of being orthogonal to the MAX-DOAS line of sights. Meteorological data from the Tesoro refinery (see Figure 4.25.) was used for the flux calculations. The FML was typically the downwind site. However, as mentioned in Section 4.3.1, during some time periods wind conditions reversed, making SPPS the downwind site. Consequently, for times with wind flow reversal, calculations were performed using SPPS as the downwind measurement. Determination on downwind site was based on analysis of the meteorological data (see Figure 4.25). The FML site was designated as downwind, when winds were coming from the direction orthogonal (± 30 degrees) to the AQMD2 line of sight. The SPPS site was designated as a downwind site for the opposite wind direction.

Figure 4.26 presents the derived NO_2 fluxes for the FML as the downwind site. These fluxes are variable in time, ranging from a few kg/hr to up to 60 kg/hr. The campaign average for the NO_2 flux with the FML as the downwind site is 22 kg/hr. Extrapolated annually, this leads to ~193 metric tons of NO_2 emissions.

Care must be taken with the interpretation of this number, as both NO and NO_2 are emitted by industrial sources, and because the NO-NO_2 system rapidly (within a few minutes) reaches a steady state. It is thus necessary to convert the NO_2-fluxes to NOx fluxes. Literature suggests that, on average, in industrial areas, the NO_2/NOx ratio is 0.3 [e.g. *During el. al.,* 2011]. Using this ratio, our measurements result in annual emissions of ~ 643 metric tons of NOx, or ~709 tons/yr.

The Tesoro and Phillips 66 facilities reported a combined total of 1033 tons of annual NOx emissions for 2012 (see

Table 2.1: Annual emissions (tons) of selected compounds reported by the refineries in Carson, CA

Facility	Pollutant ID/CAS	Pollutant	Annual Emissions 2012	Annual Emissions 2013
Tesoro Carson (formerly BP)				
	NOx	Nitrogen Oxides	650.402	698.164
	SOx	Sulfur Oxides	418.397	508.73
	CO	Carbon Monoxide	670.889	608.88
	50000	Formaldehyde	1.493	2.896
	71432	Benzene AQMD/EPA TRI	0.921 / 0.2125	0.814 / 1.906
	108883	Toluene AQMD/EPA TRI	NA / 0.043	NA / 2.84
Source:	http://www3.aqmd.gov/webappl/fim/prog/emission.aspx?fac_id=131003 http://oaspub.epa.gov/enviro/tris_control.tris_print?tris_id=90749RCPRD1801E			
Phillips 66 Carson				
	NOx	Nitrogen Oxides	332.584	335.592
	SOx	Sulfur Oxides	231.752	240.683
	CO	Carbon Monoxide	266.864	285.581
	50000	Formaldehyde	0.188	0.188
	71432	Benzene AQMD/EPA TRI	0.278 / 0.335	0.330 / 0.35
	108883	Toluene AQMD/EPA TRI	NA / 0.945	NA / 0.99
Source:	http://www3.aqmd.gov/webappl/fim/prog/emission.aspx?fac_id=171109 http://oaspub.epa.gov/enviro/tris_control.tris_print?tris_id=90745NCLCR1520E			
Valero Wilmington (formerly Ultramar)				
	NOx	Nitrogen Oxides	257.311	268.949
	SOx	Sulfur Oxides	144.477	146.518
	CO	Carbon Monoxide	102.152	116.699
	50000	Formaldehyde	1.010	1.154
	71432	Benzene AQMD/EPA TRI	0.382 / 0.046	0.532 / 0.0465
	108883	Toluene AQMD/EPA TRI	NA / 0.0785	NA / 0.108
Source:	http://www3.aqmd.gov/webappl/fim/prog/emission.aspx?fac_id=800026 http://oaspub.epa.gov/enviro/tris_control.tris_print?tris_id=90744HNTWY1651A			

). The NO_2 emissions determined by the dual MAX-DOAS system are thus ~31% lower than the values reported by the two refineries. As we will discuss in Section 4.3.4, we estimate the uncertainty of our emission flux observation at around 40%. The observed and reported values are thus in good agreement.

As refineries strive to minimize their environmental impact, it is possible that these lower estimates reflect reduction of NOx emissions since 2012. However, care must be taken when extrapolating our observations to annual emissions. Our measurements only covered daytime hours and were performed for a fraction of the year; therefore they might not capture diurnal or seasonal variations in emissions, or differences in production rates. As a first approximation however, our data generally confirms the magnitude of the reported NOx emissions. This conclusion is in agreement with mobile remote sensing observations performed in the summer of 2013 for the SCAQMD by FluxSense.

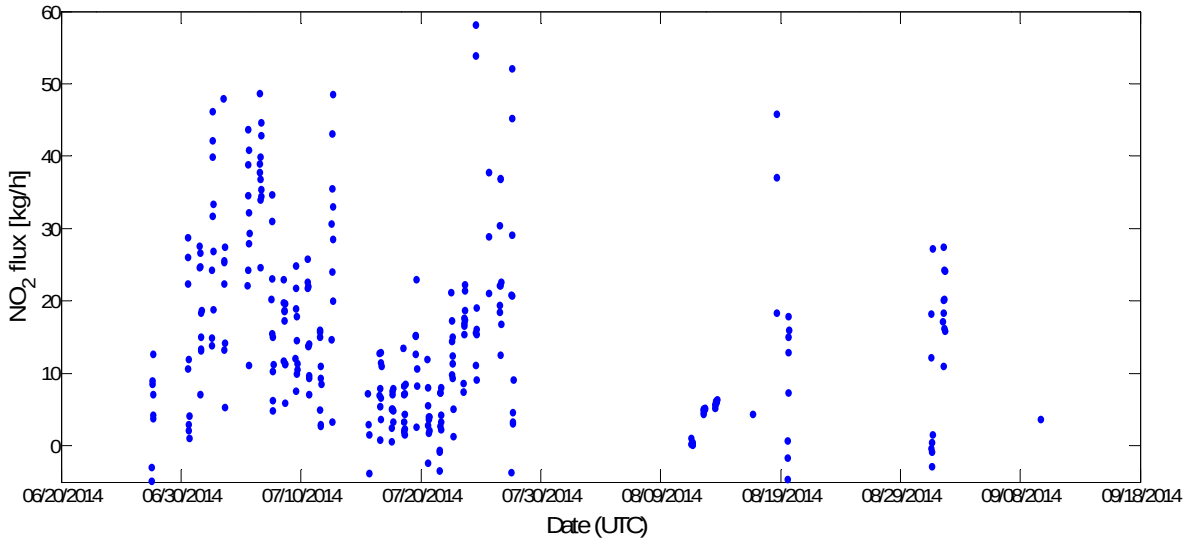

Figure 4.26: NO_2 flux (kg/hr) calculated for conditions when the FML was downwind of the refinery complex.

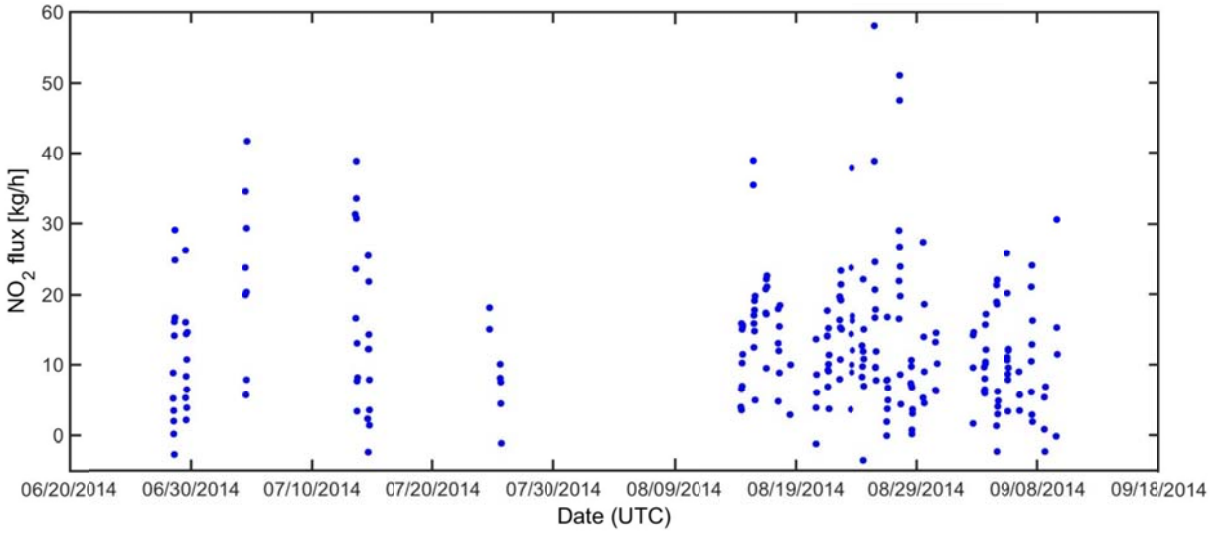

Figure 4.27: NO_2 flux calculated for conditions when SPPS was downwind of the refineries complex.

NO_2 flux calculated during times when the SPPS site (Figure 4.27) was downwind (during flow reversal) was ~14 kg/h and thus somewhat lower than for the opposite wind direction. This suggests that the NO_2 signal in the data collected from the FML is higher than in the one from SPPS. The likely cause of this discrepancy is the setup of the two MAX-DOAS systems, which look in opposite directions. The SPPS instrument viewing geometry may miss some of the NO2 close to the surface as the site is further away than optimal.

Figure 4.28 shows results of HCHO flux calculations for time periods when the FML was downwind from the refineries. Calculated HCHO fluxes are also highly variable, with an average HCHO flux of ~ 4 kg/hr. Similar to NO_2, HCHO fluxes calculated when the SPPS site is downwind are often negative, likely for the same reason as described for NO_2.

Based on our average hourly HCHO flux we can extrapolate to an annual HCHO emission of ~35 metric tons/yr. This value is greater than the 1.11 tons of annual HCHO emissions reported by the Tesoro Carson and Phillips 66 Carson combined (see

Table 2.1: Annual emissions (tons) of selected compounds reported by the refineries in Carson, CA

Facility	Pollutant ID/CAS	Pollutant	Annual Emissions 2012	Annual Emissions 2013
Tesoro Carson (formerly BP)				
	NOx	Nitrogen Oxides	650.402	698.164
	SOx	Sulfur Oxides	418.397	508.73
	CO	Carbon Monoxide	670.889	608.88
	50000	Formaldehyde	1.493	2.896
	71432	Benzene AQMD/EPA TRI	0.921 / 0.2125	0.814 / 1.906
	108883	Toluene AQMD/EPA TRI	NA / 0.043	NA / 2.84
Source:	http://www3.aqmd.gov/webappl/fim/prog/emission.aspx?fac_id=131003 http://oaspub.epa.gov/enviro/tris_control.tris_print?tris_id=90749RCPRD1801E			
Phillips 66 Carson				
	NOx	Nitrogen Oxides	332.584	335.592
	SOx	Sulfur Oxides	231.752	240.683
	CO	Carbon Monoxide	266.864	285.581
	50000	Formaldehyde	0.188	0.188
	71432	Benzene AQMD/EPA TRI	0.278 / 0.335	0.330 / 0.35
	108883	Toluene AQMD/EPA TRI	NA / 0.945	NA / 0.99
Source:	http://www3.aqmd.gov/webappl/fim/prog/emission.aspx?fac_id=171109 http://oaspub.epa.gov/enviro/tris_control.tris_print?tris_id=90745NCLCR1520E			
Valero Wilmington (formerly Ultramar)				
	NOx	Nitrogen Oxides	257.311	268.949
	SOx	Sulfur Oxides	144.477	146.518
	CO	Carbon Monoxide	102.152	116.699
	50000	Formaldehyde	1.010	1.154
	71432	Benzene AQMD/EPA TRI	0.382 / 0.046	0.532 / 0.0465
	108883	Toluene AQMD/EPA TRI	NA / 0.0785	NA / 0.108
Source:	http://www3.aqmd.gov/webappl/fim/prog/emission.aspx?fac_id=800026 http://oaspub.epa.gov/enviro/tris_control.tris_print?tris_id=90744HNTWY1651A			

). However, we would like to point out that the averaged calculated flux was based on approximately 40 days of daytime measurements over a 3 months period. Therefore, a straight extrapolation of our observations to annual emissions is likely not accurate. Refinery operations and emissions vary through a year and also have diurnal fluctuations. In addition, we did not consider secondary HCHO formation from the oxidation of hydrocarbons. Nevertheless, our results allude to the fact that HCHO emissions from refineries might be somewhat underestimated.

As in the case of NO_2, the emission determined from the period when the SPPS was downwind are again lower (Figure 4.29). This difference is even more pronounced for HCHO, which is likely due to the vertical distribution of HCHO, i.e. the SPPS instrument may not see high HCHO levels close to the surface. The average upper limit of SO_2 flux was calculated to be ~10 kg/hr.

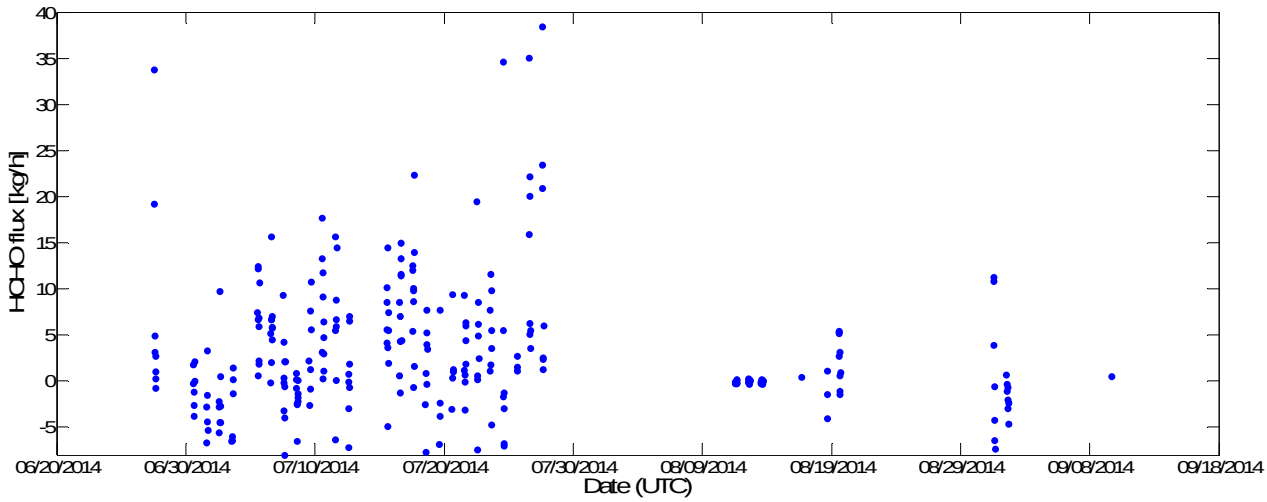

Figure 4.28: HCHO flux (kg/hr) calculated for time periods when the FML was downwind of refineries.

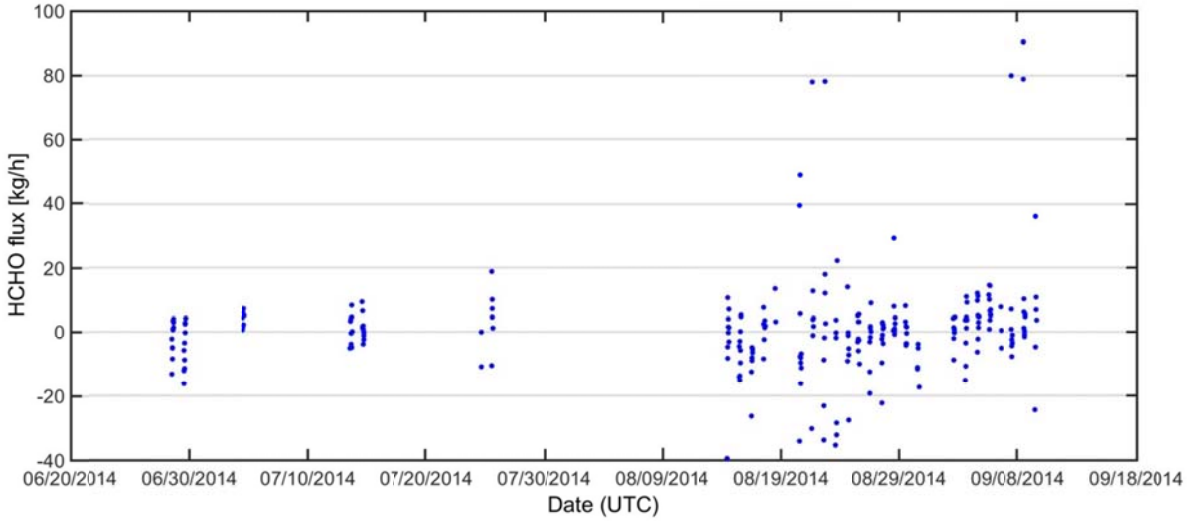

Figure 4.29: HCHO flux (kg/hr) calculated for time periods when the SPPS was downwind of refineries.

4.3.4 Uncertainties of measurements

The main sources of error in our calculation of the area-averaged fluxes are as follows:

- The meteorology of the entire region was characterized by meteorological measurements made at one location (at the Tesoro Carson refinery);

- A geometrical approximation was applied to measured slant column densities. Although we think that geometrical approximation can be used, ideally radiative transfer calculations should be applied to account for variations in aerosol and trace gases within the boundary layer.
- The boundary layer height was assumed to be 400 m and constant for all calculations. Ideally, flux calculations should be linked with either a meteorology model to produce boundary diurnally-evolving boundary layer, or real-time data from boundary layer height measurements (for example by the wind profiler LiDAR);
- Because instruments were "facing" each other in our experimental setup, the extent of the trace gas plume was assumed to be limited to a distance between the two systems.

Other, more minor, sources of error in the flux determination are:

- Accuracy in pointing of each instrument;
- Interpolation errors from putting the data from two instruments and met data on the same time scale;
- Accuracy of the reference absorption cross sections used for spectral fitting.

Based on the discussion above, we estimate the error for the area-averaged flux calculations using dual MAX-DOAS approach to be on the order of 40%.

4.4 Conclusions from the dual MAX-DOAS emission measurements

The dual MAX-DOAS approach was successfully used to measure area-wide emission fluxes of NO_2 and HCHO. Our results show that placement of the instruments is crucial, especially in an area with a high density of sources outside of the targeted area. The analysis also showed that accurate observations of wind speed and directions, as well as boundary layer height are crucial. Much of the uncertainties in our results are due to the inaccuracies of the meteorological data. Further improvement of the dual MAX-DOAS method and reduction of the emission flux error are thus possible. For an accurate comparison of the dual MAX-DOAS emission fluxes with reported values this system should be operated for an entire year, as suitability of the interpolation of our 2 month data set to an annual emission value is uncertain.

We also demonstrated the potential of a single MAX-DOAS instrument to monitor pollutants. Of particular interest is the ability to directly measure the $HCHO/NO_2$ ratio, which serves as a proxy for ozone formation sensitivity to NOx or VOC. Because MAX-DOAS instruments are fully automated and need little maintenance this measurement could be achieved with little effort over long time periods, thus allowing to monitor the success of the current AQMD 2012 Air Quality Management Plan (AQMP) (http://www.aqmd.gov/aqmp/2012aqmp/RevisedDraft/RevisedDraft2012AQMP-Main-clean.pdf) to mitigate O_3 and PM pollution.

5 Imaging Differential Optical Absorption Spectroscopy

Based on the MAX-DOAS principle, Imaging-DOAS (I-DOAS) collects scattered sunlight simultaneously in many elevation angles (Figure 5.1). The collected spectra are analyzed to retrieve differential slant column densities (DSCD) of trace gases, i.e. the number of trace gas molecules integrated along the absorption path. In contrast to traditional MAX-DOAS, where measurement results in one spectrum from a single viewing direction, I-DOAS measurement result in hyper-spectral images, where one dimension is that of wavelength of the measured light and the other is the vertical viewing direction (Figure 5.1). The wavelength dimension is used to derive trace gas DSCDs using the DOAS approach. Therefore, a single I-DOAS measurement delivers a one-dimensional array of trace gas SCDs (in the vertical direction). By adding an opto-mechanical scanner for the horizontal direction, the second (horizontal) spatial dimension can also be observed. The final result is thus an "image" of DSCDs of a single trace gas inside and outside the plume (Figure 5.1). By comparing the trace gas content in the slice in the plume and upwind of the source one can then calculate the amount of a gas added to the plume by the source. In combination with wind data an emission flux can then be directly calculated (see *Pikelnaya et al.* [2013] and Section 5.3 for details of this calculation).

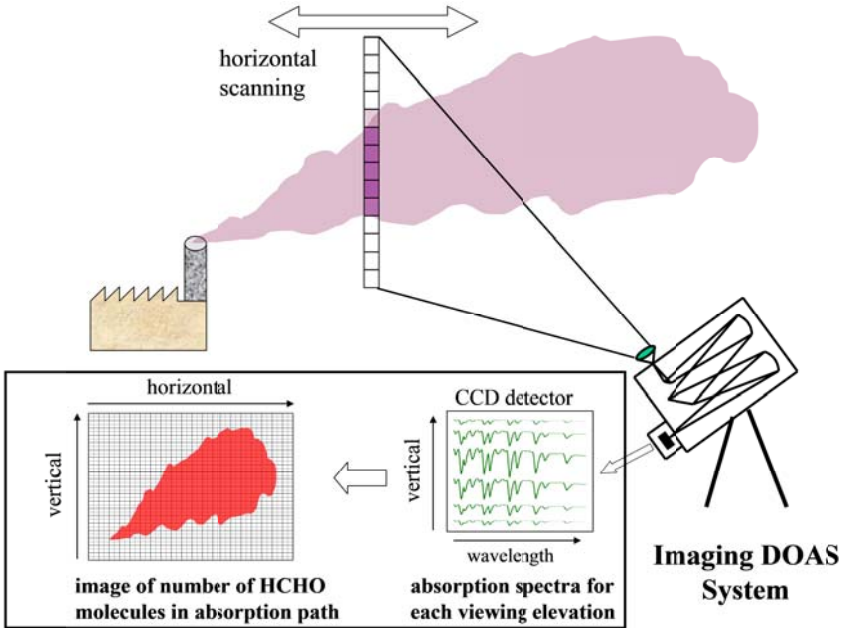

Figure 5.1: Sketch of Imaging DOAS experimental setup and data collection and processing.

5.1 Instrument Description

The UCLA Imaging DOAS instrument is designed to be portable, allowing for fast set-up and take-down, and to operate for extended periods of time from a portable power source, while still maintaining spectroscopic characteristics necessary to detect target species such as HCHO. The instrument consists of an Acton SP-2150i imaging spectrometer coupled to a Princeton Instruments PIXIS camera equipped with the 1024×256 pixel back illuminated E2V CCD30-11 CCD array (pixel size 25 µm × 25 µm) mounted in the focal plane of the spectrometer. I-DOAS measurements were performed using a 1200 grooves/mm grating, covering the wavelength range between 290 nm and 407 nm, resulting in a spectral

resolution of the instrument of 0.6 nm. A shutter is mounted directly behind the entrance slit and connected to the camera controller to ensure accurate exposure times. The CCD array is cooled to -70°C during the measurements in order to eliminate detector dark current. Five rows of the CCD array are binned into one spectrum, providing measurement of 50 separate spectra per exposure. Under nominal atmospheric conditions, exposure time for one measurement of all 50 spectra is between 50 - 200 milliseconds.

A 45° elliptical mirror collects scattered sunlight from the direction of the plume, with most of the light coming from behind the plume. The light collected by the mirror is imaged onto the entrance slit of the spectrometer by way of a Hoya 340 UV-bandpass filter, a 100mm focal length quartz lens and a turning mirror (Figure 5.2a). Translational stages are used to align the telescope and scanner assembly in the laboratory before deployment. The light on the slit represents a field of view of ~7° vertical by 0.2° horizontal. Each of the 50 vertical spectra thus represents a part of the plume 0.14° vertical by 0.2° horizontal. The scanning mirror is rotated in the horizontal (azimuth) by a small stepper motor with a minimum step width of ~0.11°. The azimuth scanner is able to cover an overall angle of ~160°, although smaller scanning intervals are typically used to characterize most plumes. Figure 5.2 shows schematics of the I-DOAS instrument and measurements setup.

The spectrometer - detector combination, together with the telescope-scanner assembly is mounted in an aluminum frame with approximate dimensions of 40 x 30 x 30 cm and ~20 kg weight, which can be tilted with a 0.1^{o} precision. The instrument is controlled by a laptop that controls the detector, spectrometer, and scanner using the DOASIS software package (Institute of Environmental Physics, Heidelberg University, Germany, https://doasis.iup.uni-heidelberg.de/bugtracker/projects/doasis/). In the field, I-DOAS is powered by a portable power system based on three commercial lead-acid batteries and a DC-AC pure-sine-wave converter.

For the imaging DOAS (I-DOAS) deployment in this project a digital camera was added to the instrument in order to improve its pointing capabilities, and to allow for the visual observation of the emission sources during the measurements.

Each individual measurement of the I-DOAS (i.e. single spectral scan at a single azimuth angle) is referred as a “measurement” and a set of measurements at consecutive azimuthal viewing angles as a “scan”.

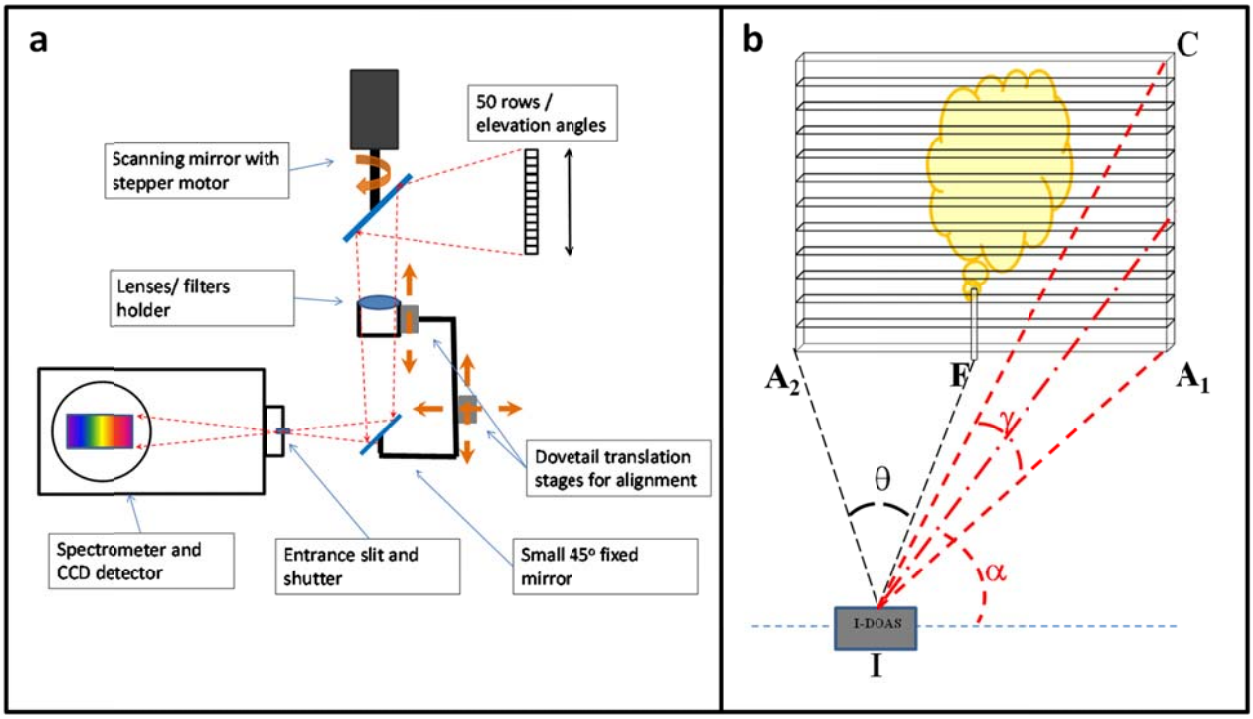

Figure 5.2: I-DOAS instrument and measurement setup. Panel a: Sketch of the I-DOAS setup. Brown arrows represent rotational movement of the scanning mirror as well as vertical and horizontal movements of the dovetail translation stages. Panel b: Sketch of the I-DOAS observation geometry. (adopted from *Pikelnaya et a*l., 2013)

5.2 I-DOAS Data Analysis

The spectral retrieval of I-DOAS measurements considers each of the 50 rows as an independent spectrometer; therefore, each row had its own wavelength-to-pixel calibration and instrument function, which are determined by measuring mercury emission lines. At the beginning of each instrument setup a mercury spectrum is recorded, and for each of the 50 rows, a set of reference trace gas absorption spectra is convoluted using an instrument function determined with the measured Hg-line at 334.4 nm. The references for the absorption cross sections used in the analysis are listed in Table 5.1.

Table 5.1: Trace Gas References used for I-DOAS analysis.

Spectral Reference	Source	Reported Uncertainties
HCHO	*Meller and Moorgat*, 2000	5%
NO_2	*Voigt et al*., 2002	4%
HONO	*Stutz et al*., 2000	5%
O_4	*Greenblatt et al*., 1990	10%
O_3	*Voigt et al*., 2001	5%
SO_2	*Vandaele et al*., 1994	5%

The spectral retrieval is performed using a combination of linear and non-linear least squares fit, as described in *Stutz and Platt* (1997). Table 5.2 presents the wavelength intervals used for detection of different trace gases from the I-DOAS. For HCHO, a small interval between 329 nm and 334.6 nm was excluded from the fit in order to minimize interference from solar Fraunhofer bands and other spectral interferences in this region. In addition to the trace gas references, an atmospheric reference is also

included in the fit. The atmospheric reference is normally obtained by performing a single measurement in an azimuth direction upwind of the targeted flare (where concentration of the target pollutant was expected to be low). This spectrum also contains absorptions of the background trace gas levels. Consequently, the atmospheric background trace gas concentration upwind of the flare are subtracted spectroscopically, considering that the radiative transfer conditions upwind and downwind of the flair are similar.

Table 5.2: I-DOAS Spectral Evaluation Information.

Trace Gas	Fitting window (nm)	Reference fitted	Degree of polynomial
HCHO	322.3 – 341.6 (329 – 334.6 excluded)	HCHO, NO_2, HONO, O_3	5
NO_2, O_4, HONO	362.8 – 378.6	NO_2, O_4, HONO	3
SO_2	305.7 – 321.1	SO_2, NO_2, HCHO, O_3	4

Simulated Ring spectra of the solar reference scan, along with the linear and quadratic expansion of the Ring spectra (*Vountas et al*., 1998; *Langford et al*., 2007) are also fitted together with a polynomial after ten-fold triangular smoothing low pass filtering. To allow for uncertainties in the grating position caused by temporal drift of the spectrometer during a measurement, spectral shift of trace gases during evaluation is allowed. During the evaluation, all trace gases are linked in shift and squeeze to each other, and spectral shift typically did not exceed one pixel. Similarly, the spectral shifts of the Ring and Fraunhofer spectra are also linked to each other. The error of the measurement is calculated by multiplying the statistical error of the fit by a factor of 3 according to *Stutz and Platt* (1997).

The results of the I-DOAS spectral retrieval from each measurement are differential slant column densities (DSCD), i.e. path-averaged trace gas concentrations, relative to the reference spectrum. Figure 5.3 shows an example of HCHO retrieval for one of the I-DOAS measurements on July 09, 2014 at 3pm local time. The HCHO differential slant column density (DSCD) was found to be $7.5 \pm 1.2 \times 10^{16}$ molec/cm^2.

The result of the I-DOAS retrieval for a scan over an individual point source is a 2-dimesional image of trace gas DSCD, with the vertical axes representative of individual rows of the CCD detector, which then can be converted to a vertical altitude using geometry of observations. The horizontal axis represents various azimuth angles that were observed using the mechanical scanner. The azimuth angles can be converted to a length scale at the source using the distance between the instrument and the source.

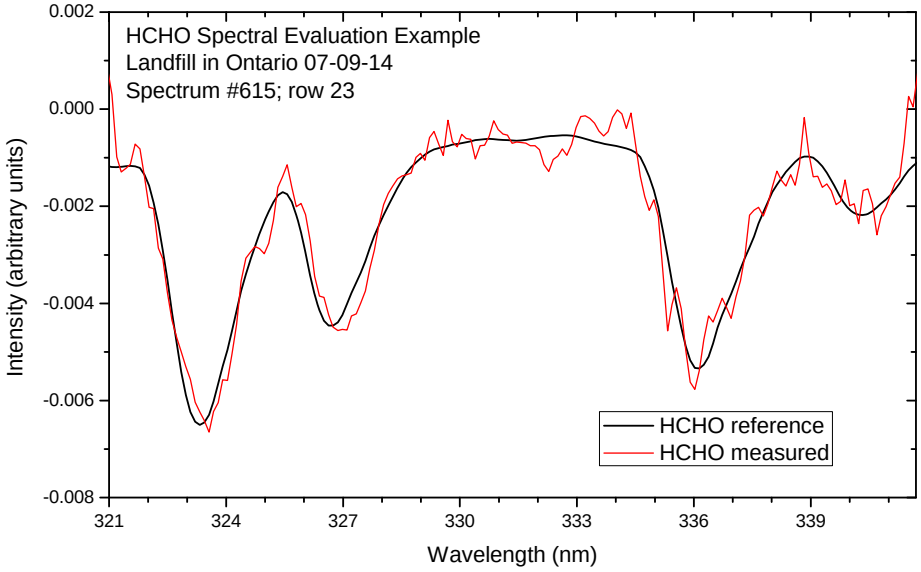

Figure 5.3: Example of spectral evaluation for HCHO for I-DOAS measurement on July 09, 2014 at 3pm local time. The comparison of the pure HCHO absorption spectrum (black line) with the HCHO absorption spectrum retrieved from the atmospheric measurements (red line) shows the quality of the measurement. The HCHO differential slant column density (DSCD) in this spectrum was $7.5 \pm 1.2 \times 10^{16}$ molec/cm^2.

5.3 Flux Calculation Procedure

Emission strengths from individual point sources can be calculated using the combination of the I-DOAS observations and meteorological data. This approach, described below, has been successfully used by our group to identify HCHO and SO_2 emissions from individual flares during the FLAIR field experiment in Houston, TX in Spring 2009 [*Pikelnaya et al.,* 2013]. The same approach was used for I-DOAS observation in the Los Angeles area for this project.

I-DOAS observations of individual sources were typically set up in a way that the instrument's line of sight (main azimuth viewing angle) was approximately perpendicular to the direction of the wind, and therefore to the direction to which pollutants emitted from the flare would travel. By summing up the 50 trace gas DSCDs in one measurement of the I-DOAS at a given azimuth viewing angle, an integrated trace gas DSCD in a vertical "slice" through the plume is obtained, as demonstrated in Equation 5.1.

$$\sum SCD_j = \sum_{j=1}^{50} SCD\left(at\ column\ j\right) \tag{5.1}$$

Taking into account the distance between the instrument and the flare, wind direction and speed, and the optical set-up of the instrument, a trace gas flux then can be calculated for each observed azimuth angle using the following equation (Equation 5.2):

$$F = \gamma * D * \sum_{j=1}^{50} SCD_j * V_w * \sin\beta \tag{5.2}$$

Where γ is the I-DOAS projection factor that relates the dimensions of the image at a distance to its projection onto the spectrometer slit ($\gamma = \frac{6mm/50}{100mm}$, where 6 mm is the slit height of the spectrometer, 50 is the number of rows in the detector, and 100 mm is the focal length of the telescope lens); D is the distance between the I-DOAS and the flare (cm), V_w is the wind speed (cm/s), and β is the angle between the I-DOAS line of sight and the direction of the wind.

In order to reduce uncertainties and the variability of the emissions, flux calculations are performed for several neighboring azimuth viewing angles to obtain an averaged flux value. For all of the calculations presented here, $\sum SCD_j$ is an average value of 8 to 10 azimuthal steps downwind from the flare. To account for the possible "background" amount of the respective trace gas the vertically integrated trace gas DSCDs from the part of the image that is upwind of the source was determined. This background value was then subtracted from the downwind $\sum SCD_j$. The "background" vertically integrated DSCD is also averaged over the 10 azimuthal steps. The final emission fluxes reported here are thus calculated using Equation 5.3:

$$F = \gamma * D * \left(\sum SCD_j(downwind) - \sum SCD_j(upwind)\right) * V_w * \sin\beta \tag{5.3}$$

5.4 Uncertainty of Flux Calculation

Systematic errors of our observations are dominated by errors associated with the reference absorption cross sections used in the spectral retrievals. Reported errors for reference absorption cross sections used for spectral evaluation are listed in Table 5.1: Trace Gas References used for I-DOAS analysis.Table 5.1.

The error of the trace gases fluxes is calculated using statistical error propagation of errors from the least squares fit of atmospheric spectra to retrieve trace gas DSCDs, errors in determination of azimuth and distance between I-DOAS and observed flare, and uncertainties in wind-speed and wind direction. The error for the DSCDs is calculated by multiplying the statistical error of the spectral fit by 3, in accordance with *Stutz and Platt* (1997). This error is the smallest contribution to the uncertainty of the flux calculation. Distance between the I-DOAS and flare/stack under observation is normally determined using Google Earth ruler tool. We estimate uncertainty of this measurement to 10 m. While Google does not provide information on accuracy of this tool, online users report it to be 10-15 m. The uncertainty for the I-DOAS azimuth viewing direction was determined to be 5 degrees.

Wind speed information used for the flux determination is estimated from the meteorological data available for the region at the time of measurements using a log wind profile relationship. Wind speed represents the largest uncertainty in the flux calculations.

5.5 I-DOAS observations at the FML in Carson

In July 2012 the I-DOAS was re-located to the monitoring site in Carson. Figure 5.4 shows a photograph of the I-DOAS performing measurements in Carson during one of the measurement days.

Figure 5.4: Photograph of the I-DOAS instrument on top of the container at the AQMD monitoring site in Carson.

The FML in Carson provides a clear view to two flares of Tesoro refinery. Directly to the west of the FML, approximately 300 m away, is a large air-assist coker flare; and to the south-west of the FML, at approximately the same distance, is steam-assist Flare #5, which serves Tesoro and well as INEOUS plants. These two flares are ideally situated for I-DOAS observations from the FML site. In addition, there is also a Tesoro tank farm that is to the west and approximately 1.5 km away from the FML. Emissions from the tank farm (if any) could also be observed by the I-DOAS system.

Prior to the Carson deployment, the UCLA I-DOAS instrument was used for flare observations in Houston-Galveston area during the 2009 FLAIR-SAHRP air quality measurement campaign. At that time, we did not have problems finding burning flares. In Carson, however, "catching" a burning flare over the Carson Tesoro refinery proved to be challenging. Based on our Houston experience, we originally expected to observe flames from the coker or #5 flares routinely. However, by May 2013 we had not observed any of these flares burning during daytime hours.

With the guidance of AQMD personnel we signed-up for flare event notifications in May 2013 – a service provided by the SCAQMD to alert about flaring events that are expected or exceeded one or more of the following daily limits: 500,000 standard cubic feet of vent gas combusted; 100 pounds of VOC emitted, and/or 500 pounds of oxides of sulfur emitted. Between June and December 2013, 7 flare event notifications for the Carson Tesoro refinery were issued (see Table 5.3). However, neither coker nor Flare #5 were observed burning during the daylight hours within the alerted periods. We did see Flare #5 burning, but in all instances it happened either late at night, after the sun set, or early in the morning before the sun rise, when I-DOAS measurements, which rely on sunlight, cannot be performed.

Despite the absence of visible flames, we performed I-DOAS observations of the coker flare and Flare #5 from the FML for 6 days. In addition, we performed numerous survey scans over the tank farm to the west of the FML. Details of these observations are outlined in Table 5.4. None of the I-DOAS measurements at the FML found emissions of HCHO, SO_2 or NO_2 from the coker flare or Flare #5, nor from the tank farm. Figure 5.5 shows an example of the I-DOAS survey scan over the Carson Tesoro refinery. The single panel at the top of the figure shows the UV intensity image derived from the measurement, and the panels below show DCSD (left) and DSCD error (right) images for SO_2, HCHO, NO_2 and O_4. Low values of the DSCD error images show the quality of the observations. No significant pollutants enhancements associated with the refinery can be observed in DSCD images. Absence of

detectable HCHO, SO_2, and NO_2 from non-burning flares at the Tesoro refinery in Carson is consistent with our previous observations in the Houston-Galveston area.

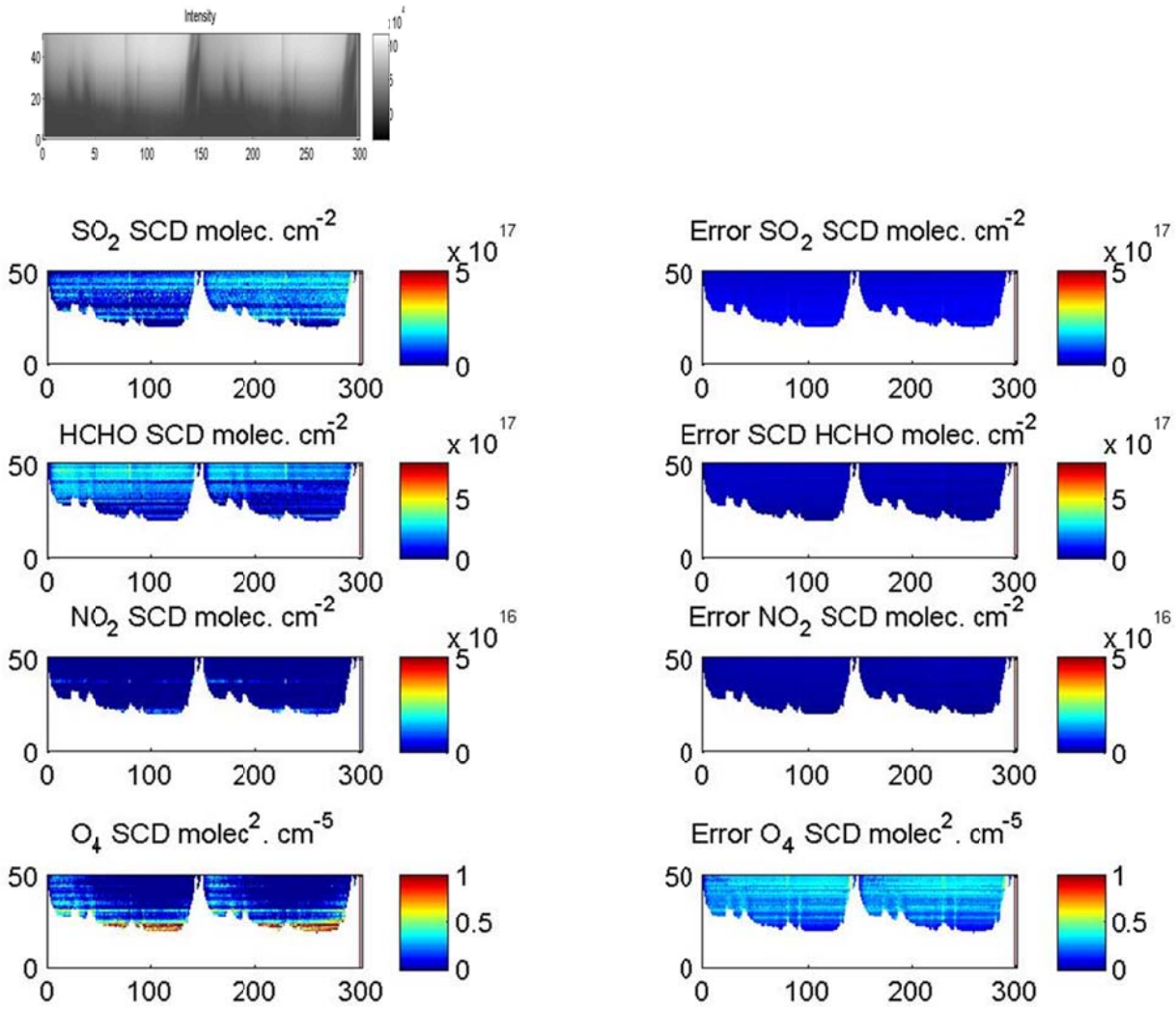

Figure 5.5: Example of I-DOAS scan over the Carson Tesoro refinery on 07/26/12. The top panel shows the UV Intensity image. All panels below show DSCD and DSCD error images for SO_2, HCHO, NO_2, and O_4. White areas on the DCSD images are obstacles (see UV intensity image on top). Values on vertical axes are numbers for rows of the CCD detector, and horizontal axis is a measurement number.

Table 5.3: Flare event notifications and burning flare observed by the UCLA personnel

Notification received through the AQMD notification system	I-DOAS measurements	Results/notes
06/07/13 5:00am – 06/11/13 11:59pm	No	No visible flames during daylight hours
06/16/13 9:00pm – 06/18/13 11:59pm	No	No visible flames during daylight hours
07/10/13 6:00am – 07/11/13 6:00 am	Yes, morning and early afternoon	By 8am Ventura Transfer opening, from the FML, no visible flames at any of the flares were observed. I-DOAS measurements of the coker flare did not detect any HCHO, NO_2 or SO_2 enhancements
07/24/13 7:30am – 07/26/13 11:59 pm	No	No visible flames during daylight hours
07/26/13 7:30am – 07/26/13 11:59 pm	No	No visible flames during daylight hours
07/27/13 12:00 am – 07/27/13 11:59 pm	No	No visible flames during daylight hours
07/29/13 11:53 am – 07/29/13 11:59 pm	No	Notification email received @ 12:34pm on 07/29/13 – not enough time to respond

Table 5.4:. I-DOAS measurements in Carson

Date	Observed	Notes
07/26/12	Coker and INEOUS flares next to the FML	• No visible flames at the flares • No HCHO, NO_2 or SO_2 emissions were detected
08/03/12	Coker and INEOUS flares next to the FML, storage tanks to the west of the FML	• No visible flames at the flares • No HCHO, NO_2 or SO_2 emissions were detected
07/02/13	Coker and INEOUS flares near the FML	• No visible flames at the flares • No HCHO, NO_2 or SO_2 emissions were detected
07/10/13	Coker flare directly in front of the FML	• No visible flames at the flare • No HCHO, NO_2 or SO_2 emissions were detected
07/11/13	Coker flare directly in front of the FML	• No visible flames at the flare • No HCHO, NO_2 or SO_2 emissions were detected

5.6 I-DOAS observations flares of landfills and air above a power plant

Since observing burning petrochemical flares during daylight hours in Carson proved to be difficult, we used the I-DOAS instrument for observation of other types of flares in the LA Air Basin for the remainder of the project. We turned out attention to other facilities in the basin, such as power plants, landfills and water treatment plants.

Originally we were directed by the SCAQMD staff to a flare of a water treatment plant in Ontario that is often burning. In order to perform I-DOAS measurements, an unobstructed field of view between the flare and the instrument is required. During the area survey we unfortunately did not find a suitable vantage point for observations outside of the facility. We approached the facility for permission to make

observations from the inside of their fenceline. However, negotiations stalled due to facility's concerns that results of the observations will be used for enforcement purposes.

Consequently we focused on flares at landfills. By AQMD regulations, flares of landfills in the LA Basin are required to have shrouds concealing the flames of the flares. Therefore, it is often hard to determine whether a landfill flare is in operation. In addition, flares of many local landfills are not visible from the public land. However, we located two landfills, one in Ontario and one in Sun Valley, which have flares that can be observed from outside of the facilities' fencelines. In addition, observations of the power plant located at the UCLA campus were performed.

During April through July 2014, three days of I-DOAS observations of flares of the landfills in Sun Valley and Ontario were conducted, as well as two days of I-DOAS observations of the power plant in West Los Angeles. Table 5.5 provides a summary of these I-DOAS observations.

Table 5.5: I-DOAS measurements of landfills

Date	Observed	Notes
04/24/14	Air above the power plant	• Plumes of elevated NO_2 and HCHO were observed in the air above the power plant
05/27/14	Air above the power plant	• No significant occurrence of HCHO, NO_2 and SO_2 were observed.
05/30/14	Flares of the landfill in Sun Valley	• Due to very close proximity to the flare, I-DOAS instrument elevation tilt was not sufficient to cover air above the flare. • Due to flare shrouds we were not able to confirm that flares were burning at the time of our measurements. • No enhancement of HCHO, NO_2, or SO_2 were detected at observed altitudes ~ ¾ of the height of the flare.
07/09/14	Flares of the landfill in Ontario	• Due to flare shrouds we were not able to confirm that flares were burning at the time of our measurements. • HCHO emissions were detected with the maximum emission strength of ~ 0.33 ± 0.1 lb/hr.
07/23/14	Flares of the landfill in Sun Valley	• Due to flare shrouds we were not able to confirm that flares were burning at the time of our measurements. • Increased I-DOAS elevation tilt in order to "cover" air above the flares. • No enhancements of HCHO, NO_2, or SO_2 were detected above the top of the flares.

5.6.1 Observations of air above a power plant

On April 24 and May 27, 2014 observations of the air above the UCLA campus were performed. During both days, the I-DOAS instrument was placed on the roof of the UCLA Math Sciences Building, with the main azimuth viewing angle looking towards the south-west. Approximately 0.25 miles along that viewing direction is UCLA's co-generation power plant. In ~1 mile the I-DOAS line of sight crossed the I405 San Diego freeway, which has a N-S orientation. Figure 5.6 shows the Google map of the area with location and main azimuth viewing angle of the I-DOAS instrument marked. On April 24, 2014 the sky was clear, with winds coming from the south at about 4m/s. On May 27, sky was also clear, but winds were very weak.

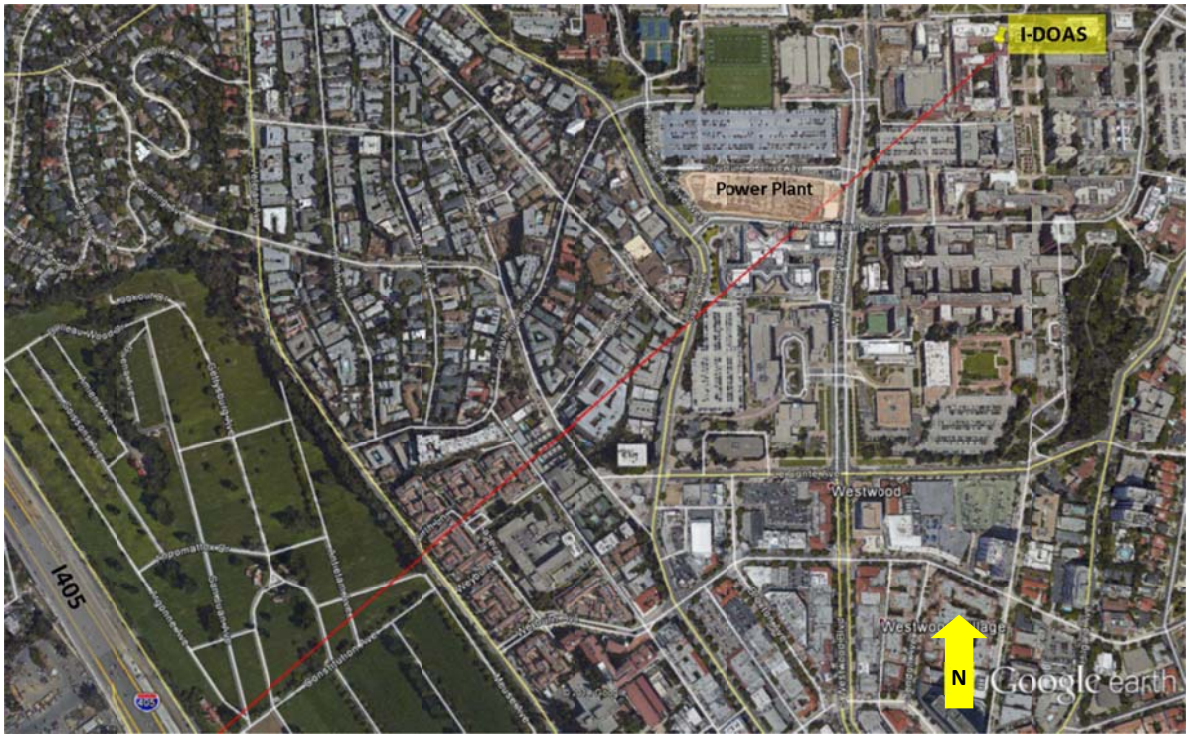

Figure 5.6: Google Earth map of area for I-DOAS measurements on the UCLA campus in April and May 2014. The yellow pin indicates the location of the I-DOAS instrument on the roof of the Math Sciences Building. The red line indicates the main azimuth viewing angle for the I-DOAS scans in the direction of the power plant.

During the I-DOAS measurements on April 24, 2014, enhancements of HCHO and NO_2 were observed in the air above the UCLA campus. While observed plumes were detected from the direction of the UCLA power plant, none of the plumes seem to have originated from the plant's smoke stacks, nor did they have smoke stack shapes. Observed plumes were more of a cloud-shape, floating above the UCLA campus, and varied with time. The origin of the observed plumes is unclear. We hypothesize that these plumes might have been older pollution plumes aloft, but they also might be outflows of the I405 freeway. Figure 5.7 and Figure 5.8 show an example of observed NO_2 and HCHO plumes, respectively.

I-DOAS measurements from the same location, with the same observation geometry were also performed on May 27, 2014. On that day, no enhancements of HCHO, NO_2 or SO_2 were observed.

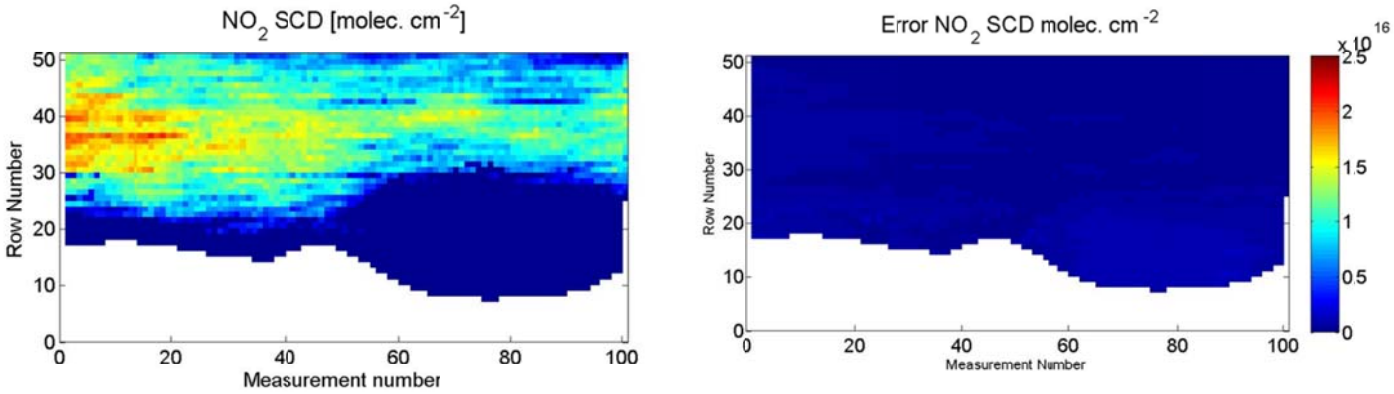

Figure 5.7: NO_2 DSCDs observed by the I-DOAS in the air above Westwood on 04/24/14. Panels show DSCD (left) and DSCD error (right) images for NO2.

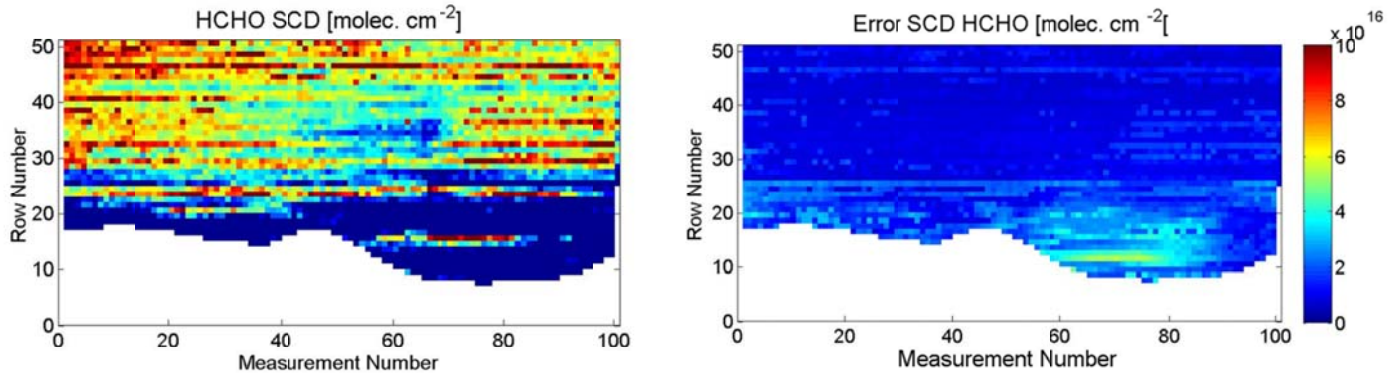

Figure 5.8: HCHO observed by the I-DOAS in the air above Westwood on 04/24/14. Panels show DSCD (left) and DSCD error (right) images for HCHO.

5.6.2 Observations of air above landfills in the Los Angeles area

On May 30 and July 23, 2014 we performed I-DOAS observations of the flares at a landfill in Sun Valley. On July 09, 2014, observations of flares at a landfill in Ontario were also performed.

On both measurement days in Sun Valley, the I-DOAS instrument was placed on a public sidewalk, directly across the street from the three flares. This observation location was not ideal, as it was very close to the observed flares and required the instrument to be considerably tilted. However, it was the only available and accessible vantage point. Since we had never before performed I-DOAS observations in such close proximity to the source, we ran into the problem that our instrument's tilting mechanism could not accommodate the required viewing geometry on the first day of measurements. On that day, measurements of the air at altitude and below the tips of the flares were performed. We adjusted the tilting mechanism and returned to the same location on July 23, 2014. During both days, the sky was clear, with very light and variable winds. On these two measurement days, we did not observe enhanced HCHO, NO_2 or SO_2 associated with the flares.

On July 09, 2014, we performed I-DOAS observations of three flares located at a landfill in Ontario. The I-DOAS instrument was placed on the grassy area across the street from the landfill fenceline, approximately 70m south-east of the three landfill flares. For most of the day skies were clear, and winds were very light and variable. On that day, we performed 6 scans over the flares, at an elevation angle of 14.5° and between azimuthal viewing angles of 309° and 319° (see Figure 5.9). Measurement at 293° azimuth (yellow line in Figure 5.9) was used as an atmospheric reference. This direction was selected during the instrument's set-up because it was upwind of the flares. Figure 5.9 shows the location and viewing geometry of the I-DOAS on July 09, 2014, and Figure 5.10 provides the view towards the flares from the location of the I-DOAS instrument.

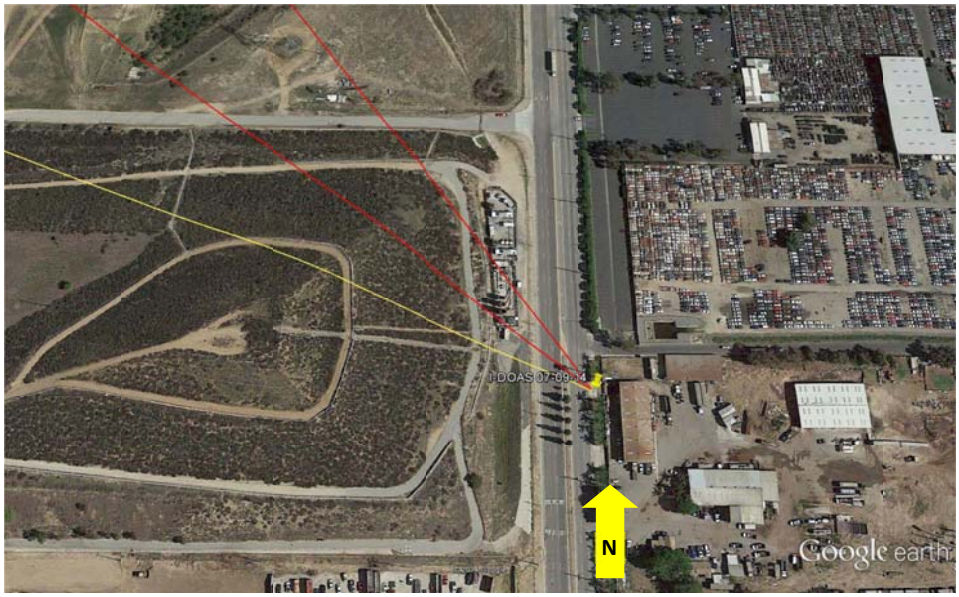

Figure 5.9: Google Earth Image of the area around the landfill in Ontario with the location of the I-DOAS instrument and instrument viewing directions marked. Yellow pin indicates the location of the I-DOAS instrument. Red lines indicate start and stop azimuths of the I-DOAS scan, and the yellow line indicates the azimuth viewing angle of the reference measurement.

Figure 5.10: View towards the flares from the location of the I-DOAS instrument.

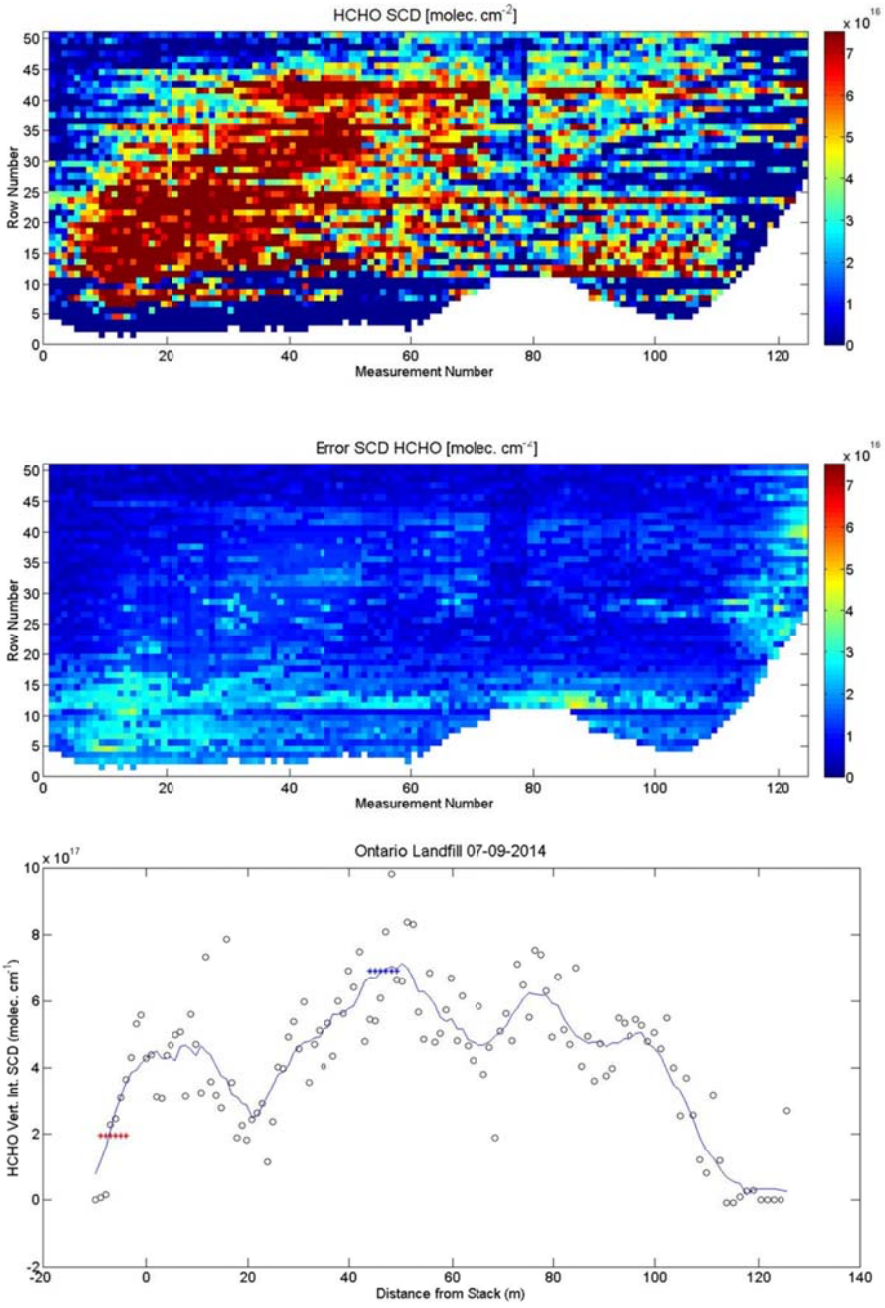

Figure 5.11: HCHO emissions from landfill flares observed by the I-DOAS at the landfill in Ontario on July 09, 2014. The top two panels show HCHO DSCD (top) and HCHO DSCD error (middle) images, and the bottom panel shows vertically integrated HCHO DSCDs. Using meteorological data from the near-by Ontario airport, the HCHO flux was estimated to be 0.14 +/_ 0.07 kg/hr.

During our measurements on that day, we did not detect NO_2 or SO_2 enhancements above our detection limit of about 0.1 kg/hr (0.22 lb/hr) and 0.5 kg/hr (1.1 lb/hr), respectively. Enhanced HCHO levels were observed from one of the flares during the scan performed between 2:49 – 3:19 pm. Figure 5.3 provides an example of the spectral analysis for HCHO on that day. HCHO DSCD and HCHO DSCD

error are shown on the top two panels of the Figure 5.11, and the bottom panel shows the vertically integrated HCHO used for the flux calculation. We calculated the HCHO emissions rate from this flare to be 0.14 ± 0.07 kg/hr (0.31 ± 0.13 lb/hr) (values for wind direction of 240^{o} and wind speed of 3 m/s were used based on meteorological information from Ontario airport).

It is important to note that, due to variable winds, conditions for I-DOAS measurements on that day were not ideal. Because flux calculation relies on wind information, wind shifts and changes during the scan could lead to under- or over- estimations of calculated HCHO flux.

Our previous experience with flares of petrochemical facilities also suggests that emissions can be variable with time. Therefore, a longer record of observations is necessary for determining overall flare emissions. It is also desirable to perform I-DOAS measurements in conjunction with any source testing done by the facility for validation of I-DOAS measurement results.

6 Open Path -Fourier Transform Infrared Spectroscopy

Large numbers of trace gases, including many pollutants and greenhouse gases, can be measured by remote sensing techniques in the infrared wavelength region. IR absorption spectroscopy is, however, rarely used for air quality research or ambient air monitoring, except in the most polluted cities, due to the higher detection limits relative to other techniques. Nevertheless, it offers a unique opportunity for fenceline monitoring of high levels of pollutants during an upset or accidental release. Some of the advantages of IR spectroscopy are the fast retrieval of concentrations, for example compared to a gas-chromatography system, the lack of sampling artifacts, and relatively easy long-term operation. While the UCLA research group does not own an IR open path system, UV-Vis and IR spectroscopy are similar enough that we proposed to explore the capabilities and operational constraints of IR absorption spectroscopy for fenceline monitoring in the Los Angeles Basin. For the IR part of our fenceline experiment, we borrowed an IMACC long-path FTIR system from the US Environmental Protection Agency, in order to determine whether this type of instrument is capable of fully automated monitoring emissions from industrial facilities. In the following sections, we will provide a short description of the setup, discuss our experience with operating this instrument and present the results from several months of measurements.

6.1 Instrument description and operational experience

Open-Path Fourier Transfer Infrared (OP-FTIR) measurements of hydrocarbon and greenhouse gas concentrations at the Carson Tesoro refinery fenceline were carried out from July 15, 2013 through January 01, 2014. The OP-FTIR instrument owned by the EPA was manufactured by the Industrial Monitor and Control Corporation (IMACC, http://www.ftirs.com) and consists of an optical telescope which transmits infrared light through the air to a passive retroreflector array at the other end of the light path. The reflector folds the light-path, sending the IR beam back to the main instrument where it is detected using Fourier transform techniques. The sending telescope is placed on the manual azimuth/elevation mount to allow for alignment to the retroreflector. The instrument is controlled through a personal computer, which also performs online data analysis. Figure 6.1 presents photographs of the IMACC FTIR system and retroreflector array in Carson. The IMACC FTIR instrument is equipped with a

Figure 6.1: Photograph of the IMACC FTIR at the Carson FML (left) and retroreflector mounted at the light post inside the Tesoro refinery (right).

HgCdTe liquid nitrogen cooled detector. The size of the instruments' dewar is such that liquid nitrogen refill is required approximately every 8 hours. Because the FML is located on the grounds of Ventura Transfer Co., we have access to the site only during business hours. Therefore liquid nitrogen refills were performed in mornings and early evenings Monday through Friday, resulting in gaps in the data during the early morning hours, as well as weekends and holidays. On-line data analysis was performed using a spectral analysis software suite proprietary to IMACC Corporation. During the instrument setup phase, an IMACC representative provided us with the analysis method optimized for our experimental setup. This analysis method contains the following species: Carbon dioxide (CO_2), Carbon monoxide (CO), Ozone (O_3), Nitrous oxide (N_2O), methane (CH_4), ammonia (NH_3), styrene, 1-3 Butadiene, vinyl chloride, ethylene (C_2H_4), propene (C_3H_6) and water vapor. While on-line data analysis is performed, raw spectra are also saved, therefore allowing for re-analysis at a later time.

6.1.1 Operation of instrument

The IMACC FTIR system was placed inside the AQMD FML at the fenceline of the Carson Tesoro refinery; and the retroreflector array was mounted on a light post on the grounds of the Tesoro refinery. The FTIR light path thus extended from the FML, across the Dominguez Channel to the retroreflector array. Figure 2.2 shows a map of the area with marked locations of the FML and FTIR light path. The instruments line of sight was almost due south (at the azimuth of 193^o). This line of sight is perpendicular to the main wind direction.

Initially, the retroreflector array was placed on the same light pole as the LP-DOAS retroreflector array. At the time of initial setup, Dr. Laush of IMACC, who helped with the initial setup, expressed concern about the low light levels through the system. A different IR source was overnighted to Carson, but it did not make a difference. After inspection of the instrument and retroreflector, Dr. Laush concluded that low light levels were due to the longer than recommended light path for the size of the retroreflector. His recommendation was to move the retroreflector closer. However, this was not an option, as relocation of retroreflector had to be performed by refinery personnel, and therefore required advanced scheduling with the refinery. A decision was made to perform measurements with the existing setup, using a longer integration time of 10 minutes. Since FTIR measurements began on July 17, 2013, we observed further steady decline of the FTIR light levels. We determined that this was due to heavy soot accumulation on the reflectors, which acted as a physical barrier and blocking a part of the light (we were located right next to the heavily traveled Alameda freight train corridor). With the declining light levels, we observed some measurements that were clearly erroneous, e.g. occasional CO_2 readings of 300 ppm. In addition, retrieved values for O_3 were highly variable (between 0 and 100 ppb within 20 minutes period) with large errors. The ozone data also did not show the expected diurnal cycle. This unreliable O_3 measurements cast doubt on the quality of all other species measured by the IAMCC FTIR instrument.

On October 16, 2013 the FTIR retroreflector was cleaned and relocated to a light post closer to the FML. The new FTIR light path length was 150 m (one way). FTIR measurements on this new light path were resumed on October 24, 2013. Light levels and data quality improved dramatically with the reflector relocation.

Figure 6.2 shows a few days of O_3 measurements obtained by the FTIR measurements after the retroreflector relocation, compared to O_3 measured by a 2B Technologies O_3 UV-absorption in-situ monitor we operate at the site. The two instruments are generally in agreement, and all other trace gases measured by the FTIR system showed reasonable values. We therefore deemed the system operation satisfactory. In the following sections we will only discuss data collected after October 24 2013.

The IMACC FTIR was equipped with a manual tripod for alignment. Prior to retroreflector relocation, realignment to the retroreflector was required at least once a day. After retroreflector relocation, we performed alignment for optimization to the retroreflector on average two times a week. In order to

maintain consistently good alignment to the retroreflector, a computerized mount with capability of auto-alignment, similar to what we use for our LP-DOAS systems, is desirable.

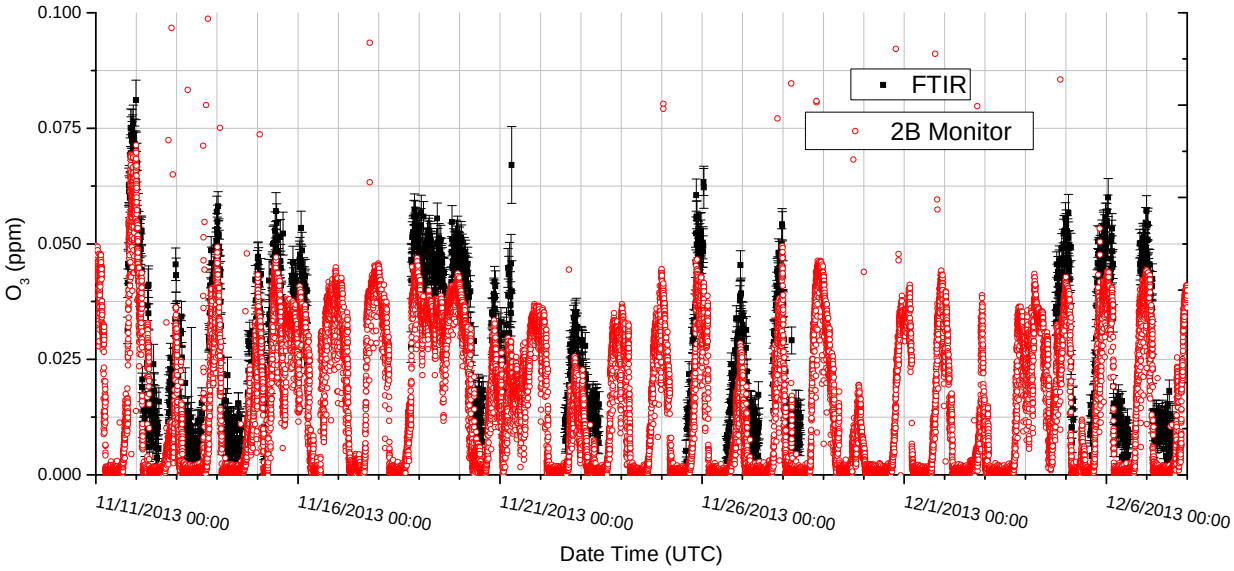

Figure 6.2: Comparison of ozone mixing ratios measured by the long path FTIR and in-situ 2B O_3 monitor.

6.2 Results

Figure 6.3 and Figure 6.4 show an overview of the FTIR measurements in Carson from October through December 2013, and Table 6.1 lists detection limits of the measurements, which were calculated as two times the average error reported by the IMACC FTIR software.

During the observational period, highly variable levels of GHG and pollutants were observed. For example, ozone levels varied between a low of only a few ppb during most nights, to a maximum of 80 ppb measured on 11/11/13 at 19:46 UTC (12:46 local). Ozone data collected after the relocation of the FTIR retroreflector showed the diurnal cycle expected from atmospheric chemistry. In addition, ozone measured by the FTIR system was in a good agreement with the in-situ 2B monitor operated by our group at the FML site (Figure 6.2), therefore giving us confidence in the quality of the FTIR data. As expected from the ozone chemistry, highest levels of ozone were observed during the mid-day hours, while the lowest ozone was during the night. However, during the night of November 19, 2013, O_3 levels did not diminish and remained above 40 ppb.

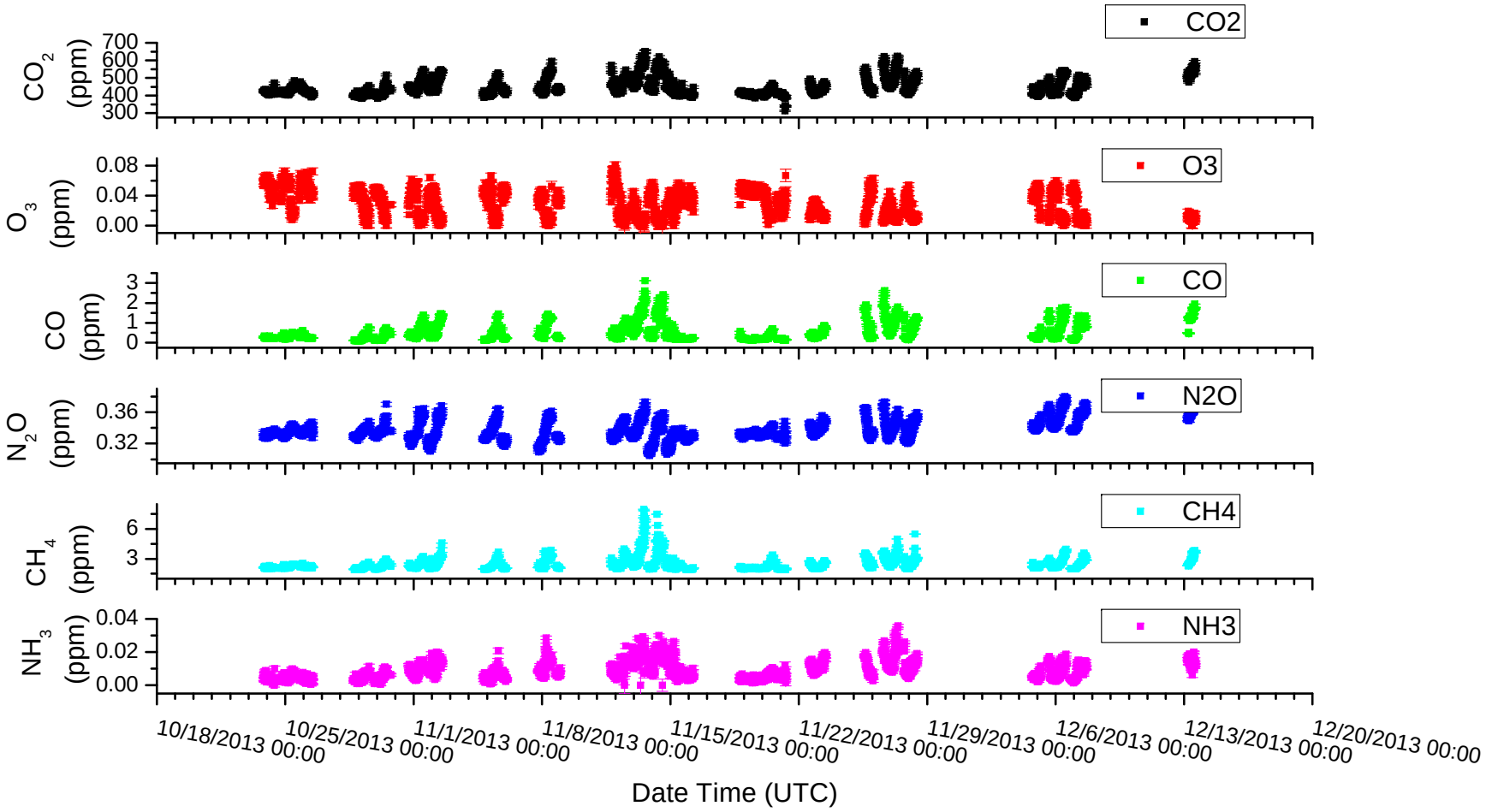

Figure 6.3: Overview of CO_2, CO, O_3, N_2O, CH_4, and NH_3 measured by the FTIR method in Carson in October – December 2013.

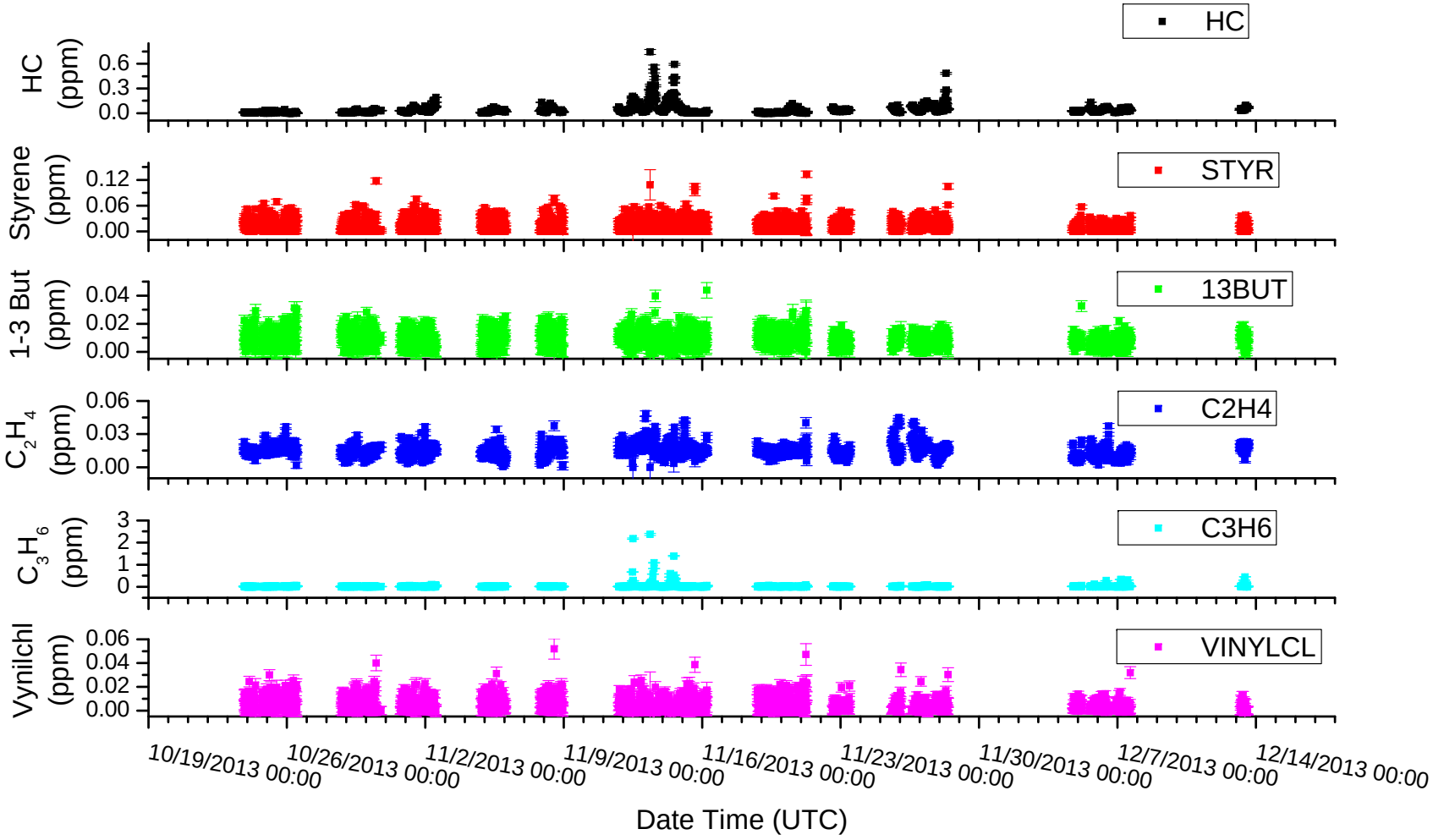

Figure 6.4: Overview of hydrocarbon continuum, Styrene, 1-3 Butadiene, Vinylchloride (Vynilchl), Ethylene (C_2H_4), and Propene (C_3H_6) measured by the FTIR method in Carson in October – December 2013.

Table 6.1: Detection limits for IMACC FTIR measurements in Carson.

Species	Average detection limit
CO_2	11 ppm
1-3 butadiene	7 ppb
C_2H_4	4 ppb
C_3H_6	9 ppb
NH_3	2 ppb
Styrene	8 ppb
Vinyl chloride	8 ppb
CH_3OH	6 ppb
O_3	6.5 ppb
CO	6.5 ppb
N_2O	5 ppb
H_2O	72 ppm
HCl	27 ppb
HC	6 ppb
CH_4	25 ppb

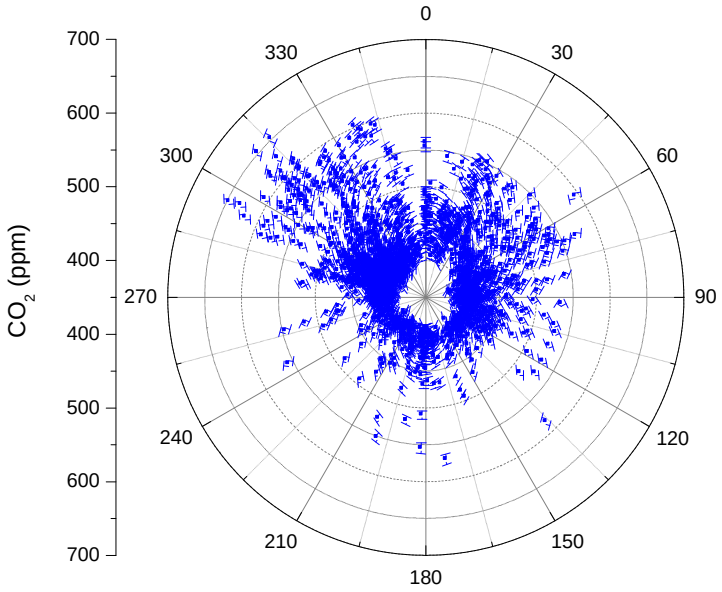

Figure 6.5: Wind rose of CO_2 mixing ratios measured by the FTIR instrument at the Carson Tesoro

CO_2 levels at the site varied between 390 ppm and 650 ppm. The highest value was recorded during the night of November 13, 2013. Figure 6.5 shows the wind rose of CO_2 mixing ratios measured at the FML. CO_2 levels above 400 ppm were frequently observed from many different wind directions. However, the highest levels of CO_2 were observed when the wind was coming from the north-western direction. The northern part of the Tesoro refinery lies in this direction (see Figure 2.1), and therefore the high CO_2 is likely due to emissions from combustion processes within the refinery, in particular from the co-generation plant. Elevated CO_2 observations were also observed from the northern and north-eastern directions. These elevated concentrations may be due to emission from the I405 and I710 freeways (see Figure 2.1).

CO levels at the site ranged from lows of 0.15 ppm to highs of 3 ppm. In general, trends of CO_2 and CO were closely correlated (Figure 6.6) with the following functional relationship (Figure 6.8):

$$[CO] = -3.44 + 0.0089[CO_2] \qquad \text{with R=0.94} \qquad (6.1)$$

Episodic elevated levels of CO_2 and CO, were observed primarily during the night. During the period of October through December 2013, elevated levels of CO_2 and CO were detected during 16 nights, between the times of 11 and 14 UTC (3 and 6 am local time) (Figure 6.6).

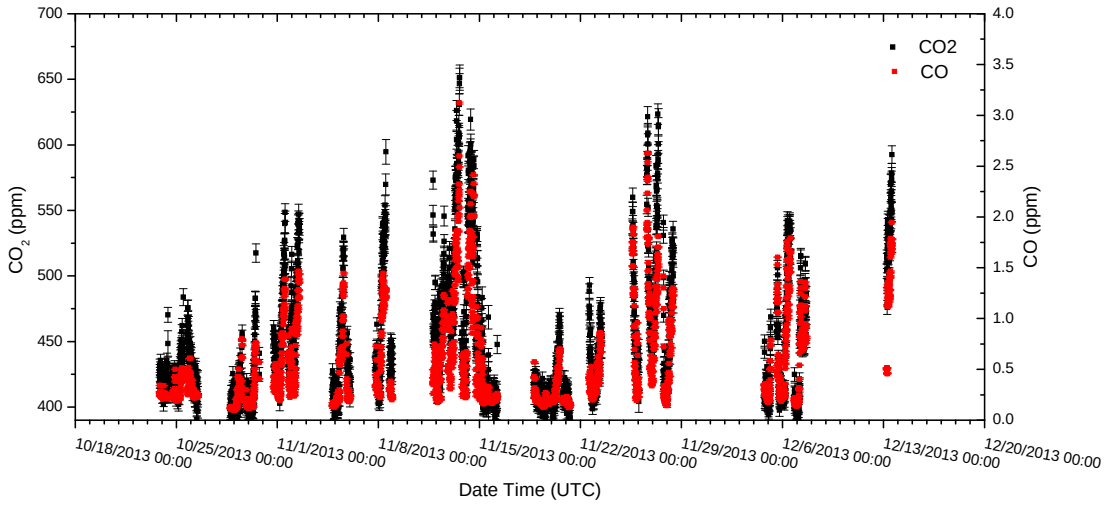

Figure 6.6: Relationship between CO_2 and CO measured at the Carson FML site.

We also observed episodic increases of other trace gases, such as NH_3 and N_2O. Similar to CO_2, these increases were primarily observed during the nighttime hours. N_2O levels varied between 0.31 and 0.38 ppm. Until the end of November, increased N_2O events above 0.32 ppm occurred at night and early morning hours. In December, the overall pattern of increased N_2O levels at night, as well as maximum observed N_2O levels, remained the same. However, daytime N_2O minimum levels increased to 0.34 ppm. NH_3 showed clear correlation with CO_2 with the following linear relationships (see Figure 6.9), the correlation with N_2O was weaker (see Figure 6.7):

$$[NH_3] = -0.33 + 9.45e^{-5}[CO_2] \quad \text{with R=0.84} \tag{6.2}$$

$$[N_2O] = 0.26476 + 1.63e^{-5}[CO_2] \quad \text{with R=0.63} \tag{6.3}$$

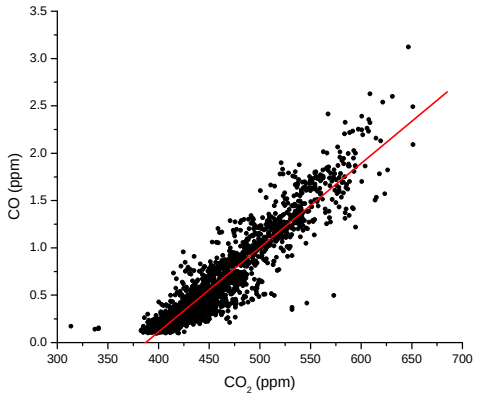

Figure 6.8: Correlation between CO_2 and CO measured at the Carson FML site.

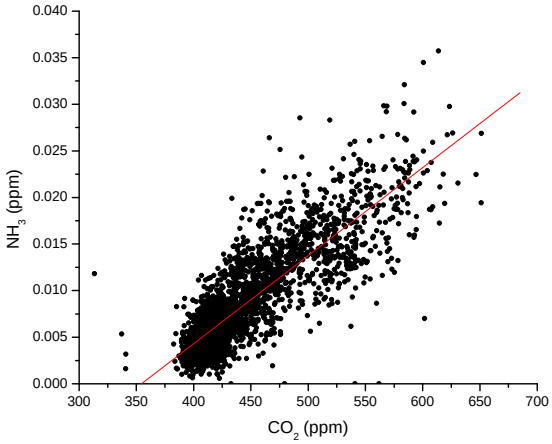

Figure 6.9: Correlation between CO_2 and NH_3 measured at the Carson FML site.

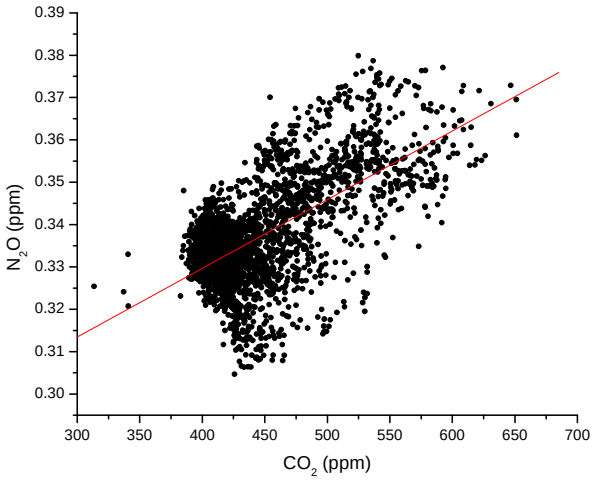

Figure 6.7: Correlation between CO_2 and N_2O measured at the Carson FML site

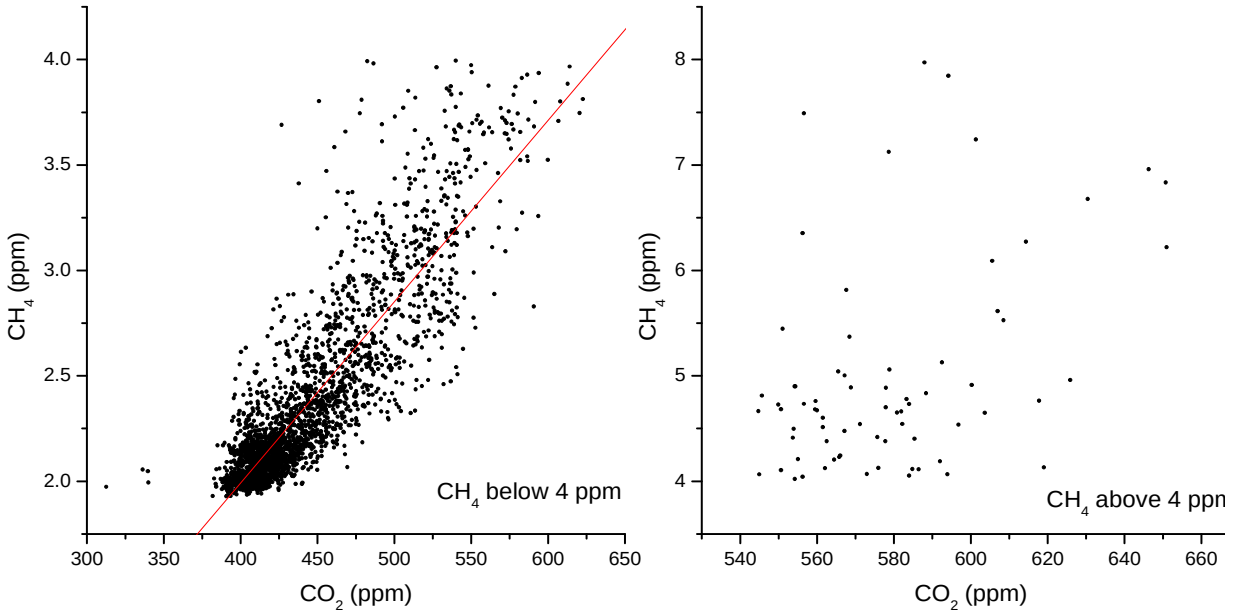

Figure 6.10: Correlation between CO_2 and CH_4 mixing ratios (ppm) measured at the Carson FML site.

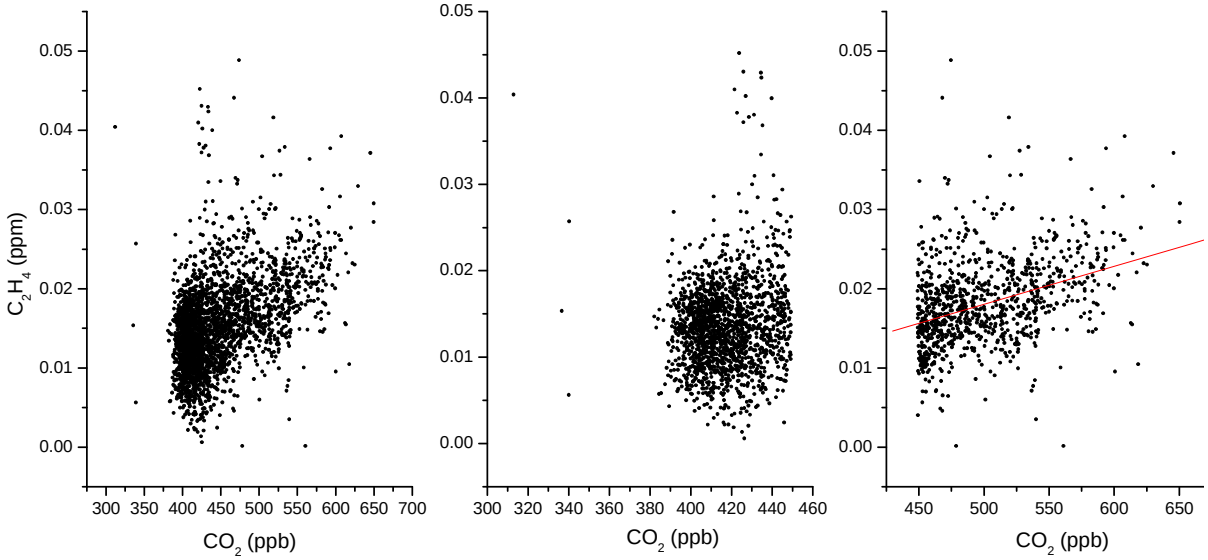

Figure 6.11: Relationship between CO_2 and C_2H_4 measured at the Carson site. Left panel shows all data points. Middle panel shows data for CO_2 levels below 450 ppm. Right panel shows data for CO_2 above 450 ppm

CH_4 levels at the site varied between minima of ~2ppm to a maximum of 8 ppm recorded at 12:35 UTC (04:35 local) on November 13, 2013. Similar levels of CH_4 were also observed the following night, at 06:24 UTC November 14, 2013 (23:24 local on November 13, 2013). Such high levels of CH_4 were only observed during these two events. During three other nights, November 02 at 12:47 UTC (04:47 local), November 27 at 09:07UTC (01:07 local) and November 28 at 08:01 UTC (00:01 local) moderate CH_4 maxima of 4.6 ppm, 4.9 ppm, and 5.5 ppm respectively were recorded. All other elevated levels of CH_4 were below 4 ppm. All observed CH_4 levels above 4 ppm were observed at CO_2 levels above 540 ppm. We therefore conclude that elevated CH_4 levels during the night of November 13 and 14 were at least partially due to a different emission source/processing unit than events observed during other nights. Therefore, in performing the correlation study between CO_2 and CH_4, we removed data associated with CH_4 levels above 4 ppm. We found that correlation between CO_2 and CH_4 followed the following linear relationship (see Figure 6.10):

$$[CH_4] = -1.4469 + 0.0086[CO_2] \qquad \text{with R=0.87} \qquad (6.4)$$

An average "background" of ~ 15 ppb of C_2H_4 was observed at the site. Higher levels of C_2H_4 (above 25 ppb) were also observed on a number of occasions, and were accompanied by varying CO_2 concentrations (Figure 6.3). The highest C_2H_4 concentration of 50 ppb was recorded during the evening of November 12, 2013 at 02:48 UTC 11/13/13 (18:48 local time). No apparent correlation between CO_2 and C_2H_4 levels were observed for CO_2 levels below 450 ppm. For CO_2 above 450 ppm, a weak correlation (R=0.4) can be described by the following equation (Figure 6.11):

$$[C_2H_4] = -0.006 + 4.8 \times 10^{-5}[CO_2] \qquad \text{with R=0.4} \qquad (6.5)$$

For C_2H_4 levels above 30 ppb, the C_2H_4/CO_2 the average emissions ratio was 7.5×10^{-5}.

C_3H_6 concentrations recorded at the fenceline monitoring site were often below the detection limit of the instrument. Three large C_3H_6 events were observed during three consecutive nights, November 12 through November 14, between the times of 09:00 UTC and 14:00 UTC (01:00 and 06:00 local), when maximum mixing ratios of 670 ppb (11/12/13 @ 11:40 UTC), 2.3 ppm (11/13/13 @ 12:00 UTC), and 1.4 ppm (11/14/13 @ 13:25 UTC) were observed. Smaller releases, between 100 ppb and 400 ppb, were observed on November 02, 21, 27, and December 6, 7, 13. These events only lasted for a couple of hours. All high C_3H_6 events were accompanied by elevated CO_2, and we estimate the average C_3H_6/CO_2 emission ratios 0.002. Figure 6.12 shows a wind rose for C_3H_6 concentrations observed at the Carson site. Most elevated C_3H_6 was observed when winds were coming from the north-west, which corresponds to the northern part of the Tesoro refinery.

The IMACC FTIR instrument also measures a hydrocarbon continuum signal, which is a broad absorption feature due to overlapping absorptions of a variety of hydrocarbons. The highest hydrocarbon continuum (HC) levels were most often observed during the times when the wind was coming from the south west and south (the direction of the Tesoro refinery), from the east (the direction of the INEOS polypropylene plant), and occasionally from the north and south (Figure 6.13).

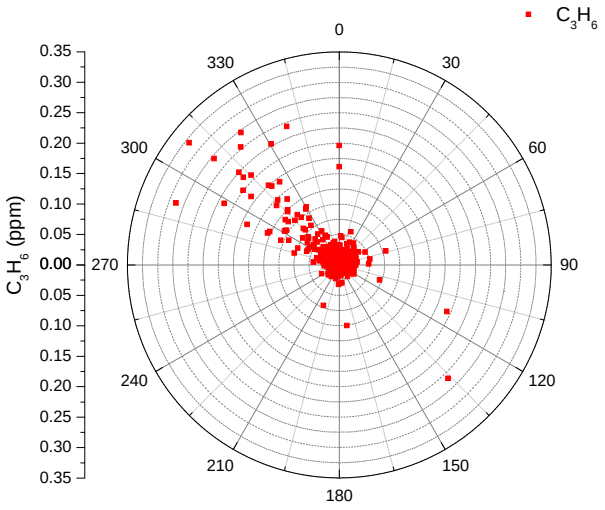

Figure 6.12: Wind rose of C_3H_6 mixing ratios (ppm) measured by the FTIR instrument at the Carson Tesoro refinery.

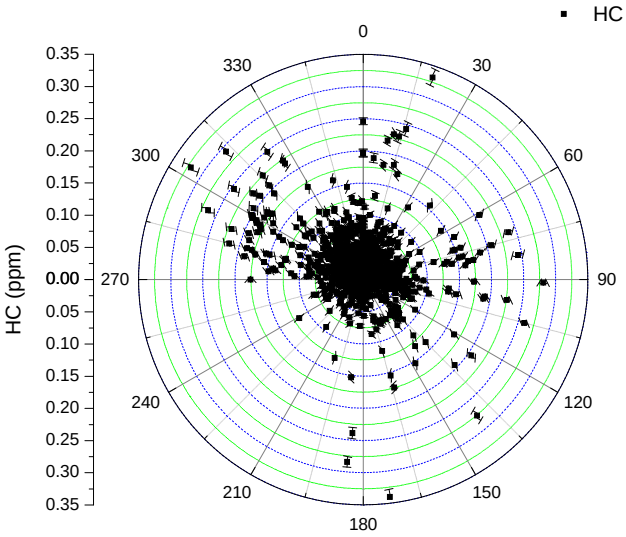

Figure 6.13: Wind rose of hydrocarbons continuum (HC, ppm) measured at the Carson site.

7 Conclusions

The goal of this project was to demonstrate the feasibility and performance of various modern remote sensing techniques for continuous fenceline pollution monitoring, and to quantify emissions from industrial and, in particular, petrochemical facilities. In addition, we investigated whether remote sensing monitoring techniques can be used as a rapid alarm system for accidental emissions at the facility fenceline.

We investigated four different remote sensing methods and applications:

- Long-path DOAS (LP-DOAS) monitoring of aromatic hydrocarbons and use of this system as an alarm tool for accidental emissions
- Imaging DOAS (I-DOAS) measurements of the emissions from point sources such as industrial flares and smoke stacks.
- Dual Multi-Axis DOAS (MAX-DOAS) measurements of facility wide emission fluxes of HCHO and NO_2.
- FTIR long-path spectroscopic measurements of various hydrocarbons downwind of an oil refinery.

Within the project we were able to investigate all four approaches and perform measurements for extended periods using each of them.

In general, we found that all four methods are capable of monitoring emissions from industrial facilities. However, each method has various challenges. For example, not all commercially available DOAS instruments have the required accuracy. However, more modern technology, such as the LP-DOAS built by UCLA for this project, has the ability to provide fast and sensitive measurements. Some of the instruments, such as the OP-FTIR used in this project, require a considerable amount of maintenance. Thus, obtaining a continuous data-set will require more engineering efforts to automate these measurements. Placement of the instruments is also crucial, as we have learned from our I-DOAS and dual MAX-DOAS observations.

A summary of the lessons we have learned in the application of each approach, and specific recommendations for future uses and applications, are provided below.

7.1 LP-DOAS measurement of aromatic hydrocarbons

The goal of this part of our project was to demonstrate the use of LP-DOAS as a long-term fenceline monitoring technique for aromatic hydrocarbons, and to explore the use of such an instrument as an alarm system for elevated levels of pollutants. Because we were unable to use the commercial OPSIS system, due to poor detection limits, we developed our own version of an LP-DOAS instrument. The preliminary version of this instrument was operated for more than 2 months at the fenceline of the refinery in Carson. The results from this deployment clearly demonstrated the potential of this system to measure various levels of toluene. Analysis of the observations with respect to the sources, using meteorological data and simultaneous observations with the OP-FTIR, showed that the observed toluene originated from the direction of the refinery. Toluene was highly correlated with CO_2, CO, and total hydrocarbons measured by the OP-FTIR. In particular, the combination of the LP-DOAS with the OP-FTIR, added another dimension to the fenceline monitoring approach, as the correlation of toluene with better known gases, such as CO_2 or CO, may allow the determination of emission fluxes.

The final version of the LP-DOAS was deployed for 3 months during summer, 2014. This system was fully automated, and besides restarting it after power failures, it did not require any manual operation or maintenance during this period. This new system has the capability to measure both benzene and toluene simultaneously, as well as other aromatic hydrocarbons if present at high enough concentrations.

The detection limits of the LP-DOAS system, calculated from the actual measurements, were ~ 0.6 ppb for benzene and ~ 0.45 ppb for toluene for a 60 second measurement time and a reflector array at 250m distance. A newly proposed EPA requirement for refineries to monitor fenceline benzene concentrations establishes a 2-week averaged benzene concentration action level of 3 ppb (http://www.epa.gov/airtoxics/petref.html). The detection limits of the new LP-DOAS system are therefore sufficient for monitoring of fenceline benzene levels for the purposes of compliance or enforcement. We also developed the tools to operate this system as a rapid alarm system. If set up correctly, benzene and toluene mixing ratios can be reported within 30-60 seconds after a measurement, provided a stable internet connection is available at the measurement site.

The following general conclusions can thus be drawn from our work for the use of LP-DOAS for the monitoring of aromatic hydrocarbons:

- LP-DOAS systems based on current state-of-the-art technology can reliably monitor ozone and air toxins such as toluene, benzene, and other aromatic hydrocarbons.
- Detection limits of these new LP-DOAS systems are sufficient for monitoring of both large accidental releases and fugitive emissions.
- The high measurement frequency of one minute, together with the near real-time data analysis, which can provide trace gas concentrations within one minute of a measurement, is sufficient to use these systems as an alarm system for accidental releases.
- The new technology employed in UCLA's new LP-DOAS allows for long-term unattended and stable operation, as well as full remote control access. This ability will considerably reduce operating cost, which largely offsets the initial cost of the instrument. No consumables, besides electricity, are needed to operate instrument.
- Co-location of an UV LP-DOAS and open-path FTIR system open new opportunities for emission measurements, as relating observations of trace gases, such as CO or CO_2, with well-known emissions, allows for the determination of emission fluxes using a ratioing technique.
- Due to its novel design, the UCLA LP-DOAS system is capable of measurements on multiple and longer light paths, thus opening up an unprecedented potential for monitoring emissions from an entire facility.

We conclude that our efforts in showing the capabilities of LP-DOAS for fenceline monitoring of aromatic hydrocarbons has been a success, and we see no obstacles in using LP-DOAS as a fenceline monitoring and alarm system at industrial facilities.

7.2 Dual Max-DOAS measurement of area-averaged emissions

The measurement of area-wide fluxes of air pollutant such as NO_2, HCHO, and SO_2, remains a challenge, as these pollutants can be mixed away from the surface, and thus would be undetected by ground-based in-situ monitors. Remote sensing offers the unique capability to overcome this challenge by providing boundary layer averaged concentration measurements. The dual MAX-DOAS approach we employed here follows this idea by measuring the trace gas amount in a slice upwind and downwind of an area. The difference between the two slices, together with information on wind speed and direction, allows the determination of the fluxes. Despite initial delays due to permitting, we were ultimately able to set up a dual MAX-DOAS system around two refineries in Carson. The setup was not ideal, as finding the optimal upwind location was more difficult than anticipated. For typical wind conditions, the dual MAX-DOAS measurements derived NOx fluxes of 709 tons/yr with a ~40% uncertainty and an assumed NO_2/NOx ratio of 0.3, which compare well with the 2012 reported emissions of 983 tons of annual NOx emissions from the refineries surrounded by the dual MAX- DOAS system. Problems with the reverse wind direction shows that the location of the two MAX-DOAS instruments, in particular in areas with a high source density, impacts the results of the method.

The success of our flux measurements was also due to the development of two new identical MAX-DOAS instruments for this project. These compact systems are unique, as much effort was spent on thermally-stabilizing the spectrometer/detector combination to allow for long-term observations.

The successful comparison of the observations from one of the newly developed MAX-DOAS instruments, using a geometric approach to convert slant column densities to mixing ratios, to measurements from a nearby air quality monitoring station showed that single MAX-DOAS instruments can also be used to monitor ambient trace gas levels. Another unique application of MAX-DOAS is the measurement of the $HCHO/NO_2$ ration, which is a proxy to the NOx/VOC sensitivity of ozone formation. Automated MAX-DOAS measurements thus could provide a long-term record of this unique measurement. It should also be noted that the newly built MAX-DOAS instruments were fully automated and do not require calibrations or consumables.

We have drawn the following general conclusions from our work with the dual MAX-DOAS system:

- The dual MAX-DOAS method is capable of measuring area averaged fluxes of NO_2 and HCHO, provided good meteorological data is available. The instruments are fully automated, and no operational effort is required once the systems are set up. On the other hand, identifying the best location for placement of the instruments is crucial for the success of the dual MAX-DOAS approach.
- Emission rates, determined by dual MAX-DOAS in Carson under normal wind conditions, compare well to those reported in 2012, considering the estimated 40% uncertainty from our observations.
- Meteorological observations are crucial for the determination of the emissions fluxes. The dual MAX-DOAS measurements could be further improved by measuring boundary layer height, for example using a relatively inexpensive ceilometer.
- Single MAX-DOAS instruments can be used for pollutant monitoring. The observations of the $HCHO/NO_2$ ratio, which provide information on the NOx/VOC sensitivity of ozone formation, could prove to be particularly useful.

In summary, we successfully demonstrated the capability of the dual MAX-DOAS approach under ideal conditions. However, the accuracy of the method depends crucially on the location of the instruments and good meteorological data. While care has to be taken in the setup of the system, it is fully automated once installed.

7.3 I-DOAS measurements.

We had previously reported the usefulness of the Imaging DOAS method to determine emissions from point sources such as flares (e.g. Pikelnaya et al., 2013). Our original proposal was thus to apply this method to monitor flares in the petrochemical facilities in Carson. Unfortunately, flaring has become so uncommon, and also typically occurs at night, so no burning petrochemical flare was observed in Carson. The first part of our measurement efforts thus did not yield any emission fluxes above the detection limits of the instrument. We thus expanded our measurements to other point sources. Our most successful deployment was the observation of a flare at an Ontario landfill. Landfill flares are encased, and it is thus difficult to assess whether they are burning. The observed plume of HCHO, with an emission rate of ~3 lbs/hour, however is a clear indication of a burning flare. We were also able to visualize trace gas plumes over the UCLA campus, but no direct attribution of these trace gases to a single source was possible. On the other hand, this example showed that I-DOAS can also be used to show plumes of elevated pollution levels over an urban area, thus giving unique insights into the distribution of pollution.

We have drawn the following general conclusions from our measurements with the I-DOAS system:

- The I-DOAS approach can measure emission fluxes from point sources. The accuracy of the methods depends, to a large extent, on an accurate measurements of wind speed and direction.

- Burning flares have become less frequent at petrochemical facilities, and thus were not successfully observed by the I-DOAS, but flares at landfills have been found to emit HCHO.
- The I-DOAS can be used to visualize plumes of NO_2 and HCHO, for example above a freeway.

In summary, the I-DOAS system performed well during all deployment days. However, it has proven more difficult to find point sources, such as petrochemical flares, in the Los Angeles area than was originally anticipated. This is likely due to the efforts of the SCAQMD to generally reduce flaring in the South Coast Air Basin. When burning flares were observed, fluxes of HCHO could be determined. It is thus clear that I-DOAS is a powerful technique to characterize source emissions from flares and smoke stacks of power plant and ships, and potentially also emission plumes from road traffic.

7.4 OP-FTIR observations

The OP-FTIR method provides a capability for monitoring a number of pollutants and greenhouse gases. In the course of this fenceline technology demonstration project, we successfully used a commercial IMACC OP-FTIR system for fenceline monitoring in Carson, CA. Based on our experience we conclude that long-path FTIR system is suitable for fenceline pollution monitoring. Our detailed conclusions / recommendations are summarized below:

- On short light paths and in close proximity to emission sources OP-FTIR is a good method for monitoring of fenceline concentrations of pollutants and greenhouse gases. Detection limits for various hydrocarbons are in the range of 5 - 10ppb. The detection limit for CO_2 is ~11ppm.
- Simultaneous measurements of pollutants, as well as CO_2 and CO, allow for calculation of ratios of individual trace gas concentrations to CO_2 concentrations. Since CO_2 emissions from facilities are better understood and constrained, these ratios can potentially be used to estimate emissions of other pollutants from the respective facility.
- Long-term operation of an OP-FTIR system is feasible only if the instrument is equipped with an active detector cooling system, in order to reduce the effort of regular refilling of coolant.
- In areas with many pollution sources, especially those that emit soot particles (e.g. proximity to busy railroad tracks), FTIR retroreflectors must be periodically cleaned in order to maintain good light levels. We recommend cleaning of the reflectors every two months.
- A motorized azimuth/elevation mount for the FTIR telescope is highly desirable to allow for automatic adjustment of the telescope aim onto the reflector.

We conclude that OP-FTIR is a powerful method for fenceline monitoring of certain greenhouse gases and hydrocarbons. The main challenge found in the operation of the OP-FTIR in Carson, was the maintenance of the detector cooling and regular manual alignment of the telescope. These are obstacles that be easily overcome with existing technology, and it is thus feasible to operate fully automated OP-FTIR systems.

In summary all four methods are capable of monitoring emissions from industrial facilities. The inherent advantages make these systems ideally suited for long-term automatic measurements with little or no maintenance. The reduced operating cost, in particular due to reduced labor for operating the instruments, offsets the initially high purchasing cost. The ability to remotely detect plumes increases the chance to detect accidental releases making these methods superior to classic in-situ measurements for fenceline alarm systems.

8 References

Chiang HL., Hwu CS., Chen SY., Wu MC., Ma SY., Huang YS., 2007, Emission factors and characteristics of criteria pollutants and volatile organic compounds (VOCs) in a freeway tunnel study, Sci Total Environ., 381(1-3):200-11.

During, I., W. Bachling , M. KETZEL , A. Baum, U. Friedrich and S. Wurzler (2011), A new simplified NO/NO_2 conversion model under consideration of direct NO_2-emissions, Meteorologische Zeitschrift, Vol. 20, No. 1, 067-073.

Fally S., Vandaele A.C., Carleer M., Hermans C., Jenouvrier A., Merienne M.F., Coquart B., Colin R., 2000, Fourier Transform Spectroscopy of the O2 Herzberg Bands. III. Absorption Cross Sections of the Collision-Induced Bands and of the Herzberg Continuum, Journal of Molecular Spectroscopy, 204, 10 – 20, doi:10.1006/jmsp.2000.8204.

Fally S., Carleer M., Vandaele A.C., 2009, UV Fourier transform absorption cross sections of benzene, toluene, meta-, ortho-, and para-xylene, Journal of Quantitative Spectroscopy & Radiative Transfer 110, 766–782.

Hwa M.Y., Hsieh C.C., Wu T.C., Chang LF.W., 2002, Real-world vehicle emissions and VOCs profile in the Taipei tunnel located at Taiwan Taipei area, Atmospheric Environment, Volume 36, Issue 12, Pages 1993–2002.

Kawashima H., Minami M., Hanai Y., Fushimi A., 2006, Volatile organic compound emission factors from roadside measurements, Atmospheric Environment 40 (2006) 2301–2312.

Merten A., J. Tschritter, U. Platt, 2011, Design of differential optical absorption spectroscopy long-path telescopes based on fiber optics, APPLIED OPTICS / Vol. 50, No. 5, pp 738-754.

Pikelnaya, O., Flynn, J. H., Tsai, C. and Stutz, J.: Imaging DOAS detection of primary formaldehyde and sulfur dioxide emissions from petrochemical flares, J. Geophys. Res. Atmos., 118, doi:10.1002/jgrd.50643, 2013.

Platt U., Stutz J. (2008), Differential Optical Absorption Spectroscopy Principles and Applications, Springer, e-ISBN: 978-3-540-75776-4.

Stutz J., Platt U. (1997), Numerical analysis and estimation of the statistical errors of differential optical absorption spectroscopy measurements with least-square methods, Applied Optics, Vol. 35, No 30, 6041-6053.

Voigt S., Orphal J., Bogumil K., Burrows J.P., 2001, The temperature dependence (203–293 K) of the absorption cross sections of O3 in the 230–850 nm region measured by Fourier-transform spectroscopy, Journal of Photochemistry and Photobiology A: Chemistry 143 (2001) 1–9.

9 Acknowledgements

We would like to thank Dr. Philip Fine, Dr. Laki Tisopulos, Dr. Andrea Polidori, and Dr. Aaron Katzenstein of SCAQMD for the support of our project and for many fruitful discussions and advice.

We would like to thank Robert Nguyen of Tesoro Environmental department, for his cooperation and support through the p[project and for providing us with the meteorological data which was essential for the data interpretation and flux calculations.

We also would like to thank Principal Nancy Kuria of Saint Peter and Paul School for allowing us to install MAX-DOAS instrument, and Rene Spenser and Tim DeMOss of Port of Los Angeles; Joel Torcolini of Leidos; and Andres Flores of TAHA for assisting with site access and instrument setup.

Many thanks are also to Steve Hurlock, Ellyn Gray, Catalina Tsai, Ross Cheung, Fedele Colosimo and James Fest – current and former UCLA DOAS group member for their contribution to the success of this project.

10 Acknowledgements

We would like to thank Dr. Philip Fine, Dr. Laki Tisopulos, Dr. Andrea Polidori, and Dr. Aaron Katzenstein of SCAQMD for the support of our project and for many fruitful discussions and advice.

We would like to thank Robert Nguyen of Tesoro Environmental department, for his cooperation and support through the p[project and for providing us with the meteorological data which was essential for the data interpretation and flux calculations.

We also would like to thank Principal Nancy Kuria of Saint Peter and Paul School for allowing us to install MAX-DOAS instrument, and Rene Spenser and Tim DeMoss of Port of Los Angeles; Joel Torcolini of Leidos; and Andres Flores of TAHA for assisting with site access and instrument setup.

Many thanks are also to Steve Hurlock, Ellyn Gray, Catalina Tsai, Ross Cheung, Fedele Colosimo and James Fest – current and former UCLA DOAS group member for their contribution to the success of this project.